BIOACTIVE THERMORESPONSIVE HYDROGELS FOR NEURAL TISSUE ENGINEERING

A Dissertation
Presented to
The Academic Faculty

by

Sarah E. Stabenfeldt

In Partial Fulfillment
of the Requirements for the
Doctorate of Philosophy Degree in Bioengineering
Department of Biomedical Engineering

Georgia Institute of Technology
December 2007

BIOACTIVE THERMORESPONSIVE HYDROGELS FOR NEURAL TISSUE ENGINEERING

Approved by:

Michelle C. LaPlaca, PhD, Advisor
Department of Biomedical Engineering
Georgia Institute of Technology

Shawn Hochman, PhD
Department of Physiology
Emory University School of Medicine

Ravi Bellamkonda, PhD
Department of Biomedical Engineering
Georgia Institute of Technology

Yadong Wang, PhD
Department of Biomedical Engineering
Georgia Institute of Technology

Andrés García, PhD
School of Mechanical Engineering
Georgia Institute of Technology

Date Approved: August 31, 2007

An idealist believes the short run doesn't count. A cynic believes the long run doesn't matter. A realist believes that what is done or left undone in the short run determines the long run.

- Sidney J. Harris

ACKNOWLEDGEMENTS

First, I would like to acknowledge my advisor, Dr. Michelle LaPlaca, for her advice and mentorship throughout my PhD career. Secondly, I want to extend my thanks to Dr. Andrés García for the countless hours of advice, peptides, and antibodies. Dr. García's lab must also be acknowledged for showing new techniques to me and letting work with them in their lab space. I thank Dr. Ravi Bellamkonda and his lab allowing me to use various equipment. To the other committee members, I thank them for the guidance and constructive criticism helped the project progress throughout the years.

To the LaPlaca lab members, from whom I learned the art of culturing "neural tissue equivalents", the proper fonts and color schemes for presentations, adventure racing, and the best places to relieve stress with an adult beverage, thanks for everything! These years would not have gone by so fast without the comradery my labmates have provided, particularly the Iron Girls, Crystal, Hillary, and Maxine. I would also like to acknowledge the undergraduates that have worked with me through the years, Ryan Riebesell, John Kroger, Linda Fong, Vishnu Amber, Scott Medway, and Gautam Muntangi. I have learned much by mentoring these students.

I would like to acknowledge my family, Mom, Dad, Josh, and Rachel for providing encouragement and a support throughout this process. Also in the past couple of years, the additional family support from the Otwells has been great. To Richard, who really put up with the late hours in lab and the fits of stress, you helped more than you will ever know.

Finally, to the other BIOE's that began this process in 2002, I thank you for your continued friendship and good times we had while in grad school. Life's lessons are not taught in the classroom, but through good friendships!

TABLE OF CONTENTS

LIST OF TABLES

LIST OF FIGURES

LIST OF SYMBOLS AND ABBREVIATIONS

2-D	Two dimensional
3-D	Three dimensional
Bax	Bcl-2-associated X protein
Bcl-2	B-cell lymphoma protein 2
bFGF	Basic fibroblast growth factor
BSA	Bovine serum albumin
CCI	Controlled cortical impact
Cn IV	Collagen IV
CNS	Central nervous system
ECM	Extracellular matrix
EGF	Epidermal growth factor
ES	Embryonic stem cells
FN	Fibronectin
GFAP	Glial fibrillary acidic protein
GFP	Green fluorescent protein
LN	Laminin-1
LCST	Lower critical solution temperature
LSM	Laser scanning microscope
MC	Methylcellulose
MC-x-LN	Methylcellulose tethered with laminin
MSC	Mesenchymal stem cell
NG2	NG2 chondroitin sulphate proteoglycan

NSC	Neural stem cell
O4	Oligodendrocyte marker 4
qRT-PCR	Quantitative reverse transcriptase polymerase chain reaction
ROS	Reactive oxygen species
SVZ	Subventricular zone
TBI	Traumatic brain injury
TUNEL	Terminal deoxynucleotidyl Transferase tetramethylrhodamine-dUTP Nick End Labeling
VZ	Ventricular zone

SUMMARY

Traumatic brain injury (TBI) results in over 50,000 deaths and 80,000 disabilities each year. Current treatment strategies aim to alleviate acute disturbances, but are not able to address the chronic disorders associated with TBI. Neural transplantation is one potential treatment that will provide multifaceted sustained therapy to degenerating injured tissue. Transplantation of multipotent neural stem cells (NSCs) has been shown to enhance functional recovery in TBI models; however, poor cell survival and integration with host tissue potentially restrict the efficacy of such transplants. This limitation may be due to the absence of inherent NSC pro-survival cues (e.g., cell-ECM interactions). Furthermore, the neural injury environment presents cell death factors to transplanted NSCs. It is hypothesized that a 3-D scaffold presenting specific CNS adhesive moieties will enhance donor cell survival and promote differentiation and migration. This project encompassed material development and *in vitro* characterization. Results highlighted the importance of ligand tethering chemistry and density and also the mechanical integrity of cell scaffold systems. Furthermore, the developed scaffold provides a controlled microenvironment to assess the influence of LN on NSC survival, migration, and differentiation. Lastly, co-delivering NSC with the MC-LN tissue engineered scaffold into a mechanically injured neural co-culture test-bed or *in vivo* TBI model confirmed the importance of ECM cues for NSC survival and migration, respectively.

CHAPTER 1: INTRODUCTION

Motivation

Each year, 1.6 million traumatic brain injuries (TBI) are reported in the United States (Rutland-Brown et al. 2006). More staggering is the estimation that 5.3 million Americans are living with a TBI related disability (Thurman et al. 1999); this number is steadily increasing as TBI is the leading cause of injury to military personnel in the Iraq war (Warden 2006). However, current clinical therapies primarily address acute secondary injuries (e.g., intracranial pressure, cerebral edema and hemorrhage) and recent pharmacological therapies have failed to benefit TBI patients in clinical trials (see review (Marklund et al. 2006)). Consequently, the deleterious sequelae following the primary insult continues to cause tissue damage for months and perhaps years. Therefore, a sustained therapy may alleviate tissue loss and degeneration and ultimately enhance the quality of life for TBI patients. Cell transplantation is one potential sustained therapy. This treatment modality has been shown to increase functional outcomes in experimental TBI models (Gao et al. 2006; Hoane et al. 2004; Riess et al. 2007; Riess et al. 2002a; Shear et al. 2004; Zhang et al. 2005), however, donor cell survival is a major limitation (Bakshi et al. 2005; Philips et al. 1999; Shindo et al. 2006). Transplanting cells with a pro-survival signal through either exogenous supplements or endogenous genetic alterations may contribute to improved donor cell survival (Bakshi et al. 2006; Bhang et al. 2007; Boockvar et al. 2005; Chen et al. 2002; Tate et al. 2002). Therefore, the goal of this project was to develop and characterize a rationally-designed scaffold that possesses both minimally invasive delivery capabilities and presents bioadhesive moieties to promote transplant survival within the traumatically injured brain.

Background

Traumatic Brain Injury

Pathological Events

The pathologic events of a traumatic brain injury (TBI) are divided into two categories: primary and secondary damage. The initial traumatic impact deforms the brain tissue initiating immediate necrosis (primary damage). The necrotic primary damage in turn activates secondary damage that includes excitotocity, ischemia, apoptosis, and release of radical oxygen species (ROS) (Chen et al. 2003). Briefly, initial cell membrane disruption due to mechanical injury leaves the cell permeable to normally impermeant molecules, thus triggering a homeostatic imbalance of ions and other regulated cytosolic molecules. This imbalance leads to alterations in immediate-early gene expression and activation of ROS, apoptotic genes, and intercellular proteases (Chen et al. 2003; McIntosh et al. 1998). Furthermore, the inflammatory response of macrophages and microglia has also been implemented in the deleterious cascade as they release cytotoxic cytokines (e.g., tumor necrosis factor and interleukins) and free oxygen radicals. Not only are these cytokines toxic to neurons, but they also activate the astrogliotic pathway that initiates the formation of the glial scar (Fawcett and Asher 1999). The acute glial scar is comprised of reactive astrocytes, oligodendrocyte precursor cells, microglia, meningeal cells, and macrophages, whereas the chronic glial scar primarily consists of reactive astrocytes (Fawcett and Asher 1999). The initial glial response is elicited in order to wall off the injured region and reestablish the blood brain

barrier. Each of the cell types within the scar releases/expresses molecules that have been found to be both permissive (growth factors and extracellular matrix proteins; ECM) and inhibitory (e.g., chondroitin sulfate proteoglycans) to endogenous regeneration (Busch and Silver 2007; Chen et al. 2003). Therefore, it is apparent that multiple intricate signaling cascades and cellular responses are prevalent in the injured brain, rendering a complex and potentially hostile environment for transplanted cells.

Modeling TBI: Controlled Cortical Impact Injury

Various experimental TBI models have been developed to investigate the associated pathophysiology and test potential therapies; the most common models are the controlled cortical impact (CCI), weight drop, and fluid percussion. The CCI injury imparts a controlled mechanical compression to the cortical surface of the brain. This injury results in an acute physiological response (e.g., cerebral edema, subdural hemotoma, and hemorrhaging) and histopathology consistent with cortical contusion in human TBI (Chen et al. 2003; Dixon et al. 1991; Fujimoto et al. 2004; Unterberg et al. 2004). The advantages of using the CCI model include control over the velocity, depth, duration, and angle of impact. Injury severity has been positively correlated with velocity and depth of impact (Dixon et al. 1991; Fox et al. 1998; Saatman et al. 2006). For this study, the injury severity utilized moderate injury parameters to produce cortical and subcortical damage and sustained sensorimotor and spatial learning deficits (Dixon et al. 1999; Fox et al. 1998; Saatman et al. 2006; Shear et al. 2004). This well-established injury model in the mouse provides a reproducible injury setting to evaluate experimental therapies for TBI.

Current Clinical Therapies

Unfortunately, the current clinical treatments for TBI are very limited. Emergency care primarily addresses the acute physiological responses (e.g., controlling elevations in intracranial pressure and cerebral perfusion pressure) and long-term therapies are largely palliative measures (Nolan 2005). A large number of pharmacological therapies have gone to clinical trials for TBI; however, such treatments either focus on a single signaling cascade or the target spectrum has collateral detrimental effects systemically and have failed in clinical trials (see review (Marklund et al. 2006)). TBI initiates an abundant number of highly complex molecular signaling pathways; thus, a multifaceted therapy is required to attenuate the degenerating injury environment. Other current clinical trials include therapies aimed at hindering the inflammatory response and provide neuroprotective effects, such as acute hypothermia (Adelson et al. 2005; Davies 2005), and early administration of erythropoietin (Grasso et al. 2007), progesterone (Wright et al. 2005), and citicoline (Calatayud Maldonado et al. 1991). Moreover, clinical trials are also evaluating pharmaceutical therapies for post-TBI behavioral issues, such as depression, irritation, and aggression. Sertraline, a selective serotonin reuptake inhibitor, is one example of this treatment that addresses behavioral disorders that persist after a TBI (Fann et al. 2001; Zafonte et al. 2002). Each of these treatment modalities target specific events that occur after injury. Neural transplantation, however, may provide a multifaceted therapeutic approach to target multiple events that occur post-injury and would greatly improve the current state of clinical therapies.

Extracellular Matrix: Laminin, an Integral Protein in the Brain

During neural development, ECM proteins are critical players. Laminin-1 (LN), laminin-10, fibronectin (FN), and collagen-IV (Cn IV) are all ECM proteins that are important to neural signaling and have been associated with cellular survival, adhesion, migration, and differentiation (Chothia and Jones 1997; Freire et al. 2002; Powell and Kleinman 1997). Moreover, recent analysis of the stem cell niche in the adult subependymal layer has identified the co-localization of LN subunits with basic fibroblast growth factor (bFGF) (Kerever et al. 2007; Mercier et al. 2002; Mercier et al. 2003). These findings indicate that the ECM not only provides direct cell support through cell-ECM interactions, but it also sequesters growth factors for neural stem cells (NSC). More specifically, LN has been shown to enhance neurite outgrowth during neurogenesis and neural differentiation and migration of neural stem cell explants (Flanagan et al. 2006; Freire et al. 2002; Kearns et al. 2003; Nakajima et al. 2007; Tate et al. 2004). Further investigation of cell-LN interactions has identified specific receptors on neuronal cells that support and promote neurite outgrowth and cell adhesion, namely $\alpha_1\beta_1$, $\alpha_3\beta_1$, and $\alpha_6\beta_1$ integrins, 67 kDa LN receptor, and 110 kDa LN receptor (Jacques et al. 1998; Leone et al. 2005; Powell and Kleinman 1997; Tate et al. 2004). Therefore, LN is a prominent ECM protein that positively influences neural cell survival, migration, and differentiation and is a candidate protein for incorporation into a NSC-based treatment formulation.

Neural Transplantation

Cell Source

Numerous cell sources are available for neural transplantation; such sources include, but not limited to, embryonic stem (ES) cells, mesenchymal bone marrow stem cells (MSCs), umbilical cord stem cells, and fetal-derived neural stem cells (NSCs). In TBI models, positive function outcomes have been recorded with the majority of these cell types (Lu et al. 2002; Mahmood et al. 2006; Riess et al. 2007; Riess et al. 2002a; Shear et al. 2004). Transplantation of ES cells in TBI models has resulted in tumor formation (Riess et al. 2007); although the propensity of ES to form tumors has been reduced by inducing neural differentiation prior to transplantation (in a degenerating striatum model) (Dihne et al. 2006). The success of MSC transplants has indicated an influence on endogenous host stem cell proliferation, potentially through the release of soluble factors from the MSCs (Mahmood et al. 2004). Moreover, neurospheres comprised of neural stem, progenitor, and precursor cells have the potential to provide critical neural cell-cell contacts in addition to trophic support in an injury environment. Therefore, we chose to use NSCs as the transplant cell type for this study.

Current Limitations

While improved function after neural transplantation has been reported, poor transplant survival potentially limits the maximum potential of this therapy (Bakshi et al. 2005; Boockvar et al. 2005; Kim et al. 2006; Marchionini et al. 2004). More specifically, apoptosis of neural transplantation has been recorded in a variety of injurious and neurodegenerative pathologies (Bakshi et al. 2005; Chen et al. 2002; Emgard et al. 2003; Marchionini et al. 2004). Activation of apoptotic signaling pathways has been detected

as early as 90 minutes after transplantation in Parkinson's model (Emgard et al. 2003) and 24 hrs in a TBI model (Bakshi et al. 2005). Furthermore, a significantly higher percentage of donor cells underwent caspase-mediated apoptosis in the traumatically injured brain compared to transplants delivered to sham brains (Bakshi et al. 2005). Recent studies have demonstrated moderate increases in donor cell survival by pre-incubation with growth factors, co-delivery with ECM molecules, or genetic modifications of the cells to upregulate molecules involved in pro-survival pathways (e.g., growth factors, Bcl-2) (Bakshi et al. 2006; Boockvar et al. 2005; Duan et al. 2000; Marchionini et al. 2003; Sinson et al. 1996; Tate et al. 2002). Therefore, in order to maximize transplant survival, additional pro-survival cues will be necessary to overcome apoptotic signaling in a pathological environment.

Neural Stem Cells

Culture methods for fetal-derived NSCs harvested from the germinal eminence of the developing subventricular zone were developed by Reynolds and Weiss (Reynolds et al. 1992). NSCs in the presence of basic fibroblast growth factor (bFGF) or epidermal growth factor (EGF) maintain a proliferative multipotent progeny. Furthermore, NSCs form clonally derived aggregates or neurospheres (Engstrom et al. 2002). Neurospheres are comprised of heterogeneous cell types with a phenotypic distribution dependent on position within the neurosphere and neurosphere size (Campos et al. 2004; Engstrom et al. 2002; Suslov et al. 2002). Moreover, the phenotypic pattern and co-localization of ECM production is similar to that observed in neural development (Campos et al. 2004). NSC adhesion, migration, and differentiation profiles have been evaluated by culturing

NSC on various ECM proteins (LN, FN, collagen I, and Col IV). Collectively, results from these studies demonstrate increased adhesion and migration on FN and LN substrates, although enhanced neuronal differentiation has been observed on LN only (Kearns et al. 2003; Leone et al. 2005; Tate et al. 2004). Moreover, NSC maintenance and migratory capacity on LN has been shown to be mediated through β_1 integrins (Campos et al. 2004; Flanagan et al. 2006; Jacques et al. 1998; Leone et al. 2005; Tate et al. 2004). Collectively, these studies established a baseline response of NSCs to ECM proteins. Developments in protein immobilization technology have elevated the level of complexity in which ECM proteins and peptide sequences can be presented on 2-D surfaces (Nakajima et al. 2007; Saha et al. 2007). Furthermore, recent *in vitro* studies have evaluated NSC response within 3-D cultures with controlled presentation of the ECM and/or growth factors (Brannvall et al. 2007; Ma et al. 2005; Mahoney and Anseth 2007). These studies demonstrate the potential bioengineered materials hold for evaluating basic biological questions, such as examination of interactions between bioadhesive and soluble factors in the extracellular environment and NSC survival, proliferation, migration, and differentiation.

Biomaterials

Thermoresponsive hydrogels

A select number of thermoresponsive polymers undergo a solution-gelation (sol-gel) phase transition *in situ* due to the difference between ambient room temperatures and physiological temperatures. Thus, a thermoreversible hydrogel system can be exploited to deliver cell- or pharmaceutics-based therapies in a minimally-invasive manner into an

injury-induced lesion cavity. Upon gelation *in situ*, 3-D microenvironment is formed to provide structural support for transplanted cells. Polymeric systems, such as methylcellulose (MC) (Tate et al. 2001), poly(N-isopropylacrylamide) (NiPAAm) (Stile et al. 1999), agarose (Yu and Bellamkonda 2003), and poly(ethylene glycol)-poly(lactic acid)-poly(ethylene glycol) tri-block polymer (Jeong et al. 1997), have been used in several biomedical applications because of this thermoresponsive property. The gelation mechanism for such thermosensitive polymers is through either covalently or physically crosslinked networks. In general, a thermosensitive free radical initiator is necessary to generate covalently crosslinked hydrogel networks, whereas physically crosslinked networks form as a function of secondary intramolecular and intermolecular interactions (Young and Lovell 1991). However, potential cytotoxic effects on the donor cells as well as on the surrounding host tissue from a free radical initiator are a concern when applying this methodology to *in situ* hydrogel for cell delivery (Temenoff et al. 2003). Therefore, a hydrogel, such as MC, based on physical crosslinks may prove to be advantageous, as the need for a secondary crosslinking initiator is eliminated. The gelation mechanism for MC arises from an increase of intramolecular and intermolecular hydrophobic interactions as the temperature increases (Desbrieres et al. 2000; Kobayashi et al. 1999). In peripheral nerve and spinal cord transection models, MC and MC polymer blends have supported neurite outgrowth and improved functional recovery (Gupta et al. 2006; Tsai et al. 2006; Wells et al. 1997). Therefore, MC is a well-established polymer system for neural tissue engineering applications.

"Bioactivation" of Materials: Incorporating Specificity

Development of release systems for growth factor delivery and tethering bioadhesive moieties to non-adhesive polymer scaffolds has been extensively investigated to increase cellular adhesion, survival, and host-implant integration in many physiological systems (see reviews (Boontheekul and Mooney 2003; Hubbell 1999; Lutolf and Hubbell 2005a). For instance, limited cell adhesion has been observed on native MC (Stabenfeldt et al. 2006; Tate et al. 2001); however, tethering LN to MC resulted in increased neuronal adhesion (Stabenfeldt et al. 2006). This technology has also enabled materials to be tailored to specific cell types depending on receptor profiles via incorporation of the appropriate ECM protein. For example, the preferential attachment of neuronal cells in the presence of astrocytes was achieved by tethering a recombinant form of L1, a cell adhesion molecule, to a substrate (Webb et al. 2001). Moreover, studies have shown that the conformation of a tethered or adsorbed bioadhesive motif is dependent on substrate surface chemistry, which ultimately modulates cell adhesion (Garcia et al. 1999; Keselowsky et al. 2003; Michael et al. 2003). Mechanical stiffness is another crucial design parameter that has been shown to influence cell-type specific adhesion and migration. A comparison of astrocyte and neuronal adhesion on substrates with differing stiffness demonstrated that astrocyte spreading was only supported on stiff substrates whereas the threshold for neurite outgrowth was much more compliant (Flanagan et al. 2002; Georges et al. 2006). Although, the relationship between stiffness and ligand density is highly intertwined as astrocyte spreading is observed in Matrigel®, a compliant hydrogel with an abundant amount of the ECM proteins and growth factors (LaPlaca et al. 2005). In summary, the tethering ligands,

surface chemistry, and mechanical strength must harmonize to render a material that supports a specific phenotype.

Neural Tissue Engineering

Neural tissue engineering strategies for both the peripheral and central nervous systems have utilized a range of biomaterials incorporating biochemical cues to ultimately elicit regeneration (see reviews (Lesny et al. 2002; Schmidt and Leach 2003; Willerth and Sakiyama-Elbert 2007)). For example, ECM proteins and neurotrophic growth factors have been incorporated into a material-based system to enhance regenerative capacity from the host tissue in spinal cord injury (Taylor et al. 2004; Tsai et al. 2006). Following peripheral nerve transection, integration of LN within a hydrogel or along the surface of a conduit has been shown to promote functional recovery (Labrador et al. 1998; Yu and Bellamkonda 2003). Moreover, collagen aligned fibrils seeded with Schwann cells have also been shown to improve the regenerative capacity of a transected nerve (Phillips et al. 2005). Collectively, these studies illustrate the growth promoting effect LN and other ECM components have when incorporated into tissue engineered scaffolds.

While similar obstacles are shared across peripheral, spinal, and brain injuries, distinction between the goal of "conduit" tissue engineering (i.e. spinal cord and peripheral nerve) and TBI tissue engineering must be made. Ultimately, conduit tissue engineering aims to elicit host regeneration to restore connection with the distal end of a severed nerve or axon bundle. Whereas the structure of brain is highly complex and organized; the cells lost in TBI potentially received inputs from hundreds of thousands of neurons throughout the brain and cell replacement with tissue engineering strategies will

most likely not recapitulate the original structure. However, if the injurious sequelae of TBI are not blocked, then degeneration will continue. Tissue engineering does have the potential to halt further degeneration and spare host tissue in the traumatically injured brain.

Thesis Objective Outline

The primary objective of this thesis was to develop a methylcellulose-laminin (MC-LN) tissue engineering scaffold for TBI. More specifically, a MC-LN scaffold was optimized to enhance cell transplant survival in neural injury environments. This objective was addresses through the following studies:

1. Optimization of LN tethering chemistry. Chapter 2 and 3 outline two tethering chemistries that were used in this study. The outcome highlighted the importance of tethering chemistry and efficiency on generating a biofunctionalized scaffold.
2. Modulation of ligand density and mechanical properties. Chapter 3 presents the neuronal survival and neurite outgrowth dependence on material stiffness and available ligand.
3. Microenvironment influences NSC fate. Chapter 4 highlights the effect of microenvrionmental cues on NSC survival, migration, and differentiation.
4. Protective effect of MC-LN on NSC survival neural injury environments. Chapter 5 evaluates the influence of co-delivering NSCs with MC-LN into neural injury environments (i.e. *in vitro* injury model and *in vivo* TBI model).

CHAPTER 2: THERMOREVERSIBLE LAMININ-FUNCTIONALIZED HYDROGEL FOR NEURAL TISSUE ENGINEERING

(As published with A. J. García and M.C. LaPlaca in the Journal of Biomedical Materials Research Part A 77A (4): 718-725.)

Abstract

Traumatic injury to the central nervous system triggers cell death and deafferentation, which may activate a cascade of cellular and network disturbances. These events often result in the formation of irregularly shaped lesions comprised of necrotic tissue and/or a fluid-filled cavity. Tissue engineering represents a promising treatment strategy for the injured neural tissue. To facilitate minimally invasive delivery of a tissue engineered system, a thermoreversible polymer is an attractive scaffold candidate. We have developed a bioactive scaffold for neural tissue engineering by tethering laminin-1 (LN) to methylcellulose (MC), a thermoresponsive hydrogel. The base MC chain was oxidized via sodium *m*-periodate to increase MC tethering capacity. Protein immobilization was facilitated by a Schiff base reaction between primary amine groups on LN and the carbonyl groups of the oxidized MC chain. Immunoassays demonstrated tethering of LN at 1.6 ± 0.5 ng of LN per mg of MC. Rheological measurements for different MC-LN constructs indicated MC composition- and MC treatment-dependent effects on solution-gelation transition temperature. Cellular assays with primary rat cortical neurons demonstrated enhanced cell adhesion and viability on LN-functionalized MC compared to base and oxidized MC. This bioadhesive

thermoresponsive scaffold may provide a robust delivery vehicle to injured CNS tissue for neural cell transplantation strategies.

Introduction

Traumatic injury to the central nervous system (CNS) is a significant socioeconomic problem. For instance, traumatic brain injury (TBI) and spinal cord injury (SCI) afflict over 90,000 people each year, and 5.3 million people in the United States are presently living with TBI-related disabilities (2004; Adekoya et al. 2002). Traumatic injury to the CNS evokes deleterious cascades that results in cell death and dysfunction (McIntosh 1994; McIntosh et al. 1996; Siesjo and Wieloch 1988) and ultimately leads to the formation of an irregularly shaped lesion cavity (Chen et al. 2003; Sutton et al. 1993). The inherent regenerative capabilities of the adult CNS are limited, and more importantly, traumatic injury to the CNS generates a complex molecular environment comprised of both inhibitory (e.g., chondroitin sulfate proteoglycans) and permissive (e.g., growth factors) molecules to endogenous regeneration (Chen et al. 2003). Therefore, therapeutic strategies aiming to enhance and restore regenerative potential represent promising treatment modalities. The complex lesion cavity creates a significant structural problem for existing tissue engineered scaffolds (e.g., poly(N-2-(hydroxypropyl) methacrylamide) (Woerly et al. 1999), poly(lactic acid) (PLLA) (Yang et al. 2004), and poly(2-hydroxylethyl methacrylate-co-2-aminoethyl methacrylate) (Flynn et al. 2003)), which generally require invasive surgical techniques for implantation and do not conform to the cavity shape. Consequently, research efforts have focused on thermoresponsive polymeric systems such as poly(N-isopropylacrylamide) (PNIPAAm) (Stile et al. 1999), agarose (Yu and Bellamkonda 2003), and poly(ethylene

glycol) (PEG)-PLLA-PEG tri-block polymer (Jeong et al. 1997). These thermoresponsive polymers undergo solution-gelation (sol-gel) transitions that facilitate a minimally invasive delivery due to *in situ* gelation mechanisms that occur from inherent differences between ambient room and physiological temperatures. Thus, a thermoresponsive hydrogel can be injected into a CNS lesion cavity in a minimally invasive manner to deliver cell- or pharmaceutics-based therapies.

Motivated by the potential advantages of thermosensitive polymer-based scaffolds, this study focused on developing a laminin-1 (LN)-functionalized methylcellulose (MC) hydrogel for neural tissue engineering applications. The gelation mechanism for MC arises from an increase in intra- and inter-molecular hydrophobic interactions as the temperature increases (Desbrieres et al. 2000; Kobayashi et al. 1999). MC exhibits minimal inflammatory reactions following implantation into a TBI lesion cavity (Tate et al. 2001) and within a conduit placed in a peripheral nerve defect (Wells et al. 1997). In addition, MC has also been investigated as a delivery agent for intraoptical (Kumar et al. 1994) and oral pharmaceutic therapies (Bussemer et al. 2003). Furthermore, MC displays limited protein adsorption and neuronal cellular adhesion (Tate et al. 2001), indicating that MC is a relatively non-bioactive hydrogel that requires immobilization of biological moieties along the polymer chain backbone to promote cell adhesion.

Tethering of protein or bioactive peptide sequences to non-adhesive polymer scaffolds has been extensively investigated to increase cellular adhesion, survival, and host-implant integration in various tissue environments (see Review (Lutolf and Hubbell 2005b)). For example, conjugation of the fibronectin-derived sequence arginine-glycine-

aspartic acid (RGD) to PEG (Dai et al. 1994; Hern and Hubbell 1998) and NIPAAm (Na and Park 2000; Smith et al. 2003) hydrogels and PLLA scaffolds (Quirk et al. 2001), TGF-β to PEG (Mann et al. 2001) hydrogels, and LN-derived peptides to fibrin (Schense et al. 2000), conveys biofunctionality to these synthetic supports.

Consequently, we hypothesized that covalent immobilization of an extracellular matrix (ECM) protein to the MC hydrogel will enable the presentation of bioactive signals essential to neuronal cell adhesion, survival, and migration. We selected LN as a candidate bioadhesive ligand, as this protein regulates neuronal cellular survival, adhesion, migration, and differentiation in the CNS (Chothia and Jones 1997; Freire et al. 2002; Powell and Kleinman 1997). When immobilized onto polymeric hydrogels, LN elicits regenerative responses in the sciatic nerve gap (Labrador et al. 1998; Yu and Bellamkonda 2003). By tethering LN to MC, we have developed a thermosensitive bioactive scaffold for neural tissue engineering applications. This study focused on the development and material characterization of this LN-functionalized MC hydrogel.

Methods

Conjugation of LN to MC

MC (M_w~65,000; Sigma Aldrich, St. Louis, MO) was oxidized via a Malaprade-type reaction facilitated by 20 mM sodium m-periodate (Sigma) in 100 mM sodium acetate buffer, pH 5.5 (Margutti et al. 2002). The reaction was performed at room temperature in the absence of light for 4 hours and was subsequently quenched with 150 mM glycerol (Sigma). After dialysis against 100 mM sodium acetate buffer, the oxidized MC (OXMC) solution underwent another dialysis against deionized H_2O (dH_2O). The OXMC in dH_2O was then lyophilized and reconstituted to a desired concentration in phosphate buffered saline (PBS; pH 7.4; Invitrogen, Carlsbad, CA). Samples were then incubated for 15 hours with dithiothreitol-reduced LN from Engelbreth-Holm-Swarm murine sarcoma (Invitrogen) to generate OXMC-LN. Negative controls included base MC and OXMC incubated with PBS and are referred to as MC and OXMC respectively. Upon completion of the conjugation scheme, unconjugated LN was rinsed from samples with PBS supplemented with 0.1% (v/v) Tween 20 (Sigma) followed by 4 rinses with PBS.

Infrared (IR) Spectroscopy

Solid phase IR spectroscopy (Thermo Nicolet Nexus 470 FT-IR, Madison, WI) was performed on lyophilized samples of MC (n=2) and OXMC (n=2) compressed into KBr prisms to verify the presence of oxidized groups on MC. The IR spectrum of each sample was measured from 4000 to 500 cm^{-1}. Band assignments were based on previous reports of MC (Zhbankov 1966) and OXMC (El-Khatib 2002; Varma and Kulkarni 2002) spectra.

Quantification of Tethered Ligand

Conjugation of LN to OXMC was quantified via a dot blot immunoassay. Briefly, 1.5 μl of each sample (OXMC-LN, OXMC, MC+LN, and MC), serial dilutions of each sample, and LN standards (45 pg to 1.5 ng) were blotted onto a nitrocellulose membrane. The membrane was blocked with a Tris-HCl buffered solution (TBS; Sigma) supplemented with 5% bovine serum albumin (BSA; Sigma) and 0.05% Tween 20 (Sigma) for 1.5 hours. The membrane was then incubated in polyclonal rabbit anti-laminin antibody (0.6 μg/ml; Sigma) in TBS-Tween with 0.1% BSA for 1 hour, followed by incubation in alkaline-phosphatase conjugated goat anti-rabbit secondary antibody (60 ng/ml; Chemicon, Temecula, CA) for 1 hour. After a 5 minute incubation in ECF substrate (Amersham Biosciences, Piscataway, NJ), fluorescence intensities were measured with a FLA-3000 Fuji Imager Analyzer (FUJIFILM Medical Systems USA, Stamford, CT). Fluorescent intensities were measured by image analysis with Photo-Paint 9 (Corel Corporation, Dallas, TX).

Thermal and Dynamic Rheological Measurements

Rheological analyses were performed on a Bohlin CVO rheometer (Bohlin, East Brunswick, NJ) with a parallel plate configuration. A temperature sweep from 22-46°C (0.5°C/min) under constant frequency (1 rad/sec) and low amplitude stress was performed on each sample group (MC, OXMC, and OXMC-LN; n=4-7). The lower critical solution temperature (LCST) was determined by the intersection of the loss (G") and storage (G') moduli (Kobayashi et al. 1999). To examine the mechanical integrity of the MC hydrogels at physiological temperatures, a frequency sweep from 0.05-10 Hz was

performed on each sample group (MC, OXMC, and OXMC-LN; n=6-8) under constant low amplitude stress upon equilibration to 37°C.

Cortical Neuron Isolation and Culture

Cortices from embryonic day 18 (E18) Sasco Sprague-Dawley rats were dissected and dissociated according to Georgia Institute of Technology IACUC-approved protocols. This well-established protocol was modified from Brewer (Brewer 1997) and optimized for cortical neuron cultures. Briefly, cortices were extracted from E18 fetuses, rinsed twice with Hank's Balanced Salt Solution (HBSS; Invitrogen), and placed in a hibernate solution consisting of L-15 supplemented with 2% B-27 (Invitrogen). Cortices were then stored at 4°C until dissociation and plating (maximum of 7 days after dissection). Dissociation of the cortical tissue began with rinsing the tissue with cold HBSS thrice, then incubated in trypsin (0.25%) + EDTA (1 mM; Invitrogen) at 37°C for 10 minutes. Following removal of trypsin, cortices were rinsed twice with HBSS then placed in HBSS supplemented with DNase (0.15 mg/ml; Sigma) and vortexed for 30 seconds. Remaining tissue fragments were removed and the resulting cell suspension was centrifuged at 180g for 3 minutes. The cell pellet was resuspended in Neurobasal medium supplemented with 2% B-27 and 0.5 mM L-glutamine (neuronal medium; Invitrogen) and placed on ice until the cells were plated. Cells were plated within 30 minutes of dissociation with no reduction in viability, as measured with a standard trypan blue exclusion viability assay.

Cell Attachment and Viability Assays

Cell attachment to native and modified MC was analyzed using a wash assay. Bovine serum albumin (BSA; Invitrogen) was tethered to OXMC to produce a negative control group (OXMC-BSA), as BSA contains no known bioadhesive sequences. OXMC-BSA was prepared according to the OXMC-LN conjugation method. Surfaces of a 24-well tissue culture plate were coated with each sample (OXMC-LN, OXMC-BSA, OXMC, MC, MC+BSA and MC+LN) to create a 50 μm thick hydrogel layer. Samples were then placed in a tissue culture incubator for 30 minutes prior to cell plating to ensure gelation of the hydrogel. Neurons were plated on top of each gel substrate (n=3 per substrate) at a density of $1x10^5$ cells/cm^2 in 500 μl of neuronal medium and maintained in a tissue culture incubator (37ºC, 5% CO_2, 95% relative humidity). After medium exchange at one day post-plating, phase-contrast micrographs (3 images per well) were captured with a Nikon TE-300 (Nikon, Japan) inverted microscope equipped with a DKC5T5/DMC Sony digital camera (Sony, Japan). Images were analyzed for both the number of cell clusters and area of attached cells on each substrate using Image-Pro Plus software (Media Cybernetics, Silver Spring, MD).

Viability of cortical neurons plated within the MC hydrogels was also examined. Neurons were harvested and dissociated according to the protocol outlined above. Three-dimensional (3-D) cell/scaffold constructs were prepared by combining dissociated primary cortical neurons (10^5 cells/mm^3) with liquid MC solution (4°C). After gentle mixing, each construct was cast in a sterilized custom-made elastomer (Sylgard 184 and 186; Dow Corning, Midland, MI) chamber mounted on a glass coverslip and allowed to gel at 37°C. Neuronal medium was then added atop of the gelled construct. Constructs

were maintained in a tissue culture incubator (37°C, 5% CO_2, 95% relative humidity). At 1 day post-plating, viability was assessed with a viability assay (calcein AM and ethidium homodimer (EthD-1); Sigma). Briefly, constructs were rinsed with PBS and then incubated with PBS containing 2 μM calcein AM and 4 μM EthD-1 for 30 minutes. Upon removal of the calcein AM/EthD-1 solution and subsequent rinsing, cellular viability was examined with a confocal laser scanning microscope (LSM 510; Zeiss, Thornwood, NY). Three random 100 μm thick z-stacks for each construct were captured and analyzed with LSM Image Browser (Zeiss) to record viability.

Data Analysis

Data are presented as one standard deviation from the mean. Results were analyzed by one-way ANOVA. If treatments were determined to be significant, pair-wise comparisons were performed using Tukey's test. A 95% confidence level was considered significant.

Results

Oxidation of MC Facilitates LN Tethering

Our strategy to functionalize MC with LN involved a Schiff base reaction between primary amine groups in LN and carbonyl groups on MC polymer chain (Figure 2.1). Native MC contains relatively few accessible carbonyl groups, and therefore does not support efficient protein tethering. To generate a reactive MC support, MC was oxidized with sodium m-periodate, which yields carbonyl groups via a Malaprade-type reaction that preferentially breaks the C_2-C_3 bond of vicinal hydroxyl groups to form a 2,3-dialdehyde (Figure 2.1, step 1). IR spectroscopy verified the formation of dialdehyde groups after oxidation of MC (Figure 2.2). Both the reduction of the alcohol band at 3460 cm^{-1} and the emergence of a carbonyl band at 1720 cm^{-1} on the OXMC spectra confirmed partial oxidation of MC (El-Khatib 2002; Zhbankov 1966). Further examination of the degree of oxidation on the MC chain was performed with a Lucifer yellow-CH assay (data not shown) derived from protocols that characterized the degree of periodate oxidation on carbohydrate moieties (Keener et al. 1994; Wolfe and Hage 1995). Our quantification revealed a reproducible degree of oxidation on the MC chain. Collectively, these results indicate that this methodology reproducibly produces an oxidized MC support.

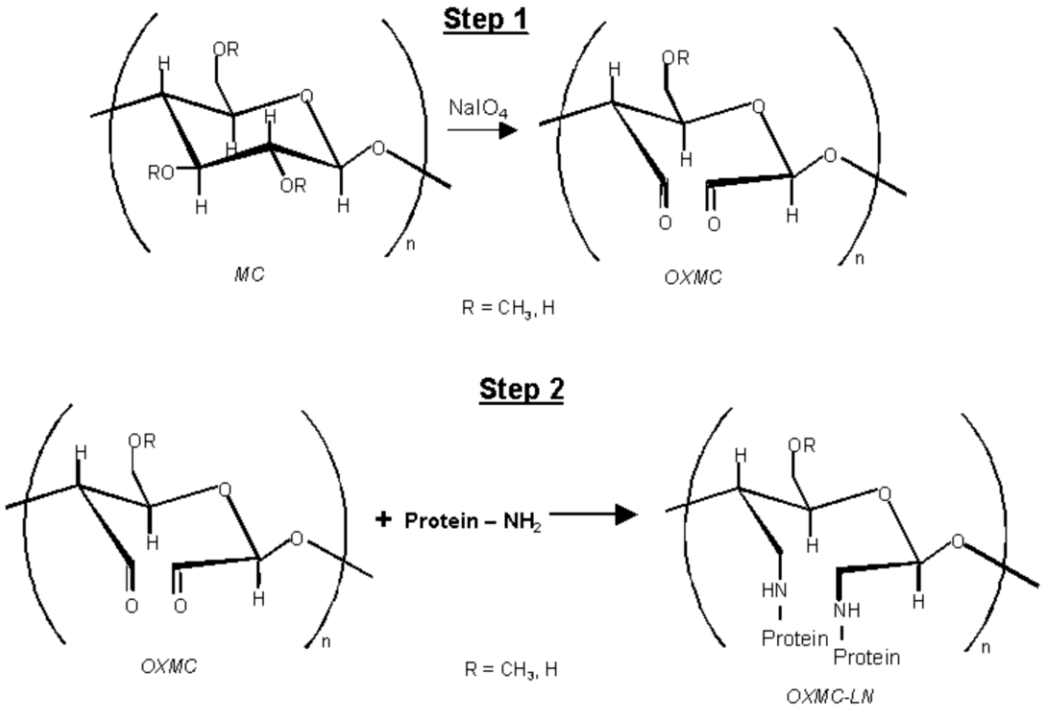

Figure 2.1 – Scheme for tethering LN to MC. Step 1: Sodium *m*-periodate ($NaIO_4$) oxidation of MC via a Malaprade-type reaction, which breaks the C_2-C_3 bond of vicinal hydroxyl groups to form a 2,3-dialdehyde structure. Step 2: Aldehyde groups of OXMC were reacted directly with primary amine groups of LN via Schiff base linkage.

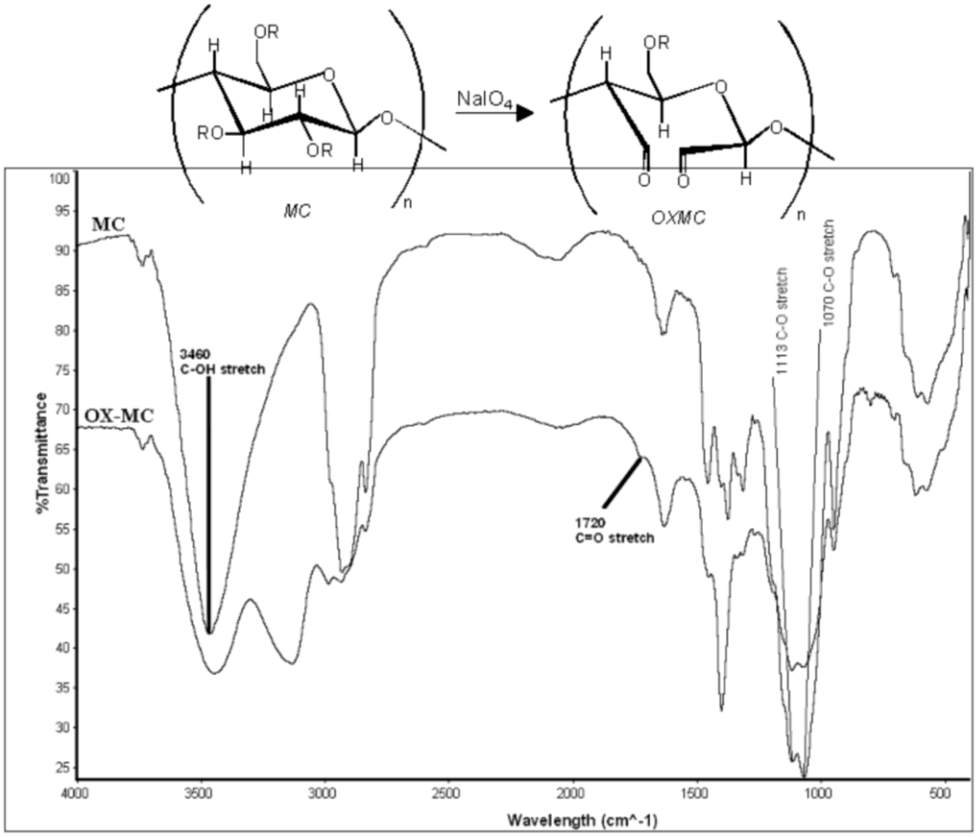

Figure 2.2 – Oxidization of MC. The IR spectra for MC and OXMC highlights the reduction of the C-OH stretch at 3460 cm^{-1} and the emergence of a carbonyl peak at 1720 cm^{-1} of OXMC compared to MC, which are key indicators of a partially oxidized MC chain.

To produce functionalized MC, oxidized MC was incubated with dithiothreitol-reduced LN. Following incubation, samples were extensively rinsed in buffer to remove unconjugated LN, blotted on a nitrocellulose membrane, and immunoprobed for LN with a polyclonal antibody. Significant amounts of LN were detected on the OXMC-LN sample compared to MC and OXMC groups (Figure 2.3), thus confirming the presence of an OXMC-LN conjugate. No fluorescence was detected in samples of MC mixed with LN (MC+LN); therefore the rinsing procedure successfully removed unbound LN from the hydrogel. Non-specific antibody binding was not observed with the negative OXMC control. Quantification of the LN content of OXMC-LN revealed 1.6 ± 0.5 ng of LN per mg of OXMC.

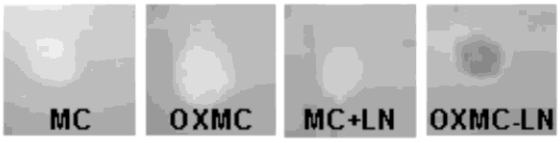

Figure 2.3 – LN tethered to OXMC. The absence of fluorescence in MC (A), OXMC (B), and MC+LN (C) indicated a deficiency of LN in these samples. Conversely, positive fluorescence was detected in OXMC-LN (D) indicating immobilization of LN to OXMC.

Material Properties of MC Depend on Conjugation State

We define the lower critical solution temperature (LCST), i.e. the characteristic temperature for solution-to-gel transition, as the temperature at which the elastic modulus (G') crosses over the viscous modulus (G") (Kobayashi et al. 1999) (Figure 2.4A). The rheological behavior as a function of temperature for MC, OXMC, and OXMC-LN at 5% and 7% (w/v) concentration in PBS is presented in Figure 2.4B. For minimally invasive delivery of MC, it is desirable for the LCST not to exceed physiological temperature (37°C) to ensure sol-to-gel transition following delivery. MC processing conditions altered the LCST as demonstrated in Figure 2.4 and Table 2.1. For example, at 5% (w/v) concentration the LCST for MC and OXMC were 33.5 ± 0.5°C and 36.15 ± 1.4°C, respectively. We attribute the increase in LCST to a reduction in hydrophobic interactions responsible for gelation as a result of oxidation of the MC C_2-C_3 vicinal bonds. Functionalization of MC with LN further increased the LCST as observed with 7% OXMC-LN (33.2 ± 0.9 ºC) compared to 7% OXMC (30.0 ± 0.9 ºC), possibly through disruptions of hydrophobic interactions among MC chains. The LCST of MC and its derivatives was also dependent on polymer concentration as decreasing polymer concentration from 7% to 5% increased the LCST.

Additional effects from polymer processing and modifications of the polymer concentration on the mechanical properties of MC and its derivatives were evaluated with dynamic rheological testing. Samples were exposed to oscillatory frequency sweeps (0.05–10 Hz) at 37ºC under low amplitude shear strain. An increase in the complex modulus, defined as the ratio of the complex stress to the complex strain, was observed by increasing the polymer concentration from 5% to 7% (Table 2.1). Interestingly,

although an alteration of LCST was observed after polymer processing, no significant differences in the complex, storage, or loss moduli were observed between MC, OXMC, and OXMC-LN after samples were allowed to equilibrate at 37ºC (Table 2.1).

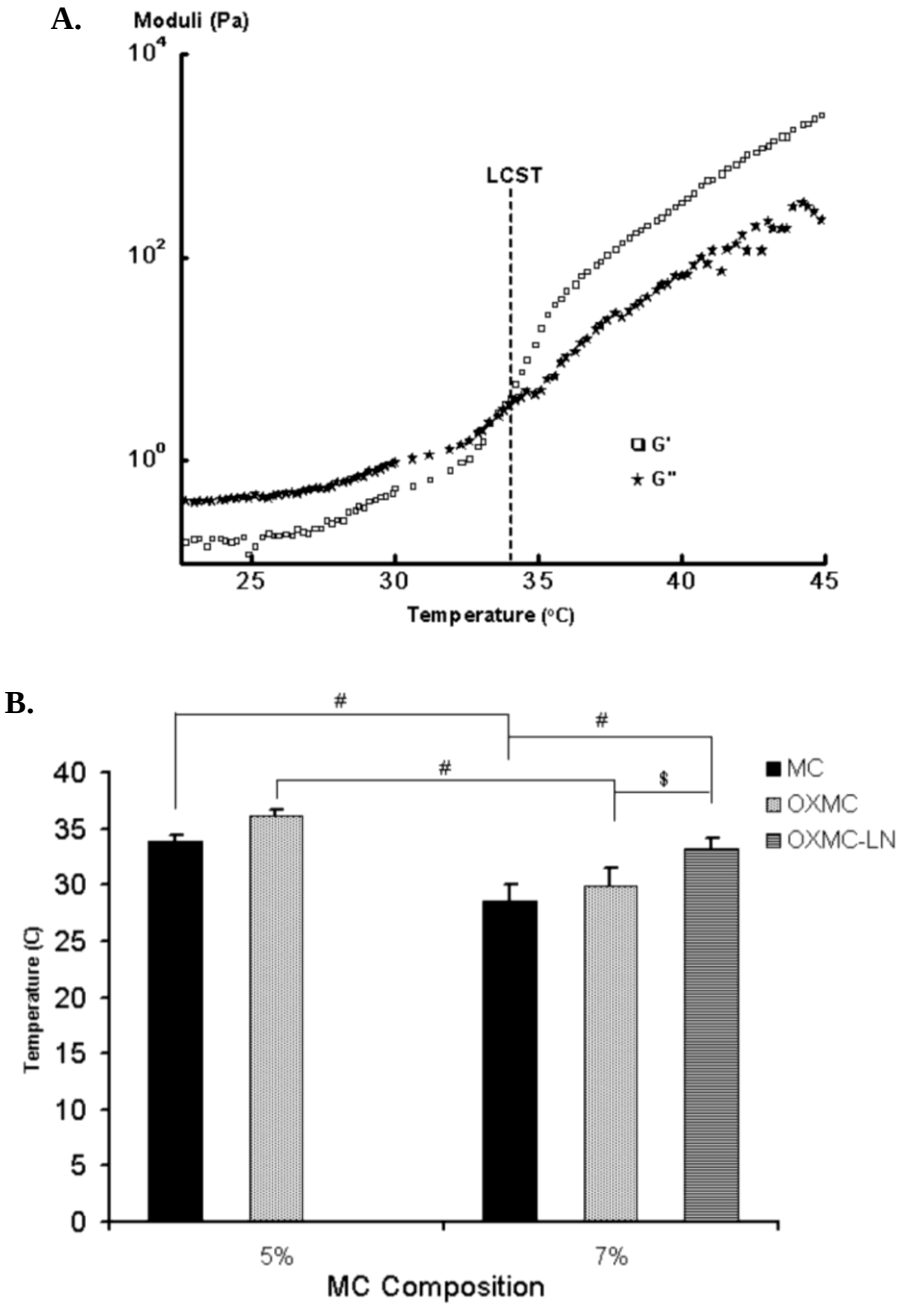

Figure 2.4 – LCST for MC modifications. (A) The LCST, marked on the figure with a dashed line, was determined as the point in which the storage modulus (G') dominates the loss modulus (G"). This plot is representative of the data collected from a 5% MC sample. (B) Gelation temperature of 5% MC was 33.5 ± 0.5°C and OXMC was 36.1 ± 1.4°C. The gelation temperature of 7% MC was 28.6 ± 1.5°C, OXMC was 29.9 ± 2.0°C, and OXMC-LN was 33.2 ±,0.9°C. Error bars represent one standard deviation from the mean. # indicates $p < 0.01$ and $ indicates $p < 0.05$.

Table 2.1 – Viscoelastic material properties of MC and its derivatives. The LCST was measured via thermal rheological tests, while the complex, elastic, and viscous moduli were measured after gelation at 37°C with a dynamic oscillatory frequency sweep. The moduli reported in this table correlate with an oscillatory frequency of 0.106 Hz. Comparison of the moduli reveled a significant statistical difference between samples of differing concentrations (i.e., 5% MC versus 7% MC).

Sample Type	**LCST (°C)**	**Elastic Modulus at 37°C (G′, Pa)**	**Viscous Modulus at 37°C (G″, Pa)**	**Complex Modulus at 37°C (G*, Pa)**
5% MC	33.5 ± 0.5	76.7 ± 18.9	19.0 ± 5.7	79.0 ± 19.7
5% OXMC	36.2 ± 1.4	112.5 ± 19.3	26.3 ± 9.2	115.6 ± 20.7
5% OXMC-LN	-	91.9 ± 14.8	20.4 ± 4.7	94.1 ± 15.4
7% MC	28.6 ± 1.5	139.9 ± 27.6	21.2 ± 4.3	141.5 ± 27.8
7% OXMC	30.0 ± 2.0	122.5 ± 38.6	17.9 ± 5.4	123.9 ± 38.5
7% OXMC-LN	33.2 ± 0.9	153.8 ± 32.3	24.4 ± 6.9	155.9 ± 31.8

LN-Functionalized MC Supports Neuronal Cell Attachment and Survival

The biofunctionality of MC and its derivatives was evaluated with both primary cortical neuron attachment and viability assays. Albumin-conjugated MC (OXMC-BSA) was included as a negative control for protein-functionalized MC as BSA does not support cell adhesion. At one day post-plating, primary neurons exhibited higher levels of attachment, in terms of number of cell clusters (data not shown) and total cell area (Figure 2.5), on OXMC-LN gels compared to OXMC-BSA, OXMC, MC+LN, MC+BSA, and base MC. The higher level of neuronal cell adhesion on OXMC-LN was attributed to functional immobilized LN.

Cell viability of the 3-D cell/MC constructs was evaluated at 1 day post-plating via a viability assay that labels live cells with a green stain (calcein AM) and dead cells with a red stain (EthD-1). Consistent with the attachment results, OXMC-LN supported significantly higher levels of cell survival compared to OXMC, MC, and MC+LN (Figure 2.6). Notably, the sample group with soluble LN (MC+LN) did not elicit enhanced survival, indicating a requirement for tethered LN. Taken together, these results demonstrate that tethering LN to the MC polymer chain enhances primary neural cell attachment and survival. The scope of this study was to examine the acute cellular response within LN-functionalized MC hydrogels; future studies will include evaluation of neuronal function at longer time points.

Cortical neurons plated within Matrigel® (2mg/ml; BD Sciences) elicited significantly higher viability than OXMC-LN at one day (data not shown). Although Matrigel® is a conventional matrix for in vitro 3D cell plating, a comparison between

OXMC-LN and this matrix is invalid due to the vast difference in ECM protein, growth factor, and cytokine composition.

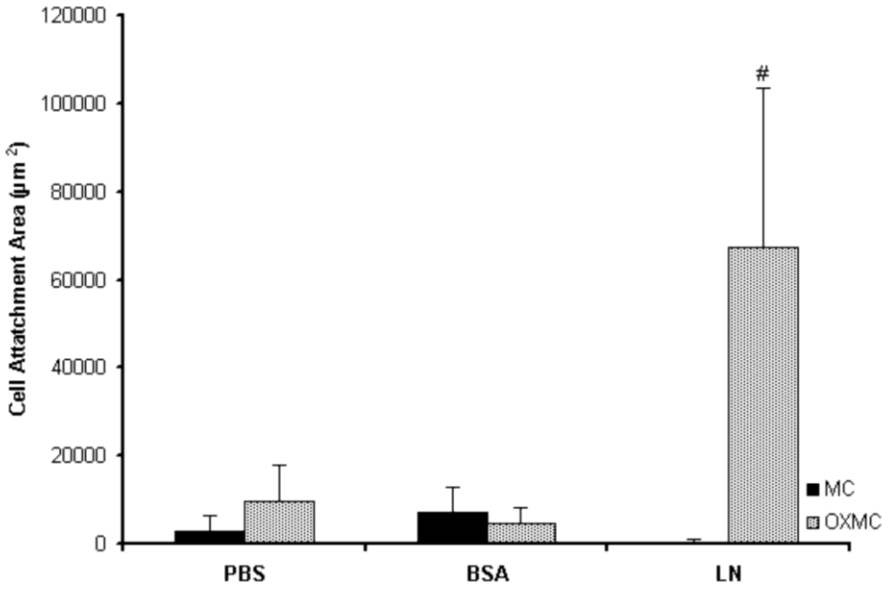

Figure 2.5 – Attachment of cortical neurons to MC scaffolds. A significant increase in cell attachment area was observed on OXMC-LN compared to the MC, OXMC, MC+BSA, OXMC-BSA, and MC+LN groups, which were not statistically different from each other. Error bars represent one standard deviation from the mean. # indicates $p < 0.01$.

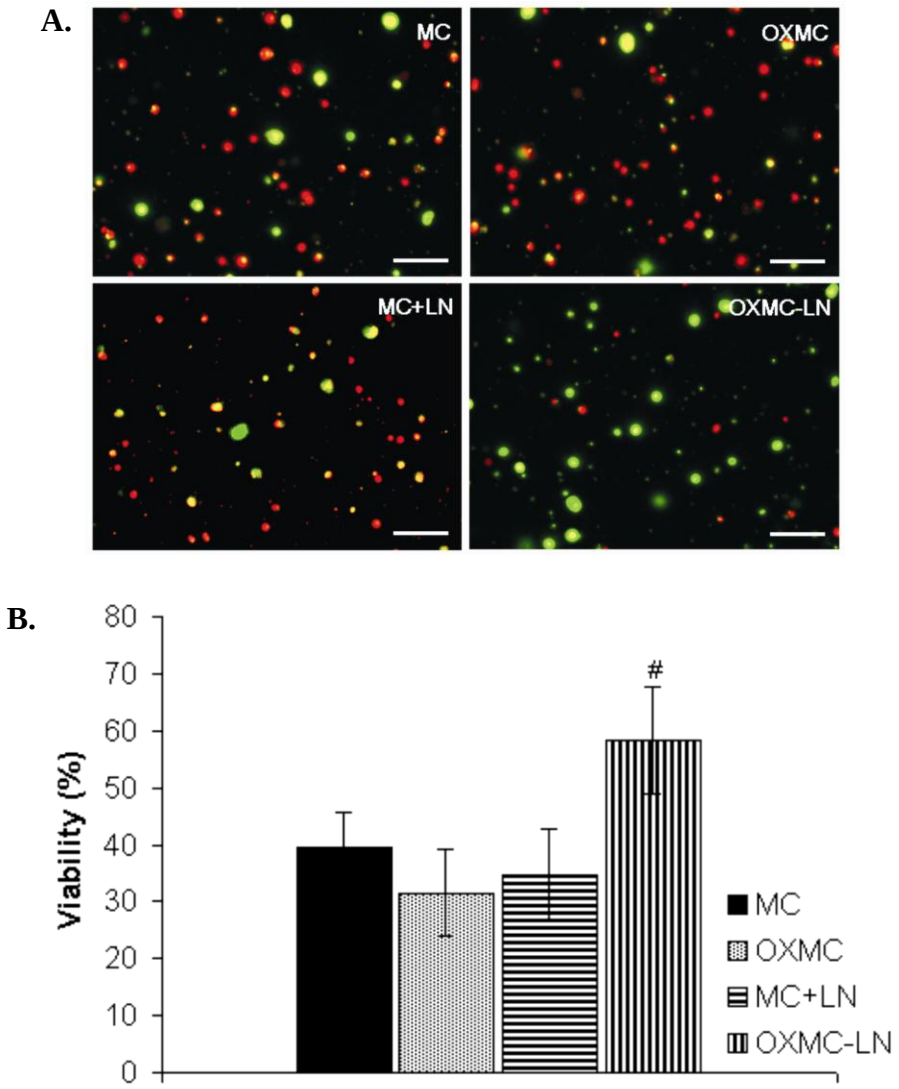

Figure 2.6 – Viability of cortical neurons plated within MC scaffolds. (A) Representative micrograph projections from 100 μm thick confocal scans of 3-D neuronal cultures in MC, OXMC, MC+LN, and OXMC-LN at one day post-plating. Each column represents one confocal projection in which calcein-AM (live) staining is shown in the top panel and ethidium homodimer (EthD-1) staining (dead) is shown in the bottom panel. Fluorescent intensities were converted to grey scale for each image. Scale bar = 50 μm. (B) A significant increase in cell viability was observed with OXMC-LN compared to MC, OXMC, and MC+LN, which were not statistically different from each other. Error bars represent one standard deviation from the mean. # indicates $p < 0.01$.

Discussion

The present study focused on the development of bioactive, thermoresponsive MC hydrogel to deliver cells and therapeutics to the injured CNS. We have validated a method to chemically modify MC in order to tether LN, thereby rendering a thermoresponsive bioactive scaffold for neural tissue engineering applications. Oxidation via a sodium *m*-periodate reaction allows for unique control over the oxidation site on the MC chain as this malaprade-type reaction breaks only the C_2-C_3 bond of vicinal hydroxyl groups to form a 2,3-dialdehyde without significant side reactions (Figure 2.1) (Margutti et al. 2002; Nevell 1963; Varma and Chavan 1995). An attractive property of MC is that the hydrogel is stabilized by a network of physical crosslinks. These physical crosslinks arise from secondary intramolecular and intermolecular hydrophobic interactions. This type of network obviates the need for a free radical initiator that is necessary for many chemically crosslinked hydrogels. Potential cytotoxic effects from a free radical initiator on donor cells as well as the surrounding host tissue has been a concern for chemically crosslinked hydrogel *in situ* formation (Temenoff et al. 2003).

The thermoresponsive nature of MC also affords a conformal scaffold with minimally invasive delivery capabilities. This is particularly important in the treatment of trauma to the CNS, as the resulting irregularly shaped lesion cavity poses structural and integration problems for pre-formed tissue-engineered constructs. The LCST, a characteristic parameter of the sol-gel transformation, is an important component in the design of minimally invasive scaffolds, as it should be set below 37°C in order to ensure transformation into a gelled conformal construct following delivery. Another key criteria for this minimally invasive scaffold is the viscosity of the MC solution at temperatures

below the LCST. A bioactive MC scaffold for future *in vivo* applications will be injected via a small gauge needle at a temperature below the LCST. Therefore, preliminary simulations of dispensing various MC polymer solutions (4-8%) through a small gauge needle and syringe were completed to determine an appropriate MC concentration as a starting point. The range of concentrations were selected based on previous examination of the cytocompatibility of MC polymer concentrations that ranged from 4% to 8% in DPBS, in which no adverse affect on viability of both primary cortical astrocytes and neurons was observed at 1 and 7 days (Tate et al. 2001). Based on the preliminary observations for the LCST and viscosity requirements, a 5% MC concentration was selected as a starting point. As shown in Figure 2.4B, the LCST of the MC hydrogel was dependent on MC processing and concentration. For the MC system described here, the LCST of the hydrogel was modified to an appropriate temperature range by increasing the polymer concentration from 5% to 7%. Additionally, the mechanical integrity of the MC hydrogels after gelation at physiologic temperature was influenced only by modification of the polymer concentration. Variation of the average polymer chain length, degrees of substitution (e.g., methyl groups for hydrogen) along the chain, and ionic strength of the solvent represent alternative methods to modify the LCST and mechanical integrity of the resulting hydrogel.

Swelling and degradation properties of the MC hydrogel are additional fundamental parameters that could affect cellular activity. While these properties of each specific hydrogel formulation was not investigated in this study, *in vitro* swelling and degradation data of 2% and 5% MC has been previously published (Tate et al. 2001). The maximum swollen volume of each MC concentration was similar (150-160%),

whereas the rate of swelling differed, with the 2% MC reaching the maximum swollen state at 1 day and the 5% at 10 days (Tate et al. 2001). Degradation for both 2% and 5% hydrogels at 1 day was between 15-30% of the initial polymer mass and were not statistically different from each other (Tate et al. 2001). For this study, each MC sample group used for the *in vitro* cellular assays was of the same polymer concentration. Therefore, variations of the hydrogel degradation and swelling properties would have minimal effect on the cellular assays.

In order to develop a MC-based scaffold for cell therapeutics, the MC hydrogel was functionalized with adhesive motifs to support neuronal cell adhesion and survival. Tethering of LN, an ECM component critical to neuronal cell activities, promoted enhanced primary cortical neuron attachment and survival compared to unfunctionalized supports. The improvements in cellular activities following immobilization of a bioadhesive component are in excellent agreement with a large body of literature (Li and Kao 2003; O'Connor et al. 2001; Shin et al. 2002; Silva et al. 2004). Biochemical cues such as ECM proteins, peptide sequences (Schense et al. 2000), and neurotrophic growth factors (Taylor et al. 2004) have been incorporated into synthetic and natural hydrogel systems to enhance regenerative capacity from the host tissue. For instance, the importance of integrating cellular adhesion moieties is highlighted in sciatic nerve gap models for the peripheral nervous system, in which nerve conduits containing LN or LN-functionalized hydrogels promoted functional recovery (Labrador et al. 1998; Yu and Bellamkonda 2003). Recently, the combination a LN-derived peptide IKVAV and a polymeric scaffold has been utilized to differentiate neural progenitor cells into neurons and glia for neural tissue engineering applications (Silva et al. 2004). Future studies will

evaluate the capacity of the LN-functionalized MC scaffold to promote neural regeneration in both the peripheral and central nervous systems.

Conclusions

A LN-functionalized thermoresponsive scaffold was engineered to support primary neuronal cell attachment and survival. This bioactive hydrogel may provide a versatile delivery vehicle for cells and pharmacological agents for the treatment of CNS injury.

Acknowledgements

The authors acknowledge support from the National Institutes of Health (R01 EB-001014) and the NSF-sponsored Georgia Tech/Emory Center for the Engineering of Living Tissues (EEC-9731643). The authors thank R.V. Bellamkonda, M.E. Levenston, J.R. Capadona, D.K. Cullen, R.K. Riebesell, and C.G. Wilson for helpful discussions and technical assistance.

CHAPTER 3: INTERACTIONS BETWEEN HYDROGEL RIGIDITY AND LIGAND TETHERING DENSITY INFLUENCE NEURONAL VIABILITY AND NEURITE OUTGROWTH

Abstract

There is a need for functionalized substrates for neural tissue engineering. We have utilized and characterized a thermoreversible polymer, methylcellulose (MC), coupled to laminin-1 (MC-x-LN) across a range of substrate rigidity and ligand densities. LN was tethered MC to generate a bioactive matrix with controlled adhesive moieties in order to evaluate neuronal viability and neurite outgrowth.. The mechanical properties of MC hydrogels were varied by altering MC polymer chain length and concentration; the complex modulus increased concurrently with increases in MC chain length and/or concentration (complex modulus range: 80 Pa to 400 Pa). Neurite outgrowth from primary cortical neurons plated in 3-D was observed only in the most rigid MC hydrogels. Moreover, outgrowth was significantly amplified when LN was tethered to MC. Subsequently, we investigated the effect of varying LN while maintaining a constant MC formulation on primary cortical neuron viability and outgrowth. A dose dependent response was observed for neuronal viability and neurite outgrowth, where the peak neurite outgrowth was observed with highest LN density. Collectively, these data demonstrate the complex interactions between material compliance and bioactive ligand concentrations and can be used to design tailor bioengineered matrices.

Introduction

Multiple factors influence cellular adhesion and migration on a natural or synthetic supports, including the physical properties and density of adhesive ligands. Non-fouling materials (e.g., polyethylene glycol, dextatran, methylcellulose hydrogels) provide a backbone to link specific biological motifs to control cellular adhesion, migration, and infiltration (Bellamkonda et al. 1995a; Dai et al. 1994; Hern and Hubbell 1998; Mahoney and Anseth 2006; Massia and Stark 2001; Stabenfeldt et al. 2006; Yu et al. 1999). With many of these polymeric substrates, control over the substrate rigidity is possible through modifications of the polymeric network properties. Consequently, researchers have studied the relationship of network structure and substrate rigidity to cell adhesion, migration, and spreading (Gray et al. 2003; Jiang et al. 2006; Yeung et al. 2005). Among neural phenotypes specifically, neurite outgrowth has been directly related to substrate compliance (Balgude et al. 2001; Flanagan et al. 2002; Georges et al. 2006; Willits and Skornia 2004), in which less rigid substrates support longer neurite compared to more rigid material. In addition to substrate, appropriate ligand presentation and density is crucial for cell spreading, migration, and/or neurite outgrowth (Cullen et al. 2007a; Jiang et al. 2006; Leach et al. 2007; O'Connor et al. 2001; Yeung et al. 2005).

Three-dimensional neurite outgrowth *in vitro* has been evaluated in a number of hydrogel matrices, in which the polymeric network structure and mechanical properties are dependent upon the organization of the polymer chains, polymer chain length, concentration, and ionic strength of the solvent. Establishing a polymeric formulation with mechanical properties that elicits maximal neurite outgrowth is crucial for developing therapeutic materials for *in vivo* applications. Methylcellulose (MC) is one

such polymer that belongs to a class of thermoreversible polymers with a sol-gel phase transition at temperatures above a lower critical solution temperature. As temperature rises, polymer chains become physically entangled due to entropic alterations that displace water molecules surrounding MC chains, thus permitting hydrophobic interactions between the MC side groups (Desbrieres et al. 2000; Hirrien et al. 1998). This property is particularly attractive for *in vivo* applications as MC can be delivered as liquid in a minimally invasive manner, then gel *in situ* (Tate et al. 2001). In addition, MC has been functionalized with the extracellular matrix protein (ECM) laminin-1 (LN), demonstrating the ability generate biofunctionalized MC (Stabenfeldt et al. 2006). Therefore, MC presents itself as suitable a matrix for both *in vivo* implantation applications and *in vitro* studies to evaluate neuronal response to alterations in stiffness and ligand density.

Numerous cell receptors interact with the 800kDa heterotrimeric protein LN, stimulating cell signaling pathways for adhesion, neuritogenesis, and survival (See Reviews (Colognato and Yurchenco 2000; Hohenester and Engel 2002; LuckenbillEdds 1997; Powell and Kleinman 1997)). LN induced neuritogenesis has been linked to interactions with $\alpha_1\beta_1$, $\alpha_6\beta_1$, and $\alpha_3\beta_1$integrins, dystroglycan, and 110 kDa laminin binding receptors. Due to this established cell-ECM interaction, LN has been incorporated within polymeric matrices to study neurite outgrowth (Balgude et al. 2001; Dodla and Bellamkonda 2006; Georges et al. 2006; Yu et al. 1999). Consequently, the interactions between substrate rigidity and bioactive support can be investigated by immobilizing LN on a mechanically tunable polymeric matrix, such as MC.

This study aimed to evaluate neuronal response to variations in both matrix compliance and ligand density. As mentioned previously, these properties have been evaluated independently (Balgude et al. 2001; Bellamkonda et al. 1995a; Willits and Skornia 2004), and recently, the concurrent evaluation of substrate rigidity and ligand density has been performed (Cullen et al. 2007a; Leach et al. 2007). The viscoelastic properties of MC and the tethering density of LN on MC were characterized and correlated with neuronal viability and neurite outgrowth. The results highlight a relationship between substrate rigidity and LN density on neuronal survival and outgrowth.

Methods

Methylcellulose – Laminin Tethering Scheme

MC (methylcellulose, M_w~40kDa; Sigma) hydrogels were prepared in 1X Dulbecco's Phosphate-Buffered Saline (D-PBS; Invitrogen) according to a dispersion technique previously reported (Kobayashi et al. 1999; Tate et al. 2001). Tethering of laminin-l (LN) to MC was accomplished via photocrosslinker N-sulfosuccinimidyl-6-[4´-azido-2´-nitrophenylamino] hexanoate (sulfo-SANPAH; Pierce Biotechnology, Inc, Rockford, IL). Briefly, LN (200 μg/mL; Invitrogen) was incubated with a 0.5 mg/mL sulfo-SANPAH solution in absence of light for 2.5 hours. Residual unreacted sulfo-SANPAH was removed with micro-centrifuge filters. LN-SANPAH (200 μg/mL) was reconstituted and thoroughly mixed on ice with MC (7.2% w/v). A thin layer of the MC+LN-SANPAH mixture was then cast onto a glass slide and exposed to UV light for four minutes (100 W, 365 nm; BP-100AP lamp, UVP, Upland, CA) to initiate the photocrosslinking reaction. Upon completion of the tethering reaction, unbound LN was removed by rinsing with D-PBS supplemented with 0.1% Tween-20 followed by three rinses with D-PBS. MC tethered to LN is referred to as MC-x-LN and unmodified MC is referred to as MC. MC tethered to bovine serum albumin (MC-x-BSA) was used as a cell culture control. MC-x-BSA was generated according to MC-x-LN procedure, in which the molar equivalent amount of BSA was substituted for LN.

Quantification of Tethered Ligand

Conjugation of LN to MC was quantified via a dot blot immunoassay. Briefly, 1.5 μl of serial dilutions of each sample (MC, MC+LN, and MC-x-LN) and LN standards

(45 pg to 1.5 ng) were blotted onto a pre-wetted PVDF membrane (Millipore). The membrane was blocked with a Tris-HCl buffered solution (TBS; Sigma) supplemented with 5% bovine serum albumin (BSA; Sigma) and 0.05% Tween 20 (Sigma) for 1.5 hours. The membrane was then incubated in polyclonal rabbit anti-laminin antibody (0.6 μg/ml; Sigma) in TBS-Tween with 0.1% BSA for 1 hour, followed by incubation in alkaline-phosphatase-conjugated goat anti-rabbit secondary antibody (60 ng/ml; Chemicon, Temecula, CA) for 1 hour. After a 5 minute incubation in ECF substrate (Amersham Biosciences, Piscataway, NJ), fluorescence intensities were measured with a FLA-3000 Fuji Imager Analyzer (FUJIFILM Medical Systems USA, Stamford, CT). Fluorescent intensities were quantified by image analysis with Multi-Gauge software (FujiFilm).

Dynamic Rheological Characterization

Rheological analyses were performed on a Bohlin CVO rheometer (Bohlin, East Brunswick, NJ) with a parallel plate configuration. To examine the mechanical integrity of the MC hydrogels at physiological temperatures, a frequency sweep from 0.05-10 Hz was performed on each sample group (n=6-8 per group) under constant low amplitude stress upon equilibration to 37°C. We evaluated MC samples of varying polymer chain length (38 kDa and 40 kDa), MC concentration in 1X DPBS (6.75%, 7.8%, and 9.0%), MC at various stages of the tethering scheme (UV irradiated MC and MC-x-BSA), and varied protein tethering densities (20 μg/ml, 200 μg/ml, and 400 μg/ml). The complex modulus over a 0.05 to 5 Hz frequency sweep were compared to determine differences in rigidity across groups.

Cortical Neuron Isolation and Dissociation

Cortices from embryonic day 18 (E18) Sasco Sprague-Dawley rats were dissected and dissociated according to Georgia Institute of Technology IACUC-approved protocols. This well-established protocol was modified from Brewer (Brewer 1997) and optimized for cortical neuron cultures. Briefly, cortices were extracted from E18 fetuses, rinsed twice with Hank's Balanced Salt Solution (HBSS; Invitrogen), and placed in a hibernate solution consisting of L-15 supplemented with 2% B-27 (Invitrogen). Cortices were then stored at 4°C until dissociation and plating (maximum of 7 days post-dissection). Dissociation of the cortical tissue began with rinsing the tissue with cold HBSS thrice, followed by incubation in trypsin (0.25%) + EDTA (1 mM; Invitrogen) at 37°C for 10 minutes. Following removal of trypsin, cortices were rinsed twice with HBSS then placed in HBSS supplemented with DNase (0.15 mg/ml; Sigma) and vortexed for 30 seconds. Remaining tissue fragments were removed and the resulting cell suspension was centrifuged at 180*g* for 3 minutes. The cell pellet was resuspended in Neurobasal medium supplemented with 2% B-27 and 0.5 mM L-glutamine (neuronal medium; Invitrogen) and placed on ice until the cells were plated. Cells were plated within 30 minutes of dissociation with no reduction in viability, as measured with a standard trypan blue exclusion viability assay.

Scanning Electron Microscopy

The pore structure and size was evaluated with scanning electron microscopy (SEM). We measured pore size variations between MC (40 kDa at 6.75% in 1X DPBS) and MC-x-LN (200 µg/ml). MC samples was cast into glass and allowed to gel at 37ºC for 15 minutes at which point the samples were snap frozen in liquid nitrogen. Samples

were lyophilized for 48 hours and then mounted onto aluminum stubs. Lyophilized samples were examined directly with a low accelerating voltage SEM to minimize destruction of the samples (Hitachi 3500H SEM). Pore size was measured with Image Pro software (n=15 pores of 2 samples).

3-D Neuronal Cultures within MC

Dissociated primary cortical neurons were mixed on ice with MC to achieve desired MC formulation and a plating density of 3.5×10^6 cells/mL. After thoroughly mixing the cell-MC solution, the solution was transferred into chambers to attain a 300 μm thick hydrogel. The plated cell-MC solution was allowed to gel at 37ºC for 45 minutes in a tissue culture incubator (37ºC, 5% CO_2, and 95% relative humidity). Upon gelation, neuronal medium was added atop of the hydrogel. Experimental groups consisted of MC-x-BSA (MC) and MC tethered to LN (MC-x-LN). Control cultures were also plated on LN coated polystyrene (5 $\mu g/cm^2$) and poly-L-lysine coated polystyrene. All cultures were maintained in a tissue culture incubator with neuronal medium exchanges every other day until the experimental endpoint.

Viability and Neurite Outgrowth

At designated endpoints, viability was assessed with calcein AM and ethidium homodimer (EthD-1; Sigma). Briefly, constructs were rinsed with PBS and then incubated with PBS containing 2 μM calcein AM and 4 μM EthD-1 for 30 minutes. Upon removal of the calcein AM/EthD-1 solution and subsequent rinsing, cellular viability was examined with a confocal laser scanning microscope (LSM 510; Zeiss,

Thornwood, NY). Three random 100 μm thick z-stacks for each construct were captured and analyzed with LSM Image Browser (Zeiss) to record viability and neurite outgrowth.

Statistical Analysis

Data are presented as one standard deviation from the mean. Results were analyzed by the appropriate one- or multi-way ANOVA, followed by pair-wise comparisons with Tukey's post-hoc test. A 95% confidence level and corresponding p value <0.05 was considered significant.

Results

Bioactive MC: LN Tethered to MC

LN was tethered to MC via the heterobifunctional crosslinker sulfo-SANPAH (Figure 3.1). The reactions of this tethering scheme occur at physiological pH without harsh organic solvents, one of the advantages of sulfo-SANPAH. The NHS esters react efficiently with primary amino groups ($-NH_2$) in the protein at pH 7-9 buffers to form stable amide bonds. This compound was then mixed with MC and exposed to UV light initiating the nitrophenyl azide end group to form a nitrene group which inserts into C-H bonds in MC. The efficiency of the reaction was evaluated by measuring the amount of LN immobilized onto MC with immunoblotting techniques. Upon completion of the reactions, unbound LN was rinsed from MC-x-LN and MC+LN. Reaction with 200 µg/ml LN yielded 8.2 ± 1.3 µg LN per ml of MC; whereas less than l µg/ml of LN was detected in MC+LN. Non-specific binding was not detected in the MC control. This efficiency was markedly increased compared to previous crosslinkers (Stabenfeldt et al. 2006). Moreover, previous studies with sulfo-SANPAH have demonstrated variation in tethering density based on the amount of LN present in during the tethering reaction (Dodla and Bellamkonda 2006). Therefore, the LN concentration during the tethering reaction was varied to generate a range of LN densities.

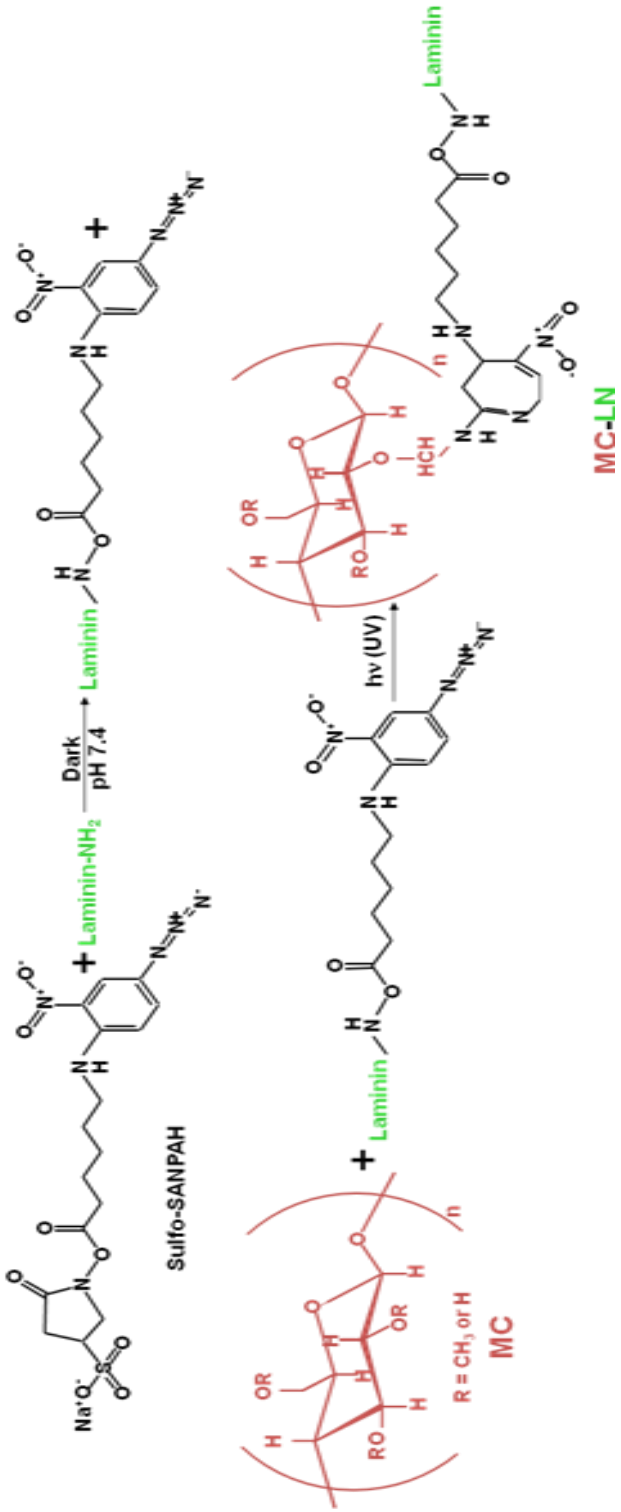

Figure 3.1 – MC-x-LN tethering scheme

Rheological Properties of MC Hydrogels

Variation of polymer chain length and concentration

Rheological analysis was utilized to evaluate the viscoelasticity of MC hydrogels of varied molecular weight (M_w) and concentration (%w/v) in D-PBS. MC samples (n = 6-8 per group; 0.5mm thick and 12mm in diameter) were placed onto a rheometer equipped with a parallel plate configuration. Upon equilibration to 37°C, the samples were subjected to a frequency sweep (0.01 to 10 Hz) under low amplitude oscillatory shear strain (0.5%). In all MC formulations, the elastic moduli (G') dominated the viscous moduli (G'') an indication that MC has transitioned from a viscous liquid to a gelled state (Figure 3.2A). Comparison of the complex modulus (G*) demonstrated significant differences in rigidity between the MC groups (Figure 3.2B). Increasing the concentration of MC (38 kDa) from 7.8% to 9.0% resulted in a more rigid gel by nearly threefold. However, a more prominent increase in G* was observed by increasing M_w chain from 38 kDa to 40 kDa, albeit the concentration of the 40 kDa MC solution was lower (6.75%) than the 38 kDa (7.8%). Elevating the M_w increases the number of monomeric groups with hydrophobic regions. Thus, the results demonstrate that this increase of hydrophobic groups enhanced the propensity of hydrophobic interactions to a greater extent than a 1% increase in concentration MC.

Biofunctionalization influenced hydrogel viscoelasticity

The LN tethering scheme includes a UV photoinitiated crosslinker. Researchers previously reported breakdown of the MC polymer under UV irradiation (Wach et al. 2004). Therefore, we measured the viscoelasticity throughout the tethering scheme to ensure the properties of the end product (MC-x-LN and MC-x-BSA) were not

substantially affected by the tethering scheme. Moreover, we measured the rheological properties of the MC-x-BSA groups with varying BSA tethering densities. This comparison was performed to delineate rigidity and protein tethering densities. The viscoelasticity of MC was measured according to the protocol outlined above. Two experimental groups were evaluated. The first group was native MC, UV irradiated MC, MC-x-BSA, and MC-x-LN; all MC groups were of the same M_w (40kDa and 6.75% in 1X DPBS). The second group consisted of MC (40kDa and 6.75% in 1X DPBS) with varying BSA densities (20 µg/ml, 200 µg/ml, 400 µg/ml).

We determined that UV irradiation to MC alone significantly decreased the complex modulus from 400 Pa to 150 Pa (Figure 3.3A). This phenomenon is consistent with previous reports and is due to breakdown of the MC polymer chain (Wach et al. 2004). However, completing the tethering scheme with either LN or BSA, the complex modulus increased to the original range of native MC (Figure 3.3A). A potential explanation for this phenomenon may be that the incorporation of a protein with hydrophobic regions may contribute to the degree of MC gelation. More importantly, within the range of BSA densities we evaluated, the complex modulus resulting tether MC products was not significantly dependent upon the protein density (Figure 3.3B). We observed an upward trend directly related to BSA density, potentially indicating that BSA densities greater than 400 µg/ml may increase the rigidity of MC.

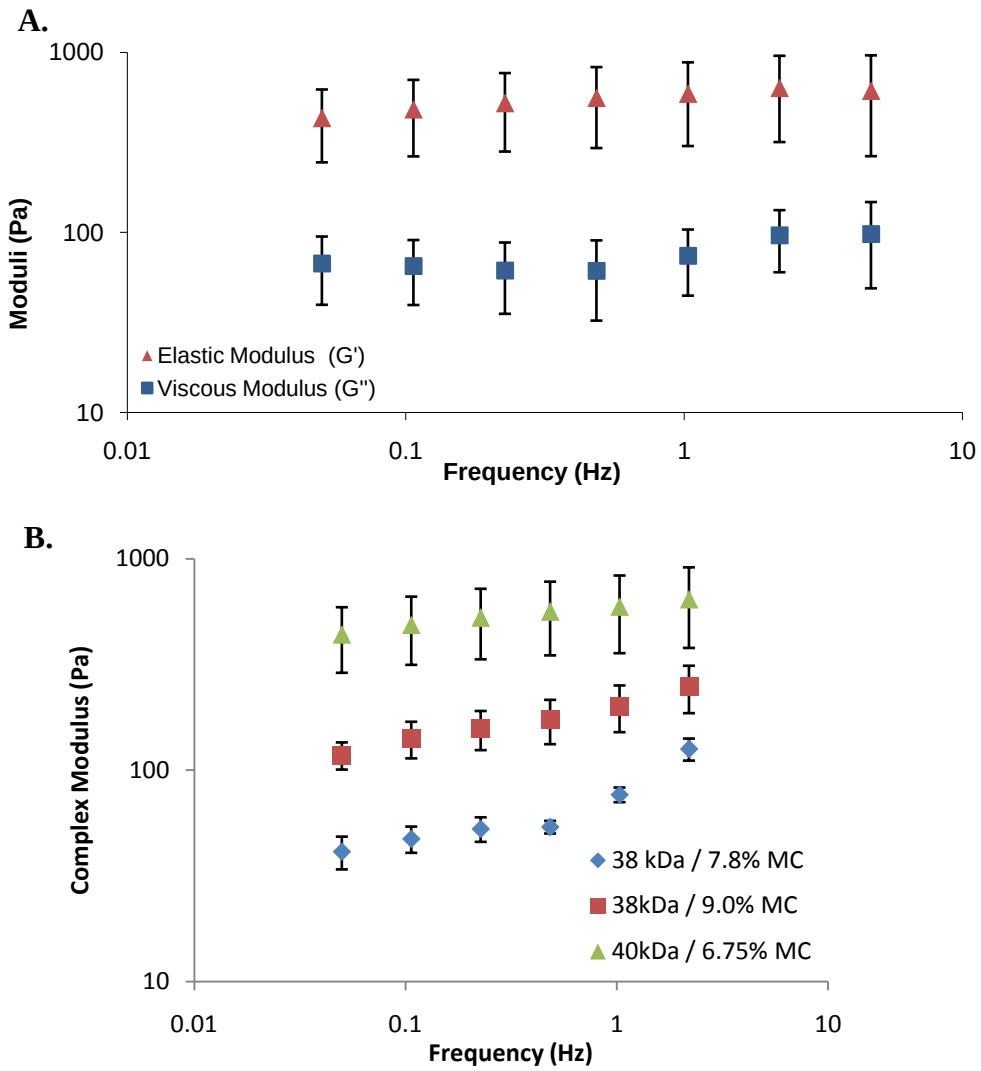

Figure 3.2 – Complex modulus is dependent on chain length and concentration. (A) Plot of loss (G'') and storage moduli (G') demonstrated a gelled state as G' is greater than G". (B) The complex modulus depended on molecular weight and MC concentration (w/v) in 1X D-PBS. Data presented as mean ± standard deviation. Statistical analysis of the complex modulus at 0.8 Hz revealed a significant difference between all groups.

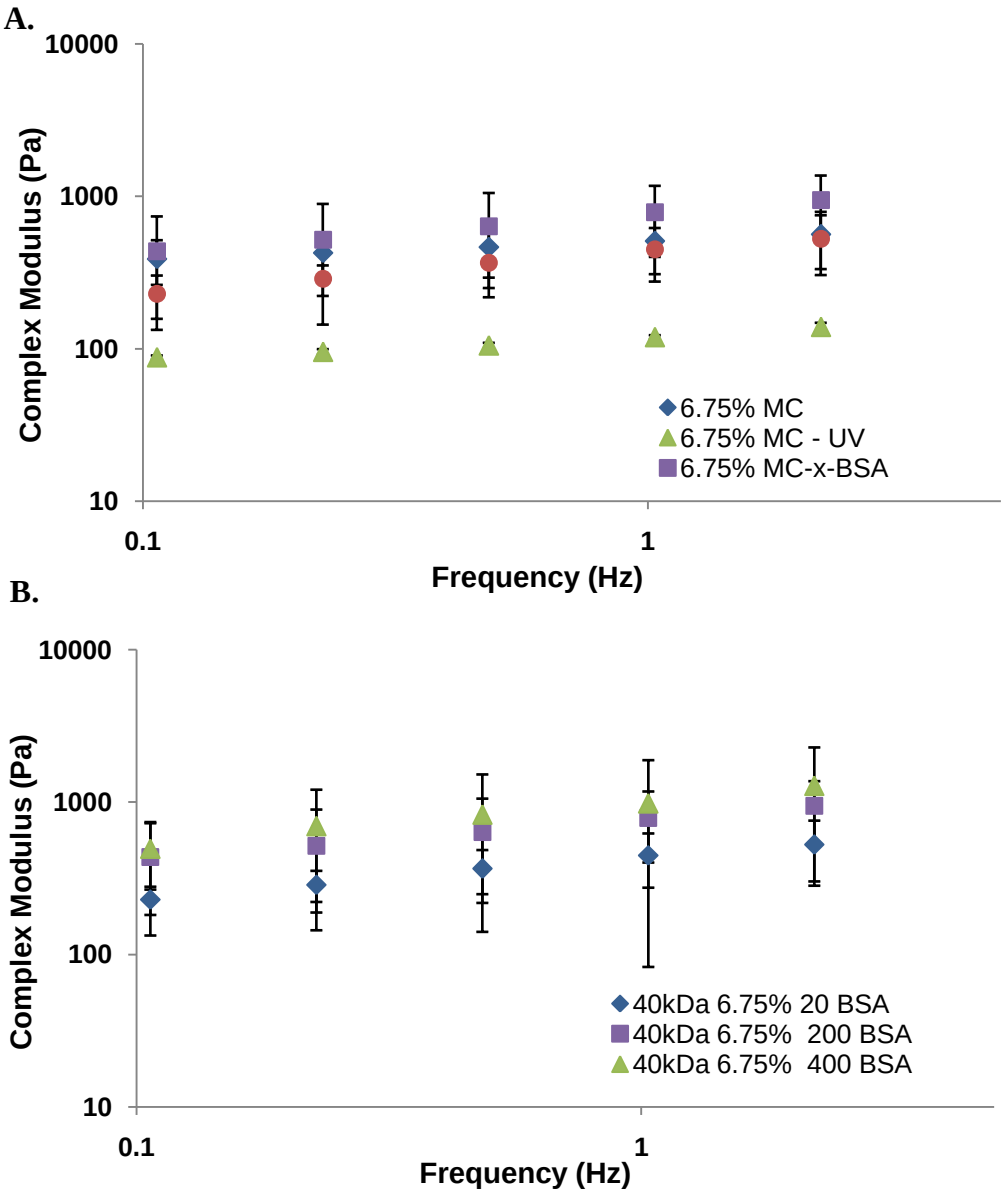

Figure 3.3 – Complex is altered due to UV irradiation. (A) UV irradiation of MC significantly reduced the complex modulus by 5-fold. This reduction was not observed with MC-x-BSA and MC-x-LN. The moduli of MC tethered with proteins were near native MC. (B) Variation in the protein concentration did not significantly alter the complex modulus. Data presented as mean ± standard deviation.

SEM: Analysis of MC structure and pore size

Previously, our lab has reported the pore size of 38 kDa MC at 8% to be relatively homogenous at 30-50 μm (Tate et al. 2001). SEM analysis of a hydrogel represents the polymeric network structure in a dehydrated state resulting in potential preparation artifacts (e.g., contraction or collapsing of network). In an effort to minimize artifacts, MC hydrogels were snap frozen, lyophilized, and then examined on the SEM. The pore size of 40 kDa MC at 6.75% was consistently 20-40 μm; the structure was highly tortuous across samples (Figure 3.4A). MC-x-LN (Figure 3.4B) had similar pore size as MC (20-40 μm); however, the macro structure did not appear as tortuous as MC. This observation could be attributed to artifacts inherent to the dehydration of a hydrogel for SEM analysis. We attempted to use an environmental SEM to evaluate the hydrogels in a hydrated state, but the SEM did not have a high enough resolution to distinguish between the water and polymer molecules. Ultimately, this characterization lead to the conclusion that MC provides a porous and tortuous matrix that permits cellular migration and neurite outgrowth.

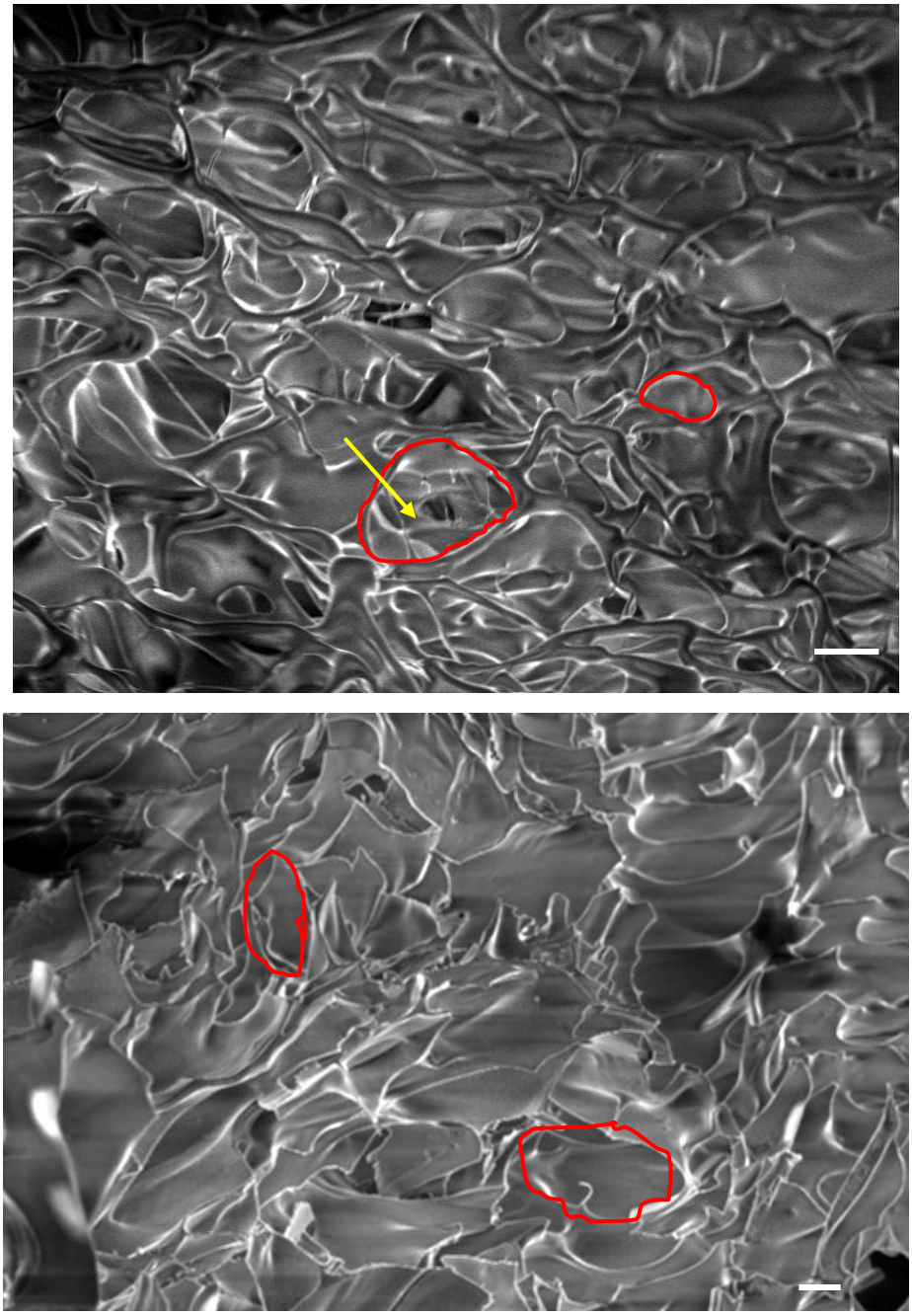

Figure 3.4 – Pore sturture and size of MC. Scanning electron micrograph of 40 kDa MC at 6.75% (A) and MC-x-LN (B) demonstrated the microstructure of the MC hydrogels. The pore size ranged between 20-40 µm; representative pores are highlighted in red. The arrow point outs pores within pores, indicative of a tortuos scaffold (A. magnification = 705X, scale bar = 10 µm, voltage = 2.00 kV; B. magnification = 423X, scale bar = 10 µm, voltage 2.00 kV).

3-D Neuronal Cultures in MC-x-LN

Neurite Outgrowth Dependent on MC Chain Length and Concentration

To examine the effects of the MC rigidity on neuronal culture viability and neurite outgrowth, both the polymer chain length and the MC concentration in solution were varied (38kDa / 7.8%, 38kDa / 9.0%, and 40kDa / 6.75%). To control for potential artifacts from the LN tethering scheme, we used MC tethered to BSA (MC-x-BSA) as a control. At 4 days post-plating *in vitro*, the viability of the neurons plated in all three MC-x-BSA groups ranged between 30-35% (Figure 3.5). Functionalizing MC with LN significantly enhanced the viability only in the 40kDa / 6.75% gels, while tethering of LN did not significantly increase viability in either of the 38kDa groups compared to the respective MC-x-BSA formulations. Most notably, neurite outgrowth occured predominantly within the 40kDa / 6.75% gels (Figure 3.6). The percentage of viable neurons extending neurites increased in the presence of tethered LN. Based on these positive observations, we used the 40kDa / 6.75% MC-x-LN for the remainder of the studies. These results underscored the significance substrate rigidity has on neuronal response.

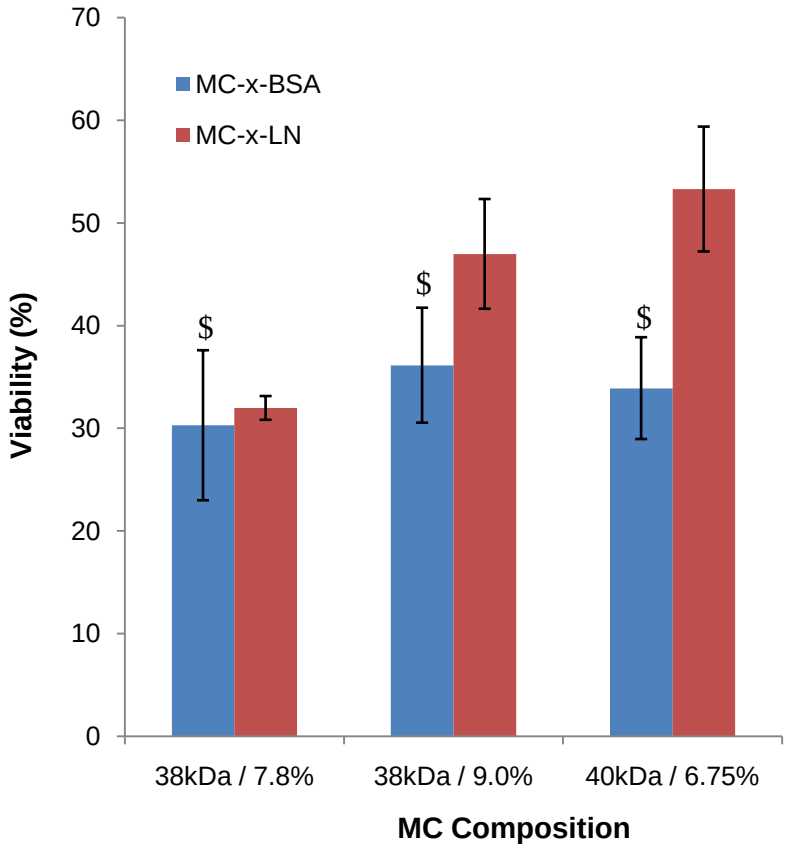

Figure 3.5 – Neuronal viability dependent on MC composition. Viability of cortical neuronal cultures was measured 4 days post-plating. Compairing the MC-x-BSA groups, no statistical differences were observed. When LN was tethered to MC, viability was siginficantly increased only within the 40kDa / 6.75% gels. (n = 4-7, error bars represent ± one standard deviation, $ $p \leq 0.05$ relative to 40kDa / 6.75% MC-x-LN)

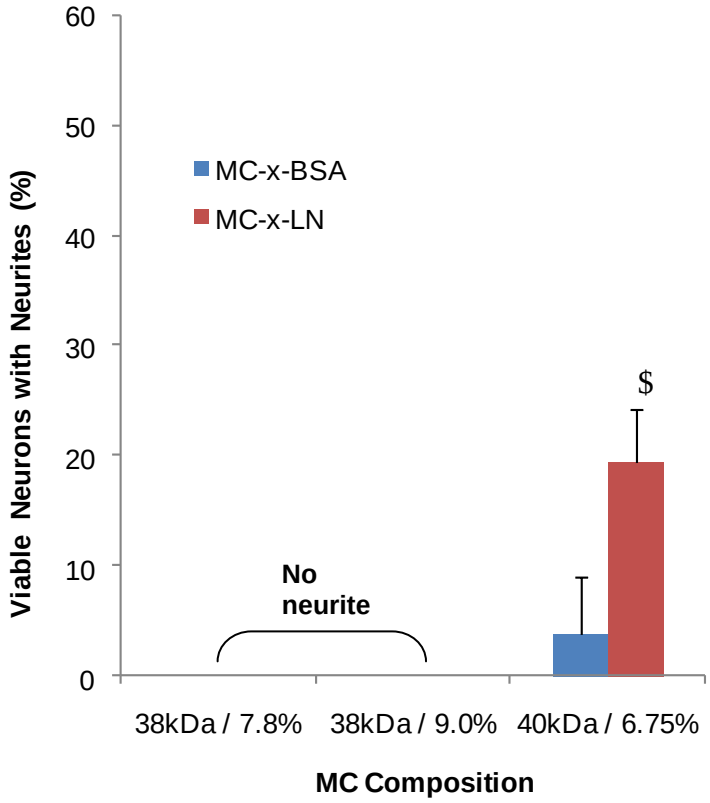

Figure 3.6 – Neurites were preferentially supported in stiffer MC-x-LN hydrogel. Quantification of the percentage of viable neurons extending neurite processes revealed that outgrowth was greater in 40kDa / 6.75% gels. Furthermore, significantly higher percentage of neurons had neurites in MC-x-LN versus uncoupled MC. (n = 4-7, error bars represent ± one standard deviation, $ represents $p \leq 0.05$).

Viability and neurite outgrowth dependent on tethered LN concentration

To evaluate the effect of varied LN densities on neuronal viability and neurite outgrowth, the MC formulation was maintained constant (40kDa / 6.75%) while a range of tethered LN concentrations was examined (n=4-8 per group). The amount of LN present in the tethering reaction was 20, 200, or 400 μg/ml. MC-x-BSA served as the negative control group to examine the specificity of the LN. As in the study above, we cultured primary cortical neurons in the 3-D MC hydrogels for 4 days *in vitro*, at which point we measured viability and neurite extension. The viability in MC-x-LN with tethering reaction concentrations of 200 and 400 μg/ml significantly increased compared to MC-x-BSA and 20 μg/ml (Figure 3.7). Moreover, the percentage of live cells with one or more neurite extensions significantly increased in all MC-x-LN groups compared to MC-x-BSA (Figure 3.8). Neurons cultured within the 400 μg/ml LN MC hydrogels supported a significantly higher percentage of neurite extension than the 20 and 200 μg/ml LN MC hydrogels (Figure 3.8). Therefore, for this study, we observed a critical threshold of LN ligand (≥ 200 μg/ml) to increase viability, whereas the lowest concentration of LN (≥ 20 μg/ml) enhanced neurite outgrowth compared to MC-x-BSA. These results demonstrated the importance of providing bioactive motifs to maintain viable cells in a synthetic matrix and encourage neurite outgrowth.

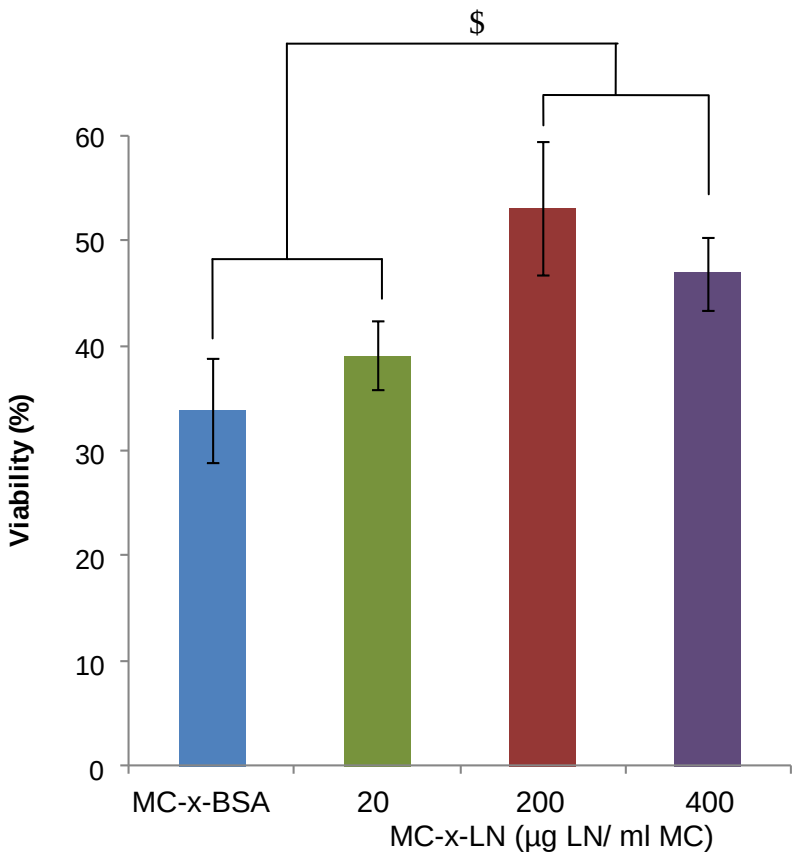

Figure 3.7 – Tethered LN enhanced viability. At 4 days *in vitro*, a critical concentration of LN was necessary to enhance neuronal viability in MC. Viability significantly increased in 200 and 400 µg/ml compared to MC-x-BSA and 20 µg/ml. (n = 4-7, error bars represent ± one standard deviation, $ represents $p \leq 0.05$).

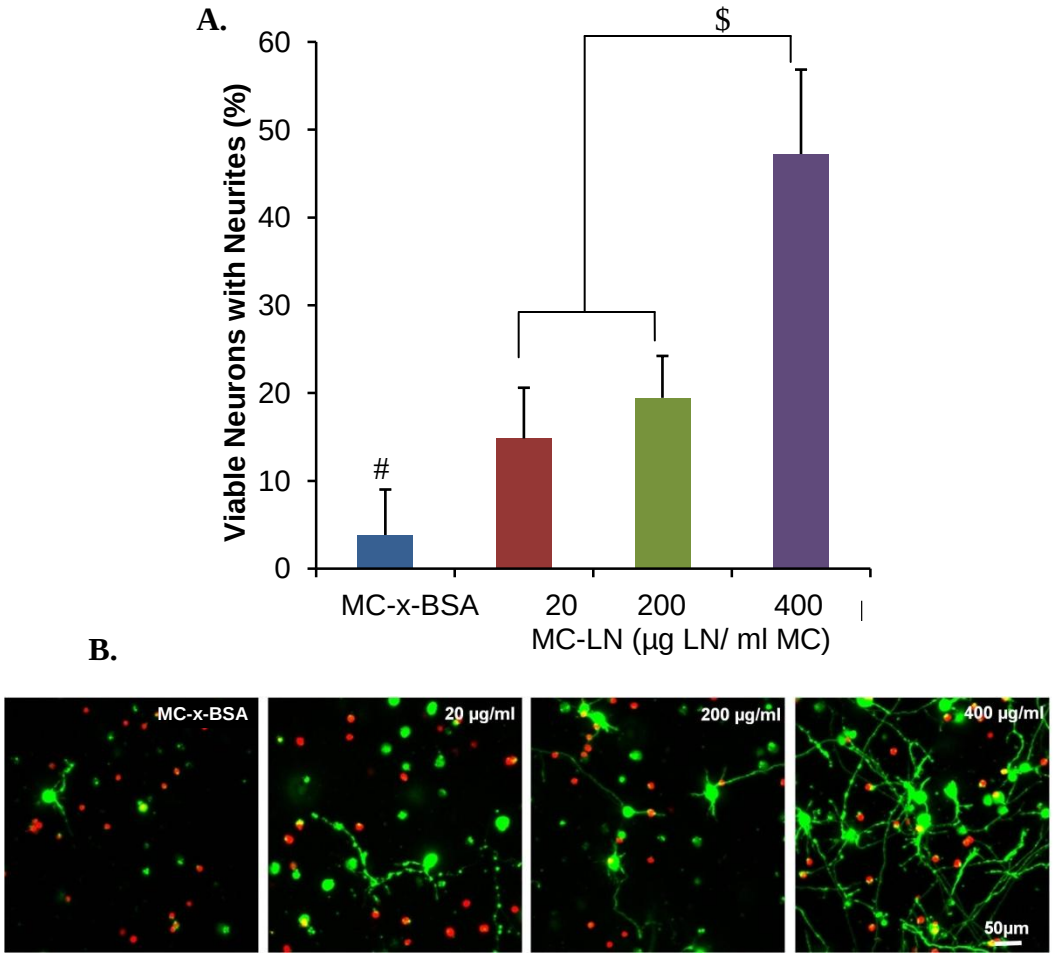

Figure 3.8 – Neurite outgrowth was directly influenced by LN concentration. (A) The percentage of viable neurons possessing one or more neurite extensions significantly increased in the presence of tethered LN. A substantial increase of neurite extensions was observed in the 400 µg/ml groups. (n = 4-7, error bars represent ± one standard deviation, $ represents $p \leq 0.05$, # represents $p \leq 0.05$ relative to all groups). (B) Confocal micrograph projections of 100 µm z-stacks clearly demonstrate the stark differences in viability and neurite extension among the experimental groups.

Discussion

The significance of substrate rigidity/structure, ligand density, and cell type/source on neural cell adhesion, spreading, and neurite outgrowth has been well-documented (Balgude et al. 2001; Bellamkonda et al. 1995a; Cullen et al. 2007a; Flanagan et al. 2002; Georges et al. 2006; Leach et al. 2007; Willits and Skornia 2004). The results of this study further verified the dependency of neuronal viability and neurite outgrowth on complex interaction between substrate rigidity and ligand density. Since cell motility and neurite outgrowth requires specific traction forces, culture substrates need to have mechanical properties near to that of *in vivo* tissue to accurately model cell behavior *in vitro*. The complex modulus of the developed MC-x-LN (~350 Pa) is comparable to *in vivo* brain tissue (G' = 150 – 500 Pa), depending on the region, age, and species (Coats and Margulies 2006; Gefen and Margulies 2004; Prange and Margulies 2002; Thibault and Margulies 1998). Therefore, we have developed a relevant hydrogel system to assess the influential properties of neuronal viability and neurite outgrowth. Moreover, the complex modulus of the MC hydrogels correspond to other synthetic polymer matrices used for neurite outgrowth studies (e.g., agarose and polyacrylamide) (Balgude et al. 2001; Cullen et al. 2007a; Dodla and Bellamkonda 2006; Flanagan et al. 2002; Georges et al. 2006; O'Connor et al. 2001). In comparing the rigidity to naturally-derived polymeric matrices (e.g., collagen and Matrigel), we noted that the complex modulus of the naturally-derived polymeric matrices were an order of magnitude lower (2 - 30 Pa) than the synthetic matrices (Cullen et al. 2007a; Willits and Skornia 2004). Therefore, we postulate that the bioactive moieties found in abundance within the natural matrices regulate the propensity for neurite outgrowth.

Neurite outgrowth has been shown to be inversely proportional to substrate rigidity (Balgude et al. 2001; Georges et al. 2006; Leach et al. 2007; Willits and Skornia 2004). The neuronal cell types analyzed in these studies were of various origins including PC-12 carcinoma lines, dorsal root ganglia, and mammalian primary spinal cord and cortical tissue. In comparing the cell culture types, studies with either PC-12 cells or DRGs had an increase in neurite outgrowth inversely proportional to substrate stiffness (Balgude et al. 2001; Willits and Skornia 2004). However, the study presented in this paper and Cullen et al. assessed primary cortical neuron cultures and cited a threshold stiffness support neurite outgrowth (Cullen et al. 2007a). Softer MC-x-LN formulations did not support neurite outgrowth, yet the stiffer 40 kDa / 6.75% supported outgrowth. Moreover, tethered ligands integrated into the matrix further influenced neurite outgrowth. Recently, a similar mechanical threshold was observed in 2-D study with PC-12 cells on a substrate of constant FN density and altered stiffness (Leach et al. 2007). Collectively, these observations demonstrate heterogeneous responses among neuronal cell types to substrate stiffness and ligand presentation.

Researchers have also examined the response of astrocytes to substrate rigidity. Astrocyte adhesion and spreading on a 2-D surface is directly proportional to substrate rigidity with limited astrocyte spreading on substrates with G' of 200 Pa (Georges et al. 2006). Similarly, astrocytes dispersed in 3-D a compliant poly(N-(2-hydroxypropyl)-methacrylamide) (HMPA) maintained a rounded morphology (Woerly et al. 1996). Astrocytes and neurons co-habitat amidst tissue of similar rigidity *in vivo*; however, the response of theses cell types to substrate rigidity differs substantially *in vitro*. These observations further support the hypothesis that complex interactions between the

mechanical properties, bioadhesive ligands, and the presence of other phenotypes determine the potential for a matrix to support healthy neuronal cultures.

Ligand-dependent neurite outgrowth has been observed with the ECM proteins collagen IV, LN, and fibronectin (Bellamkonda et al. 1995a; Cullen et al. 2007a; Leach et al. 2007). A multitude of studies have shown that neurite outgrowth correlates not only to isotropic ligand concentrations, but also anisotropic gradients for directed neurite outgrowth (Bellamkonda et al. 1995a; Cullen et al. 2007a; Dodla and Bellamkonda 2006; Kapur and Shoichet 2004; O'Connor et al. 2001; Pittier et al. 2005; Sakiyama-Elbert and Hubbell 2000; Yu et al. 1999). These examples demonstrate that substrate compliance alone does not dictate cell response; the complex relationship among matrix stiffness, adhesive ligands, cell-cell interactions, and soluble factors ultimately determines cell fate.

Conclusion

This study evaluated the effects of MC hydrogel formulation (polymer chain length and concentration) and protein tethering density on primary cortical neuron viability and neurite outgrowth. The formulation of MC contributes to the micro-matrix structure (e.g. pore size and tortuosity) as well as rigidity, both of which have been identified as key factors for cellular viability and motility in scaffolds (Bellamkonda et al. 1995b). The results indicated that neuronal viability in MC-x-BSA groups was similar regardless of concentration or molecular weight. However, neurite outgrowth was only observed within the 40kDa MC group, the largest complex modulus. Moreover, significant neurite outgrowth was not observed until LN was tethered to the 40 kDa MC. A LN-density dependency was identified with respect to neurite outgrowth, while a significant increase in viability compared to MC-x-BSA required 200 μg/ml.

Collectively, these results demonstrated that neuronal response, as measured through viability and neurite outgrowth, are related to the interplay of substrate mechanical properties and ligand density.

Acknowledgments

This work was supported by the NIH NRSA Fellowship (F31 NS054527; S.E.S.), NSF EEC-9731643, and NIH EB001014 (AJG). We thank the following people for their technical assistance: R. Bellamkonda, M. Dodla, M. Levenston, and C. Wilson. We acknowledge the following people for assisting with image quantification and rheology analysis: R. Riebesell, J. Kroger, and G. Munglani.

CHAPTER 4: BIOADHESIVE MICROENVIRONMENT INFLUENCES NEURAL STEM CELL SUVIVAL, MIGRATION, AND DIFFERENTIATION

Abstract

The extracellular matrix (ECM) provides critical signals during neural development to direct cellular migration and differentiation. 2-D culture systems have been used to characterize neural stem cell (NSC) behavior on various adhesive ECM proteins. We postulate that ECM proteins presented in a controlled 3-D configuration better mimic *in vivo* cell-ECM interactions and allow for more robust examination of signals that contribute to NSC behavior. Accordingly, we developed a methylcellose (MC) scaffold system to which we tethered a controlled density of laminin-1 (LN) and monitored the activity of neurospheres cultured within this 3-D microenvironment. Specifically, we examined NSC survival, apoptosis, migration, differentiation, and matrix production over a period of 1 week. MC tethered to LN (MC-x-LN) enhanced NSC survival compared to controls of MC coupled to bovine serum albumin or MC plus uncoupled LN. Analysis of apoptosis death mechanisms identified significantly lower levels of apoptotic NSC activity in MC-x-LN compared to MC controls, as measured by bcl-2 and bax expression and TUNEL. Over 7 days, the presence of tethered LN did not significantly alter the total migrational area out of the initial neurospheres. However, MC-x-LN supported a significantly higher percentage of neurospheres extending neurite-like processes compared to MC controls. Using functional blocking antibodies, this migratory behavior was shown to be mediated by β_1 integrins. Most interesting, the differentiation profiles within the neurospheres depended on tethered LN, where MC-x-

LN fostered higher levels of neuronal and oligodendrocyte precursor cells compared to the control MC groups. Additionally, the production of LN and corresponding $\alpha_6\beta_1$ integrins were markedly increased within MC-x-LN, whereas the production of fibronectin and $\alpha_6\beta_1$ integrins were more pronounce in MC-x-BSA and MC+LN. These findings demonstrated that the microenvironment surrounding NSC modulates cellular activity that propagates to the neurosphere's center and contributes to our understanding of the NSC response to LN, critical factors that can be exploited to develop pro-survival transplant couriers for novel neurotransplantion methodologies.

Introduction

Neural stem cells (NSCs) transplanted in neural injury or neurodegenerative diseases models result in only modest functional recovery and tissue sparing (Kelly et al. 2004; Longhi et al. 2005; Riess et al. 2002a; Shear et al. 2004; Studer et al. 1998; Subramanian 2001; Tate et al. 2002). Limitations of neural transplants are, in part, due to poor donor cell survival that occurs at acute time-points post-transplantion (Bakshi et al. 2005; Emgard et al. 2003). It is postulated that co-delivering NSCs with pro-survival cues will prevent apoptosis, thereby markedly improving transplant survival. The design of tissue engineered scaffolds that take advantage of inherent pro-survival cell signals may be a promising approach to overcome current transplant limitations (Review(Boontheekul and Mooney 2003)).

NSCs derived from the developing germinal eminence can be maintained in proliferative neurosphere cultures (Reynolds et al. 1992), resulting in a highly complex 3-D microenvironment that mimics characteristics of the stem cell niche *in vivo* (Campos et al. 2004). During neural development, the ventricular and subventricular zones, remnants of the germinal neuroepithelium, are rich in neural precursor cells and NSCs. Within this region, laminin (LN) chains co-localize with α_6 and β_1 integrins on NSCs (Campos et al. 2004). The co-localization of laminin and NSC remains prominent in the ventricular NSC niche throughout adult life (Kerever et al. 2007; Mercier et al. 2002). Coincidentally, NSC neurospheres cultured *in vitro* produce laminin and β_1 integrins co-locally (Campos et al. 2004). This expression of β_1 integrins is critical for NSC proliferation and survival (Leone et al. 2005). Moreover, *in vitro* migration on fibronectin (FN) and LN is dependent of β_1 integrins, as functional antibody blocking of

β_1 integrins hinder migration from neurospheres plated on FN and LN (Leone et al. 2005; Tate et al. 2004). Collectively, these studies indicate that ECM-integrin interactions are fundamentally required for maintaining NSC survival and strongly regulate the migratory potential of NSCs. Furthermore, due to production and deposition of ECM proteins and cell-cell interactions within the neurosphere, it is hypothesized that this resulting complex 3-D microenvironment leads to directed differentiation and asymmetrical proliferation (Campos 2004). Therefore, we postulate that NSC-derived neurospheres enveloped within an exogenous LN microenvironment will exhibit a markedly altered spatial distribution of differentiated cells; foremost, the peripheral edge of the sphere will possess a higher population of committed cells.

Recently, innovative bioengineered scaffolds have been used to investigate the response of NSC activity to controlled concentrations of soluble and/or immobilized ligands (Ilkhanizadeh et al. 2007; Mahoney and Anseth 2007; Nakajima et al. 2007; Saha et al. 2007; Soria et al. 2006). While these studies include both 2-D and 3-D substrates, cell receptor-ECM engagement depends on the dimensionality of the presented protein (Cukierman et al. 2001; Cukierman et al. 2002). Therefore, controlled presentation of ligands in 3-D provides a more *in vivo*-like cell-ECM interaction. 3-D bioengineered systems typically consist of a non-fouling polymeric scaffold decorated with biofunctional ligands, enabling specific interactions between the cells and the ligand(s) of interest. In this study, we utilized methylcellulose (MC) as the polymeric foundation to evaluate the effect of the 3-D presentation of LN on NSC activity. MC is a unique temperature sensitive polymer used in multiple neural tissue engineering applications (Gupta et al. 2006; Hirrien et al. 1998; Stabenfeldt et al. 2006; Tate et al. 2001; Tsai et al.

2006; Wells et al. 1997). Therefore, this system allowed us to not only investigate the impact of LN presented in 3-D on NSC neurosphere activity, but also the utility of MC tethered to LN as a potential delivery vehicle for neural transplantation.

The objective of this study was to examine the influence of LN presented in a controlled 3-D manner on NSC survival, migration, and differentiation. The results from this study indicated that surrounding NSC neurosphere microenvironment with exogenous LN significantly augments NSC activity, particularly cell survival, differentiation, and matrix production. Moreover, we show that dimensionality of ligand presentation modifies the cell-ECM interactions resulting in altered intracellular processes and NSC fate, a phenomenon that has been observed in other cell types (see Reviews (Cukierman et al. 2002; Friedl and Brocker 2000)).

Methods

Neural Stem Cell Harvest and Culture

Colony breeding and harvest procedures were approved by the Institutional Animal Care and Use Committee of the Georgia Institute of Technology. NSC neurospheres were obtained from primary fetal transgenic B6-TgN(β-act-EGFP)osbY01 mice (C57/BL6 background) (mice were generously donated by M. Okabe). The use of NSCs constitutively expressing GFP enabled time-course 3-D imaging on a confocal microscope to evaluate migration and neurite outgrowth. This protocol was based on previously published methods (Reynolds et al. 1992; Tate et al. 2004). Briefly, pregnant mice (gestational day 14.5) were anesthetized with isoflurane and sacrificed. The fetuses were then isolated by Caesarian section and decapitated; the scalp and skull were removed. Next, the germinal zone was isolated and mechanically dissociated in HBSS. Cells formed spheres and were maintained in suspension culture in NSC medium comprised of serum-free DMEM/F12 (Invitrogen, Carlsbad, CA) containing insulin (25 μg/mL; Sigma Aldrich, St. Louis, MO), transferrin (100 μg/mL; Sigma), putrescine (60 μM), sodium selenite (30 nM), progesterone (20 nM), and glucose (6 μg/mL; Sigma) at 37ºC, 5% CO2, and 95% relative humidity. Human recombinant basic fibroblast growth factor (FGF, 20 ng/mL; Peprotech, Rockhill, NJ) supplements were added every other day to maintain proliferating neurospheres. The resulting neurospheres were passaged every 7-10 days and were used at passages 3-5.

Tethering of Laminin-1 to Methylcellulose

MC (methylcellulose, M_w~40kDa; Sigma) hydrogels were prepared in 1X Dulbecco's Phosphate-Buffered Saline (D-PBS; Invitrogen) according to a dispersion technique previously reported (Kobayashi et al. 1999; Tate et al. 2001). Tethering of laminin-l (LN) to MC was accomplished using the photocrosslinker N-sulfosuccinimidyl-6-[4´-azido-2´-nitrophenylamino] hexanoate (sulfo-SANPAH; Pierce Biotechnology, Inc, Rockford, IL). Briefly, LN (200 μg/mL; Invitrogen) was incubated with a 0.5 mg/mL sulfo-SANPAH solution in absence of light for 2.5 hours. Residual unreacted sulfo-SANPAH was removed with microcentrifuge filters. LN-SANPAH (200 μg/mL) was reconstituted and thoroughly mixed on ice with MC (7.2% w/v). A thin layer of the MC+LN-SANPAH mixture was then cast onto a glass slide and exposed to UV light for four minutes (100 W, 365 nm; BP-100AP lamp, UVP, Upland, CA) to initiate the photocrosslinking reaction. Upon completion of the tethering scheme, unbound LN was removed by rinsing with D-PBS supplemented with 0.1% Tween-20 followed by three rinses with D-PBS, resulting in 8.2 ± 1.4 μg LN per ml of MC. MC tethered to LN is referred to as MC-x-LN and control MC tethered to BSA is referred to as MC-x-BSA. A control of MC+LN was included to account for residual non-tethered LN trapped within MC. MC+LN was generated in the same manner as MC-x-LN except the LN was not reacted with sulfo-SANPAH. After rinsing, less than 1 μg LN per ml of MC remained in the hydrogel.

3-D NSC Cultures within MC

NSC neurospheres of passage 3-5 were suspended in NSC medium and mixed on ice with the MC formulations at a 1:5 ratio. After thoroughly mixing the cell-MC

solution, the solution was transferred into Sylgard (Dow Corning, Midland, MI) chambers to obtain a 300 μm thick hydrogel. The Sylgard chambers consist of a circular Sylgard ring fixated to a coverslip, enabling real-time confocal imaging. The plated cell-MC solution was allowed to gel at 37ºC for 45 minutes in a tissue culture incubator (37ºC, 5% CO_2, and 95% relative humidity). Following gelation, NSC medium was added on top of the hydrogel. Experimental groups consisted of MC tethered to BSA (MC-x-BSA), MC supplemented with soluble LN (MC+LN), and MC tethered to LN (MC-x-LN). The control groups included NSCs plated on LN coated polystyrene (5 $\mu g/cm^2$), and NSCs cultured in suspension with and without FGF. All cultures were maintained in a tissue culture incubator with media exchanges every other day until the experimental endpoint.

Cell Viability

Release of LDH into the cell medium is an indicator of compromised cellular membranes, thus an indirect measure of cell death (Decker and Lohmann-Matthes 1988; LaPlaca et al. 1997; Legrand et al. 1992). At 2, 4, and 7 days, NSC medium was collected and the LDH content was determined with an LDH Assay (Sigma). Briefly, 50 μl of media was transferred into a 96-well plate and mixed with 100 μl of LDH reagent solution (1:1:1 LDH substrate: LDH reagent: LDH enzyme). After a 30 minute incubation, the reaction was stopped with 15 μl of 1.0 N HCL. At this point, the absorbance was measured at 490nm on a spectrophotometer. The LDH content was normalized with a standard curve using active LDH (Sigma).

At 2, 4, and 7 days, viability was also assessed by ethidium homodimer (EthD-1) staining and GFP intensity; the transgenic GFP was driven by a β-actin promoter,

therefore production of GFP diminished with cell death (unpublished observations). EthD-1 (Invitrogen) was used to evaluate cell death as this normally impermeable molecule enters cells with compromised membranes and binds to nucleic acids (Invitrogen). At the specified endpoints, cell-gel constructs were rinsed three times with 1X DPBS, and then incubated a 4.0 μM EthD-1 solution in 1X DPBS at 37 ºC. After 30 minutes, the stain was removed and the constructs were rinsed with 1X DPBS. A laser scanning confocal microscope (LSM 510; Ziess, Thornwood, NY) was used to image the constructs. For each sample (n=3-4 per group), three 200 μm thick z-stack images were acquired, allowing for qualitative viability analysis to corroborate the quantitative analysis of the LDH assay.

Apoptosis

Quantitative Reverse Transcriptase Polymerase Chain Reaction (qRT-PCR)

Apoptotic signaling cascades have established the involvement of B-cell lymphoma-2 (bcl-2) and bcl-2-associated protein X (bax), in which bcl-2 acts as anti-apoptotic molecule and bax is pro-apoptotic (Chao and Korsmeyer 1998). The ratio of bcl-2 to bax is indicative of the apoptotic state of a cell; a high ratio signifies a healthy state whereas a low ratio suggests the levels of bax is increasing leading to an apoptotic state(Chao and Korsmeyer 1998). At 7 days post-plating quantitative reverse transcriptase polymerase chain reaction (qRT-PCR) was performed on RNA extracts to determine the levels of bcl-2 and bax using previous methods developed (Byers et al. 2002; Gersbach et al. 2004). Briefly, RNA was isolated and cDNA synthesis was performed on DNaseI-treated total RNA by oligo(dT) priming using the Superscript™

First Strand Synthesis System (Invitrogen). Real-time PCR with SYBR Green intercalating dye was performed with the ABI Prism 7700 Sequence Detection System (Applied Biosystems, Foster City, CA; 40 cycles; melting, 15 s at 95°C; annealing and extension, 60 s at 60°C). Sequences for bax and bcl-2 oligonucleotide primers have been previously published (Boley et al. 2002): bax: forward – 5' ATGCGTCCACCAAGAAGCTGA 3', reverse – 5' AGCAATCATCCTCTGCAGCTCC 3'; bcl-2: forward – 5' TTCGCAGCGATGTCCAGTCAGCT 3', reverse – 5' TGAAGAGTTCTTCCACCACCGT 3'. Primer specificity was confirmed with ABI Prism 7700 Dissociation Curve Software. Standards for each gene were from cDNA using real-time oligonucleotides, purified using a Qiagen PCR Purification kit (Qiagen, Valencia, CA), and diluted over a functional range of concentrations. Transcript concentrations in template cDNA solutions were quantified from a linear standard curve and normalized to 1μg of total RNA. Detection limits for each gene were determined by reactions without cDNA at least an order of magnitude below the most dilute sample.

Terminal deoxynucleotidyl Transferase tetramethylrhodamine-dUTP Nick End Labeling

Cellular apoptosis was evaluated by Terminal deoxynucleotidyl Transferase tetramethylrhodamine-dUTP Nick End Labeling (TUNEL; Roche Applied Science, Indianapolis, IN). At 7 days post-plating, NSCs cultured in MC samples were rinsed with PBS and fixed with 3.7% formaldehyde (Sigma) for 30min. Samples were rinsed three times in PBS, embedded in OCT Compound, then snap frozen in liquid nitrogen. Frozen cultures were cryosectioned at 15 μm thickness (Microm Cryo-Star HM 560MV Cryostat; Walldorf, Germany). Prior to TUNEL, sections were permeablized with freshly prepared 0.1% Triton X-100 in a 0.1% sodium citrate solution for 30 minutes at room

temperature. TUNEL labeling followed the protocol provided by manufacturer (*In Situ* Cell Death Kit, TMR). Subsequent image acquisition and analysis was performed with a LSM confocal microscope (LSM Image Browser). For each group, n = 4-6 samples (5-8 neurospheres per sample) were evaluated to quantify the percentage of $TUNEL^+$ cells.

Migration and Outgrowth

NSCs were harvested from transgenic mice that constitutively express GFP enabling the ability to observe migration and outgrowth from a neurosphere over time. At 2, 4, and 7 days cultures, confocal z-stacks were collected for each experimental group (n = 3-5). To minimize cell death from imaging, cultures were exposed to low power laser excitation. The 2-D projections from each z-stack were then analyzed with Image Pro-Plus software. The images were quantified by counting the number of extensions protruding from the neurosphere and measuring the area of migration (total area of sphere normalized to an inner circular area; n = 10-25 per culture).

Differentiation and ECM and Integrin Production

Immunocytochemistry was employed to evaluated markers of differentiation, pro-survival signaling molecules, and proliferation after 7 days in culture. MC cultures were cryosectioned at a thickness of 15 μm prior to staining. Fixation and sectioning was performed in a similar manner as outlined above. Phenotypic markers for neural progenitor (nestin), astrocyte (glial fibrillary acid protein; GFAP), neuronal (β-tubulin III), oligodendrocyte (NG2), and oligodendrocyte precursor (marker 4; O4) lineages were probed. Other markers evaluated included LN (laminin-1 specific), fibronectin (FN), and integrins $\alpha_5\beta_1$ and $\alpha_6\beta_1$. Cryosections for immunocytochemistry were then blocked and permeablized with a 4% goat serum solution supplemented with 0.1% Triton-X100 at

room temperature for 1 hour. Primary antibodies for nestin (1:100, Promega, Madison, WI), GFAP (1:100; Millipore, Billerica, MA), β-tubulin III (1:1000; Covance, Harrisburg, PA), O4 (1:100; Millipore), Bcl-2 (1:60; Millipore), LN (1:50; Sigma), FN (1:100; Millipore), integrin $\alpha_5\beta_1$ (1:50; Millipore), and integrin α_6 (1:50; Millipore) were diluted in 4% goat serum and incubated for 2 hours at 37°C. Sections were rinsed 3 times with PBS followed by 2 hour incubation with the secondary antibodies of Alexa 546nm and Alexa 633nm (Invitrogen) at room temperature. After rinsing with PBS, sections were mounted with Fluoromount-G aqueous mounting medium, coverslipped and stored at 4°C. Immunostaining was analyzed on a LSM confocal microscope. For each immunolabel, n = 3 per group where 5 to 8 neurospheres were analyzed per group. A blinded observer rated each image with a relative intensity scale ranging from no positive immunostaining (–) to high positive immunostaining (+++).

β_1 Integrin Blocking

NSC cultures were cultured with functional β_1 integrin blocking antibodies in order to evaluate the dependence of migration and outgrowth on integrin-mediated adhesion. NSC-MC 3-D cultures were prepared as described above. Experimental treatment groups (n=3) received NSC media supplemented with anti-rat CD29 (250 µg/ml; BD Pharmingen, San Jose, CA). Control groups consisted of regular media (n=3) and media supplemented with IgG isotype control (250 µg/ml; BD Pharmingen; n=3). At 2, 4, and 7 days, neurite outgrowth was evaluated according to the above mentioned protocol.

Statistical Analysis

Data are presented as mean ± one standard deviation from the mean. Results were analyzed by the one- or multi-way ANOVA, followed by pair-wise comparisons with Tukey's post-hoc test (SigmaStat; Systat Software, Inc., San Jose, CA). A 95% confidence level and corresponding p value <0.05 was considered significant.

Results

Tethered LN enhances NSC survival in a 3-D synthetic microenvironment

Levels of LDH release from the NSCs in the MC cultures were evaluated as an indirect measure of cell viability. MC tethered to BSA (MC-x-BSA) served as the negative control group, generated according to the MC-x-LN coupling protocol. Additionally, we used MC plus unmodified LN to control for residual non-tethered LN within MC; the LN was not reacted with intermediate crosslinker sulfo-SANPAH. MC+LN contained less than 1 μg LN per 1 mL of MC (non-tethered LN) and MC-x-LN contained 8 μg LN per 1 mL of MC (tethered LN). At 2 days post-plating, the highest concentration of LDH release was observed with NSC cultured within MC, indicating an elevated level of cell death (Figure 4.1A). MC+LN resulted in a significant decrease in LDH compared to MC-x-BSA ($p < 0.01$). An even more pronounced reduction was observed within tethered LN (MC-x-LN), as LDH levels were significantly lower compared to MC ($p < 0.001$) and MC+LN ($p < 0.05$). The significant decrease in LDH levels observed between MC+LN and MC indicated that residual soluble LN in MC (<1 μg/ml) initially delayed cell death at 2 days; however, the density and/or presentation (i.e. soluble versus tethered) was not sufficient to maintain viable NSCs compared to MC-x-LN over 7 days *in vitro*. Qualitative analysis with EthD-1 staining and GFP intensity confirmed the results from the LDH assay. The representative confocal micrograph projections (Figure 4.1B-1D) illustrate increased EthD-1 uptake in the MC-x-BSA and MC+LN groups compared to MC-x-LN over 7 days *in vitro*. Concurrently, GFP intensity was maintained most prominently in MC-x-LN, providing additional evidence

of NSC survival. Collectively, these results demonstrated the critical need to present ECM signals in an immobilized fashion mimicking *in vivo* ECM to prevent cell death.

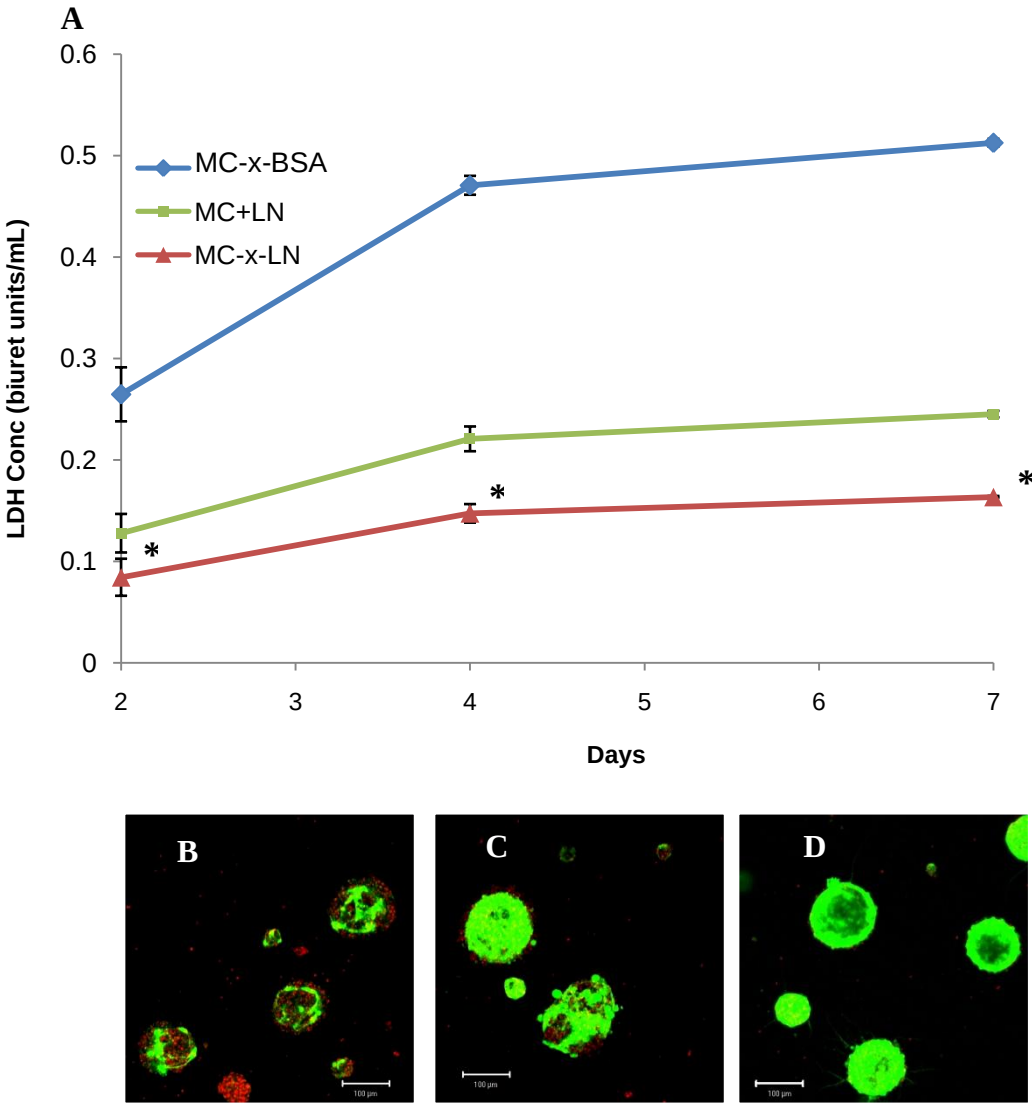

Figure 4.1: NSC viability – (A) Elevated LDH release from NSCs cultured within MC-x-BSA is indicative of cell death. NSCs cultured within MC-x-LN had the significantly lowest level of LDH release ($p<0.05$). (B-D) Confocal micrograph projections of 150µm z-stacks at 7 days post-plating of GFP on actin promoter (green) and Eth-D1 (red). Eth-D1 uptake was highest for NSCs plated within MC-x-BSA (B), decreased with MC+LN (C), and lowest within MC-x-LN (D). Scale bar = 50 µm

MC-x-LN Reduced Apoptosis

Similar to the cell survival results, apoptotic activity measured by bcl-2/bax levels and a TUNEL assay further supported the hypothesis that MC-x-LN provides pro-survival signals to NSCs. At 7 days *in vitro*, qRT-PCR was used to examine the expression of bcl-2 (anti-apoptotic) and bax (pro-apoptotic). The ratio of these molecules is indicative of the apoptotic state of the cell; lower bcl-2/bax ratio signifies an upregulation of bax driving the cell into a pro-apoptotic state (Chao and Korsmeyer 1998). The ratio of bcl-2 to bax levels was significantly higher in MC-x-LN compared to all groups including the 2-D LN control (Figure 4.2F). The results from the TUNEL assay further demonstrated the contribution of MC-x-LN to anti-apoptotic NSC signaling. TUNEL identifies cells with DNA fragments, one hallmark indicator of apoptosis. The micrographs in Figure 4.2 (A-D) are representative TUNEL images for the MC groups and LN control. NSCs cultured on LN coated 2-D control substrates displayed the pro-survival potential of LN with minimal $TUNEL^+$ cells. Within MC-x-BSA, a large number of $TUNEL^+$ cells (~70%) were distributed throughout the neurosphere; a similar percentage and distribution of apoptotic bodies was observed with MC+LN. However, significantly few $TUNEL^+$ cells were observed in MC-x-LN (~30%), which were localized in the center of the neurosphere. Therefore, NSCs will undergo apoptosis when cultured within a microenvironment devoid of bioadhesive signals and mitogenic support. Collectively, these results support the hypothesis that cell-ECM interactions are critical for NSC survival.

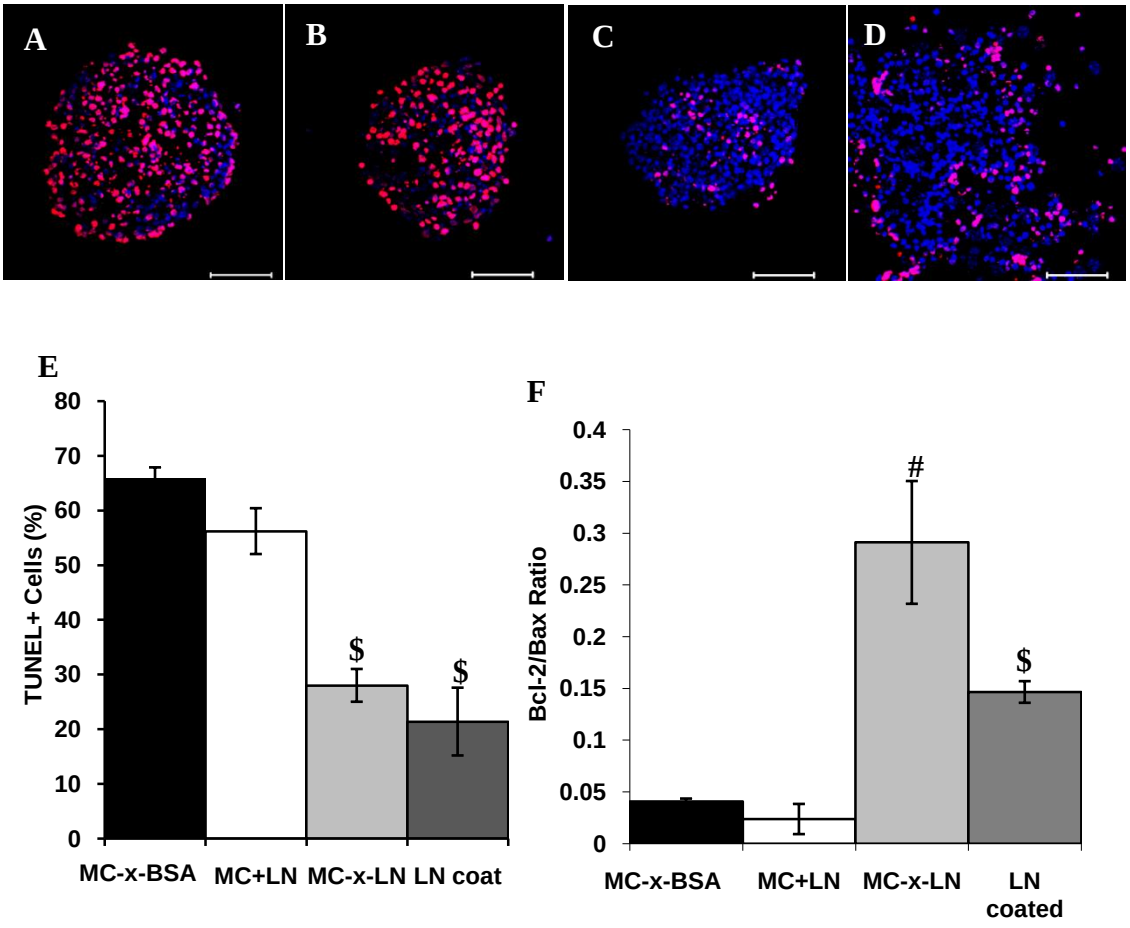

Figure 4.2 – Apoptosis decreased within MC-x-LN – (A) At 7 days, significant numbers of apoptotic cell bodies (red = $TUNEL^{+}$, blue = Hoechst nuclei stain) was observed within MC-x-BSA (A) and MC+LN cultures (B), but not within MC-x-LN (C) and on LN coated substrates (D); scale bar = 50 μm. (E) A significantly lower percentage of TUNEL+ cells were observed with MC-x-LN and LN coated compared to MC-x-BSA and MC+LN. (F) At 7 days, the ratio of bcl-2 to bax, as measured by qRT-PCR, showed significantly higher levels of anti-apoptotic signaling in MC-x-LN and LN coated control compared to MC-x-BSA and MC+LN. Mean ± standard deviation, # $p < 0.05$ relative to all groups, $ $p < 0.05$ relative to MC-x-BSA and MC+LN.

Neurite Outgrowth, but Not Migration, is Modulated by MC-x-LN

LN stimulates migration and outgrowth from NSC neurospheres (Kearns et al. 2003; Tate et al. 2004). Therefore, we measured both the migration and outgrowth from neurospheres with confocal microscopy to determine the impact LN had on these activities in 3-D. For this study, we defined migration as the total area of the neurosphere normalized to the largest inner circle (Figure 4.3A). At 7 days *in vitro*, migration from the viable neurospheres significantly increased when LN was present in either MC+LN or MC-x-LN compared to MC-x-BSA (Figure 4.3). However, no significant difference was observed between MC+LN and MC-x-LN. In addition to migration, we quantified the percentage of neurospheres extending projections. The outgrowth was not compared to LN controls as in previous experiments due to the significant migration out of the neurosphere that occurs on 2-D substrates coated with LN over 7 days. Therefore, only 3-D MC groups were compared to each other. The results showed a significant increase in outgrowth within MC-x-LN compared to MC and MC+LN (Figure 4.3). Importantly, the addition of a function-perturbing β_1 integrin antibody to the culture media significantly blocked outgrowth in MC-x-LN at all time points and MC+LN at 3 days. Therefore, the outgrowth in LN matrices was through β_1 integrin-dependent mechanisms, which corroborates previous 2-D studies on LN (Tate et al. 2004). Immunocytochemistry on cryosectioned cultures revealed that the observed projections were β-tubulin III positive, indicating a neuronal phenotype (Figure 4.4). Together these data revealed that while non-biofunctionalized MC supports NSC migration from neurospheres, the generation of neurite-like projections require a LN-presenting matrix and β_1 integrin activity.

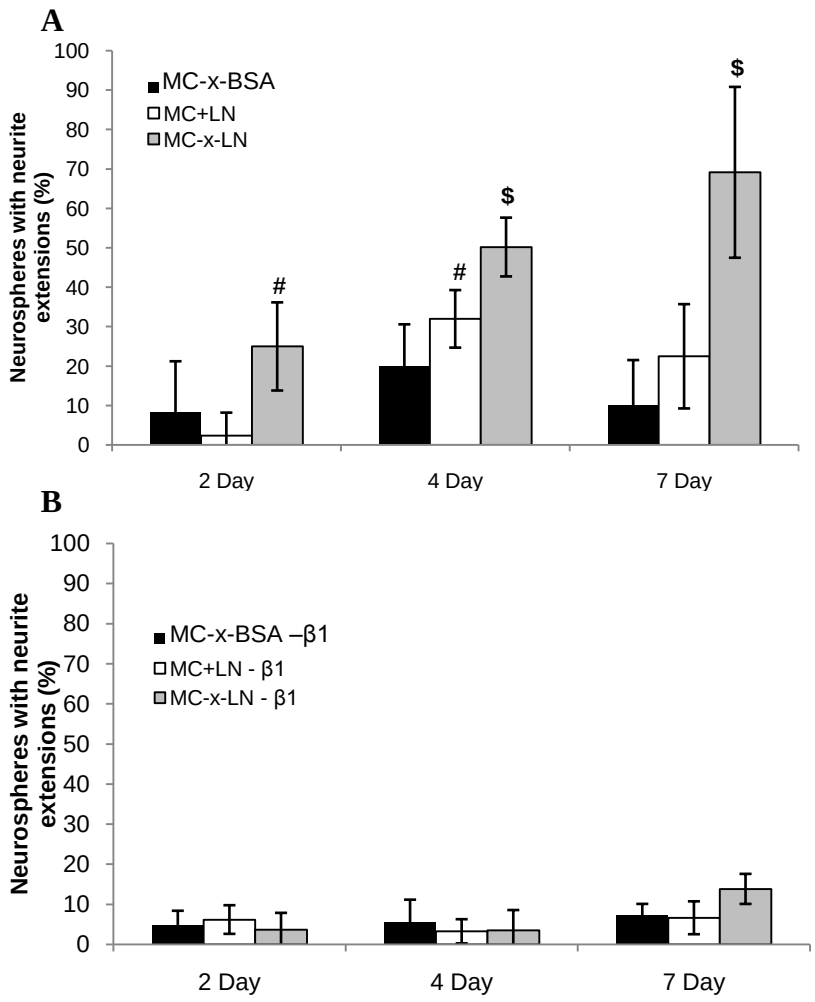

Figure 4.3 – MC-x-LN supports β_1 integrin dependent neurite extension – (A) At 4 and 7 days post-plating, the percentage of viable neurospheres with neurite-like extensions was significantly higher in MC-x-LN compared to MC-x-BSA and MC+LN. (B) β_1 integrin function blocking significantly blocked neurite extension in MC-x-LN across all time points. Mean ± standard deviation; \$ $p < 0.05$ relative to all groups; # $p < 0.05$ relative to matching β_1 integrin blocked group.

3-D Presentation of LN Modulates Differentiation

Markers of neural phenotypes were evaluated via immunocytochemistry. At 7 days, cultures were cryosectioned (15 μm) and stained for neural progenitor (nestin), neuronal (β-tubulin III), astrocyte (GFAP), oligodendrocyte precursor (O4), and oligodendrocyte (NG2) lineages (Figure 4.4 and Table 4.1). For this study, all culture conditions were without bFGF supplements except the $bFGF^+$ control; removal of this mitogen inherently induces differentiation (Campos et al. 2004). Our findings demonstrate that the extracellular microenvironment surrounding the neurosphere modulates and directs the differentiation of NSCs. As expected, nestin expression was maximum in NSCs cultured in bFGF supplemented media; expression diminished across all MC conditions and LN coated control (Figure 4.4A, D, G, J). Residual $nestin^+$ staining in the MC groups was limited to the peripheral edge of the neurosphere. Immunostaining for GFAP and β-tubulin III on LN coated 2-D controls clearly demonstrates the effect of LN on differentiation toward astrocytic and neuronal lineages, specifically the astrocytic lineage (Figure 4.4K). In all MC culture conditions, GFAP expression was noted, however, maximum levels were observed in MC+LN (Figure 4.4E). β-tubulin III positive staining was detected primarily on the peripheral edges of neurospheres cultured within MC-x-LN (Figure 4.4H), indicating the extensions observed in the outgrowth study were of neuronal origin. NG2 positive staining was absent throughout all culture conditions. Detection of marker O4 was limited to MC-x-LN and LN coated control cultures (Figure 4.4I, L). Collectively, these data indicated that MC provides an environment that cultivated primarily astrocyte and minimal neuronal

differentiation; however, the spectrum of phenotypes increased to include a more prominent neuronal population and oligodendrocyte precursors by tethering LN to MC.

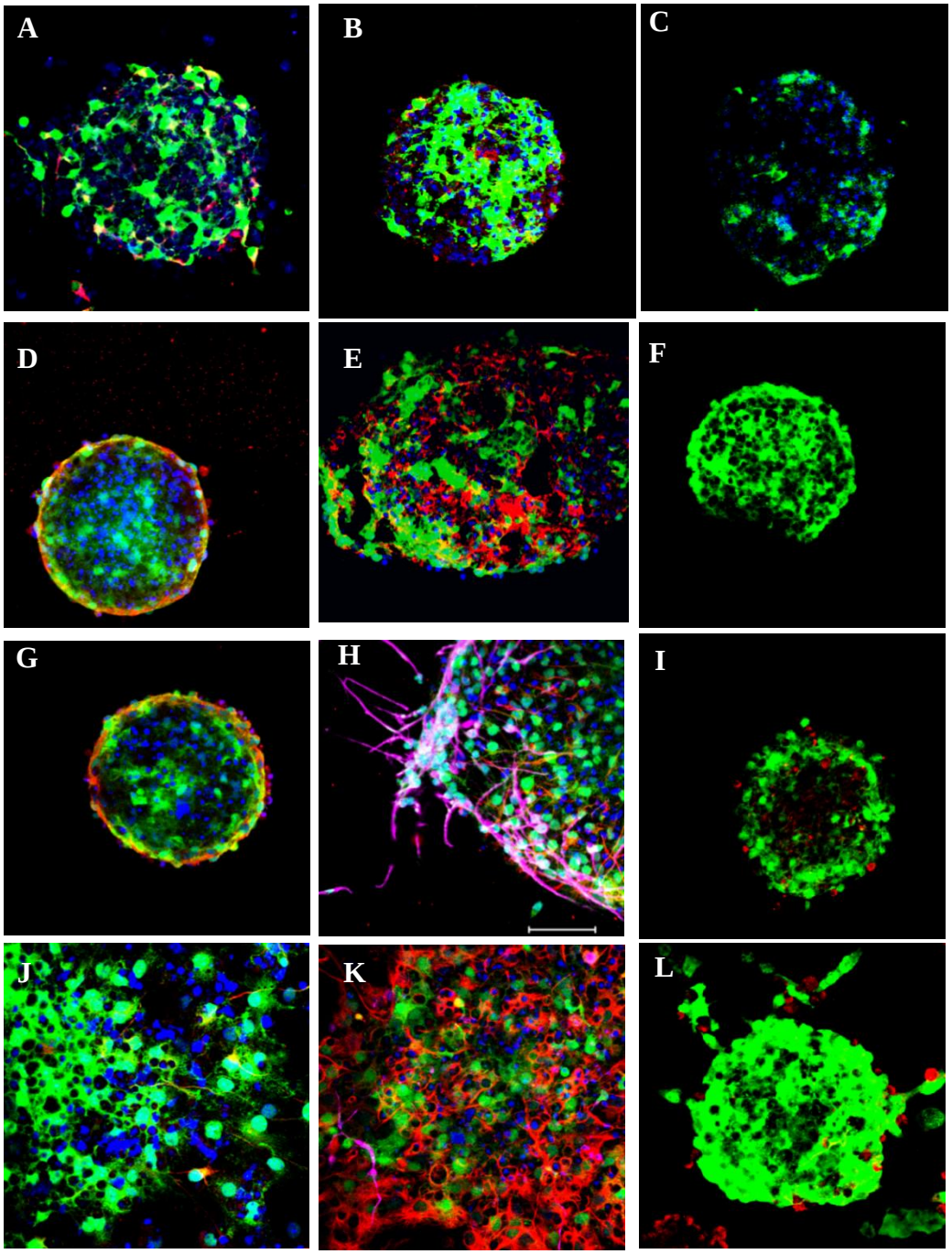

Figure 4.4: Differentiation – Immunocytochemistry at 7 days revealed substantial differences in phenotype profiles within each culture condition. Representative images of MC-x-BSA (A, B, C), MC+LN (D, E, F), MC-x-LN (G, H, I), and LN coated control (J, K, L). Compared to bFGF treated cultures, nestin staining (red; A, D, G, J) diminished in all culture conditions. Increased GFAP staining (red; B, E, H, K) was most pronounce in MC+LN (D) and LN coated control (J). β-tubulin III (pink; B, E, H, K) was predominantly observed in MC-x-LN (H) and LN coated contro (K). O4 staining (red; C, F, I, L) was only observed in MC-x-LN (I) and LN coated controls (L). Green = GFP on actin promoter, blue = Hoechst nuclei stain, scale bar = 50 μm.

Table 4.1: Relative scale of phenotype expression as observed with immunocytochemistry at 7 days (high = +++, moderate = ++, low = +, not detected = –).

Sample	Phenotypic Markers				
	Nestin	**GFAP**	**β-Tubulin III**	**O4**	**NG2**
+FGF	+ + +	**+**	**+**	**-**	**-**
- FGF	**+ +**	**+ +**	**+ +**	**-**	**-**
LN coated	**+**	**+ + +**	**+ + +**	**+ +**	**-**
MC	**+ +**	**+ + +**	**+**	**-**	**-**
MC+LN	**+**	**+ + +**	**+**	**-**	**-**
MC-x-LN	**+**	**+ + +**	**+ + +**	**+**	**-**

Extracellular Environment Modulates ECM Production

To further examine the functional impact LN has on NSCs, we measured the production of LN and FN and co-localization with their corresponding integrin binding receptors $\alpha_6\beta_1$ and $\alpha_5\beta_1$, respectively (Figure 4.5 and Table 4.2). Antibody to the integrin subunit α_6 was used to detect $\alpha_6\beta_1$; this antibody also binds to $\alpha_6\beta_4$, however, based on previous integrin characterization, β_4 integrins are minimally expressed on NSCs (Hall et al. 2006; Jacques et al. 1998). Therefore, positive α_6 staining was considered to indicate the presence of $\alpha_6\beta_1$ integrins. NSCs plated in all MC groups stained for all probed markers, though the intensity and distribution of both ECM proteins and integrins varied across sample type (Figure 4.5 and Table 4.2). FN and $\alpha_5\beta_1$ immunostaining intensity levels were elevated in both MC-x-BSA and MC+LN cultures compared to MC-x-LN (Figure 4.5A, B, C). We observed more intense immunostaining at the periphery of the neurospheres. The majority of the staining was observed at the periphery of the neurosphere. Conversely, the production of LN and $\alpha_6\beta_1$ in neurospheres as measured by immunostaining was elevated in MC-x-LN compared to MC-x-BSA and MC+LN (Figure 4.5D, E, F). Furthermore, the production of both LN and $\alpha_6\beta_1$ integrins within MC-x-LN was distributed across the entire neurosphere with enhanced intensity at the peripheral edges. During the immunostaining protocol, residual MC hydrogel matrix was rinsed from the slide, indicating that the LN staining was not from MC-x-LN, but of cellular origin. Therefore, presenting a 3-D LN microenvironment to NSCs resulted in an upregulation of LN and $\alpha_6\beta_1$ integrins across the neurosphere. Together these data further demonstrate the influence of microenvironmental factors on the synthesis of ECM and regulation of corresponding receptors.

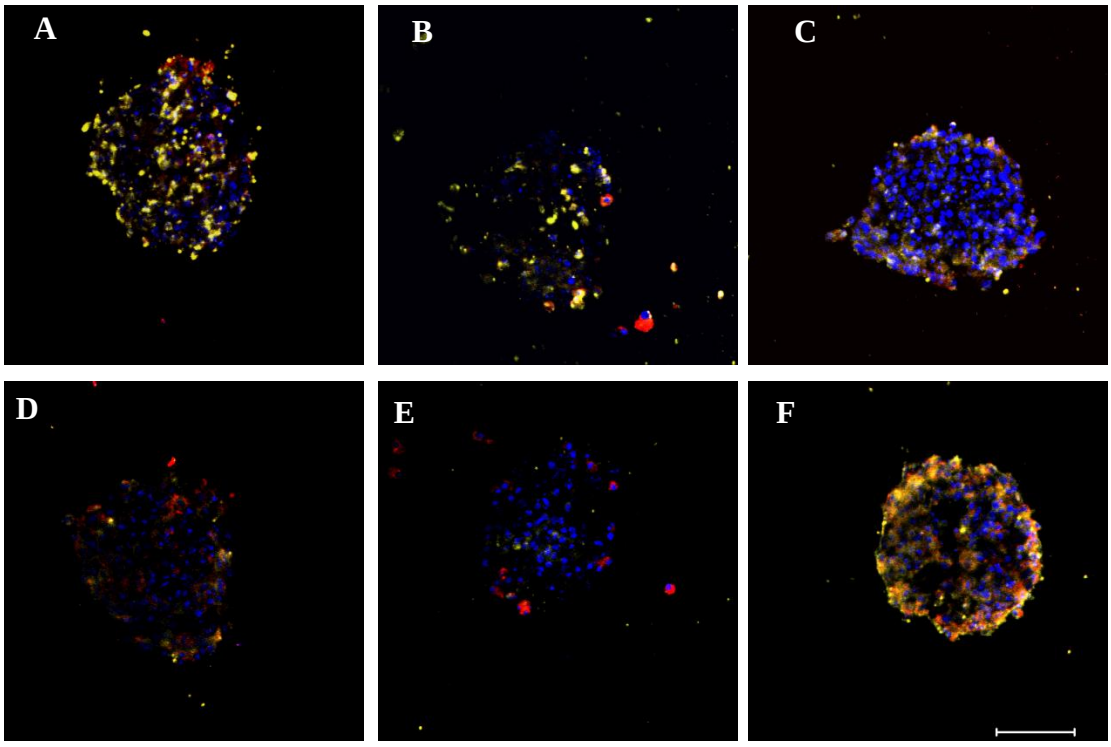

Figure 4.5: Altered ECM and integrin production within MC-x-LN – Immunocytochemistry at 7 days revealed alterations in the ECM matrix and integrin production that were dependent culture condition. (A-C) FN production (yellow) and integrin $\alpha_5\beta_1$ (red) were distributed throughout the neurosphere within MC-x-BSA (A) and MC+LN (B); however, FN and $\alpha_5\beta_1$ were predominately found on the peripheral edges in MC-x-LN (C). Minimal LN (yellow) and $\alpha_6\beta_1$ (red) were observed within MC-x-BSA (D) and MC+LN (E), yet the peak ECM/integrin production was LN and $\alpha_6\beta_1$ in MC-x-LN, distributed across the neurosphere with a maximum at the periphery (F). blue = Hoechst nuclei stain, scale bar = 50 μm.

Table 4.2: Relative scale of expression of ECM and integrins as observed with immunocytochemistry at 7 days (high = +++, moderate = ++, low = +, not detected `

Sample	ECM and Integrin Expression			
	LN	**$\alpha_6\beta_1$ integrin**	**FN**	**$\alpha_5\beta_1$ integrin**
+FGF	+ +	++	+	+
- FGF	+ +	+ +	+	+
LN coated	++	+ + +	+	+
MC	+	+	+++	+++
MC+LN	+	+	++	++
MC-x-LN	+++	+ + +	+	+

Discussion

We assessed the regulatory effect of LN presented in a 3-D matrix on NSC maintenance. We established that LN tethered to MC promoted NSC viability, reduced apoptosis, provided an environment that fostered differentiation, and enhanced neurite outgrowth from neurospheres. Moreover, the neurite outgrowth from the neurospheres was dependent on β_1 integrin signaling signifying the specificity of the cell-LN interaction within MC-x-LN. These data further established the importance of extracellular matrix signaling cues for positive NSC fate.

Cellular signaling involves complex synergistic and antagonistic interactions between cell-ECM engagements, cell-cell contacts, and soluble molecules. We demonstrated that NSCs placed in a microenvironment devoid of bioadhesive signals and/or extrinsic mitogenic support signals will undergo anoikis−apoptosis attributed to the absence of ECM support. In many transplantation paradigms, donor cells are injected in suspension form, void of direct ECM support. Donor cell apoptosis at acute time-points post-transplantation has been linked to anoikis (Marchionini et al. 2003; Pinkse et al. 2006; Pinkse et al. 2004; Smets et al. 2002; Thomas et al. 1999). Moreover, lower donor cell transplantation into injured tissue exposes donor cells to pathological signaling molecules contributing to lower donor cell survival (Boockvar et al. 2005; Marchionini et al. 2003; Molcanyi et al. 2007). We and others hypothesize that low levels of donor cell survival are due to the imbalance of pro-survival cues (e.g., cell-cell contact, cell-ECM interactions, growth factor signaling) with inducers of necrosis and apoptosis. For instance, Marchionini et al. found that donor cell survival in a Parkinson's lesion model was increased by pre-incubating transplant cell suspensions with tenascin or an antibody

for cell adhesion molecule L1, possibly by reducing anoikis (Marchionini et al. 2003). In this study, we demonstrated that NSC viability was maintained and apoptosis was reduced only when cultured within MC hydrogels presenting tethered LN. Similar observations of cell-ECM interactions have been made with pancreatic islet and hepatocyte isolations as direct plating of both cell types onto LN, FN, or collagen IV substrates decrease apoptosis (Pinkse et al. 2006; Pinkse et al. 2004; Smets et al. 2002). In a previous study, we injected NSCs into an *in vitro* 3-D model of traumatic neural injury consisting of a co-culture of mechanically injured neurons and astrocytes (Cullen et al. 2007c). NSCs injected into injured co-culture contained high levels of active caspase; whereas the number of caspase positive donor cells was significantly reduced when co-delivered with MC-x-LN (Cullen et al. 2007c). Thus, by incorporating pro-survival cell-ECM interactions to the transplant delivery vehicle, the cytotoxic transplant environment may effectively be reduced and improve donor cell survival.

During development, LN-1 is found predominantly in the basement membrane and provides guidance signals for cell migration and differentiation (Reviews (Colognato and Yurchenco 2000; Kleinman et al. 1988; LuckenbillEdds 1997; Powell and Kleinman 1997)). As development progresses (> murine postnatal day 0), LN-1 is synthesized predominantly near to the blood vessels (LuckenbillEdds 1997); conversely, other isoforms of LN are expressed in a region specific manner (Zhou 1990). For example, laminin-α2 isoform is predominately expressed in the VZ/SVZ of adult mice where NSCs reside with co-localization of β_1 integrins (Campos et al. 2004). In addition, growth factor (e.g., FGF and epidermal growth factor) gradients participate in concert with ECM cues to direct cell migration and differentiation (Review (Campos 2005)). In the present

study, providing a LN milieu profoundly affected NSC fate as measured by survival, apoptosis, neurite outgrowth, and differentiation. MC-x-LN enhanced neuronal and oligodendrocyte precursor differentiation and promoted neurite extension from the neurospheres. These results corroborate with previous studies that evaluated NSC adhesion, migration, and differentiation on 2-D LN coated surfaces (Flanagan et al. 2006; Kearns et al. 2003; Leone et al. 2005; Tate et al. 2004).

NSCs maintained in proliferative neurosphere cultures result in a heterogeneous cell population with a supporting 3-D microenvironment that mimics characteristics of the stem cell niche *in vivo* (Campos et al. 2004). In this study, surrounding the NSCs in a LN rich microenvironment perturbed the spatial distribution of phenotypic markers across the neurosphere. NSCs maintained under proliferative culture conditions (e.g., bFGF or EGF supplemented medium) possess a phenotypic distribution that is dependent on the spatial location within the neurosphere (Aarum et al. 2003; Campos et al. 2004). In the presence of bFGF, nestin positive cells are located on the peripheral edges and more mature phenotypes (neuronal and astrocyte) are located in the center of the neurosphere (Aarum et al. 2003; Campos et al. 2004). However, NSCs cultured without bFGF expressed minute traces of nestin and mature phenotype markers were observed at the periphery (data not shown). Similarly, NSCs cultured in MC-x-BSA without bFGF resulted in GFAP expression across the neurosphere and diminished nestin expression. Introducing tethered LN to MC resulted in neuronal, astrocytic, and oligodendrocyte differentiation at the periphery; nestin expression was reduced overall and peripherally located. Similar to *in vivo* signaling, the LN bioadhesive moieties provided differentiation signals to the NSCs.

Related to the altered phenotypic profile, the production of ECM proteins and corresponding integrin profiles depended upon the culture conditions. Neurospheres maintained with mitogens (bFGF or EGF) have shown expression of LN predominantly in the center (Campos et al. 2004). In contrast, the production of LN and $\alpha_6\beta_1$ integrins was upregulated in MC-x-LN compared to MC and MC+LN. The corresponding spatial phenotype in MC-x-LN indicates that the production of LN is of neuronal or astrocytic origin as both cell types have been shown to produce LN (Jucker et al. 1991; Liesi et al. 2001; Zhou 1990). Deposition of this ECM further perpetuates the formation of a niche that promotes migration and differentiation. In contrast, FN and $\alpha_5\beta_1$ integrins were expressed at higher levels in MC-x-BSA and MC+LN compared to MC-x-LN. The differentiation profile within these MC groups consisted predominantly of astrocytes, a cell type known to produce FN (Liesi et al. 1986). Therefore, we established that a LN enriched environment modulates the ECM production of NSCs, presumably correlating with phenotype alterations.

In conclusion, by controlling the presentation LN within a novel engineered 3-D scaffold we were able to evaluate the influence of cell-ECM interactions on NSC fate. We observed a significant improvement of NSC survival using the tethered MC-x-LN scaffold and profound enhancement of neurite outgrowth and differentiation compared to MC matrices void of specific ECM interactions. While NSCdevelopment is directed by other signals in addition to cell-ECM interactions, LN presentation through bioengineered scaffolds can be utilized to control NSC fate and begin to understand the complex signaling that occurs with multiple biological inputs (Mahoney and Anseth 2007; Nakajima et al. 2007). These studies demonstrate both synergistic and contrasting

effects of matrix and growth factor interactions that occur with NSCs, providing a baseline for future studies of cell-ECM interactions. Therefore, this controlled matrix provides a novel platform in which additional stimuli could be introduced in order to evaluate multiple stimuli on NSCs for improved therapeutic approaches that require NSC control.

Acknowledgements

The project was partially funded by an NIH NRSA award (SES; F31 NS054527) and NIH EB-004496 (AJG). The authors thank Tim Petrie for technical assistance with the antibody blocking studies. We also thank M. Okabe at Osaka University for the generous gift of the GFP mice. We acknowledge Scott Medway, Vishnu Ambur, and Gautam Munglani for assisting with the image quantification.

CHAPTER 5: A MULTI-LEVEL EVALUATION OF METHYLCELLULOSE TISSUE ENGINEERED CONSTRUCTS IN TRAUMTATICALLY INJURED NEURAL ENVIRONMENTS

Abstract

Neural transplantation is a promising treatment modality for traumatic brain injury (TBI). However, the full potential this therapy is limited by low levels of donor cell survival. Moreover, while deleterious cellular signaling cascades have been identified after TBI in the host tissue, the consequence of subjecting donor cells to these pathological factors is not fully understood. The aim of this study was to evaluate the influence of a tissue engineered scaffold on neural stem cell (NSC) function within injured neural tissue using both *in vitro* and *in vivo* models of TBI. First, acute NSC survival was evaluated in a 3-D neuron-astrocyte co-culture subjected to a mechanical deformation, which induces key components of astrogliosis at 4 days after injury. NSCs in Hank's balanced salt solution (HBSS), MC, or MC-x-LN were delivered into mechanically injured or control co-culture. Subsequent evaluation of NSC active caspases revealed a significant increase when delivered without MC-x-LN into injured co-cultures. To evaluate the longer term effect of the MC-x-LN scaffold on the NSC response, a controlled cortical impact *in vivo* injury murine model was used in which adult male mice sustained moderate brain injuries and received transplants 1 week after injury. Over the course of 8 weeks, an injury deficit in fine motor skills measured with a beam walk task was sustained; however, none of the treatment groups resulted in significant recovery of function using this measure. Histological analysis of glial response of the host tissue was comparable across groups. Qualitative evaluation of NSC

migration patterns indicated a dependency on the delivery vehicle (HBSS vs. MC-x-LN). NSCs delivered in MC-x-LN were primarily observed in corpus callosum or the medial lining of the injury cavity, whereas HBSS group engraftment was more random. In both NSC delivery mediums, donor cells residing in the lining of the injury cavity were $GFAP^{+}$. The results from the *in vitro* model system indicated that MC-x-LN enhanced NSC survival when exposed neural injury components for an acute period of time. The *in vivo* model evaluated a more chronic time point that indicated that MC-x-LN potential influenced engraftment location of donor cells. Collectively, this unique multi-level analysis demonstrated the importance of providing critical survival cues to transplants exposed to a pathological environment.

Introduction

Neural stem cells (NSC)-based therapies for traumatic neural injuries, neural degenerative diseases, and stroke have shown promise in providing beneficial functional outcomes (Bakshi et al. 2006; Riess et al. 2002b; Shear et al. 2004; Subramanian 2001). However, the underlying limitation in transplantation for each of these pathologies is poor donor cell survival (Bakshi et al. 2005; Boockvar et al. 2005; Kim et al. 2006; Marchionini et al. 2003; Tate et al. 2002). Cell signals (e.g., trophic support, cell-cell signaling, and cell-extracellular matrix interactions) within the microenvironment of donor cells are crucial to cell survival, maintenance, and function. Conventional transplantation methods generally deliver donor cells in liquid suspension form. Donor cells are consequently delivered directly into pathological host tissue void of homeostatic survival cues. Disruption of this homeostatic state via pathological, mechanical, or enzymatic disturbances can lead to apoptosis. Recently, studies examining NSC transplantation as a potential treatment for traumatic brain injury (TBI), have implicated caspase-mediated mechanisms of donor cell apoptosis (Bakshi et al. 2005).

Pro-survival signaling pathways have been targeted via pre-incubation with growth factors, co-delivery with ECM molecules, or genetic modifications of the cells to upregulate molecules involved in pro-survival pathways (i.e., growth factors, Bcl-2) (Bakshi et al. 2006; Boockvar et al. 2005; Duan et al. 2000; Marchionini et al. 2003; Sinson et al. 1996; Tate et al. 2002). Some success has been observed; however, the consequence of immersing cells in a pathological environment has not been fully elucidated. Recently, *in vitro* models of neural injury and/or activated astrocyte / microglia cultures have shed light on the effect of removing NSCs from a homeostatic

environment and subjecting it to a pathologic milieu (Aarum et al. 2003; Cullen et al. 2007c; Faijerson et al. 2006). It is acknowledged that such models have inherent limitations, as the complex injury environment is simplified, yet these models permit mechanistic analysis and incremental addition of pathological components. Therefore, models may aid in identifying dominant factors that influence donor cell survival.

The tissue engineering scaffold used in this study targets cell-ECM interactions by delivering donor cells within a scaffold decorated with specific ECM proteins. This methodology strives to develop bioinspired and/or rationally designed materials to support a prosperous cellular network for the repair, replacement, and/or restoration of damaged neural tissue due to traumatic injury. Design of such a scaffold must encompass material and mechanical properties of the desired applicative tissue/system. In the case of TBI or spinal cord injury (SCI), materials such as agarose (Jain et al. 2006), collagen gels (Woerly et al. 1999), and fibrin matrices (Taylor et al. 2004) have been investigated. However, the lesions produced by such injuries often include a cavity, thus therapeutic treatments in scaffold form must have the capacity to conform to irregularly shaped cavities to ensure a stable host-scaffold interface. The thermoreversible polymer methylcellulose (MC) is a potential scaffolding material that has several attractive features for neural tissue engineering applications (Stabenfeldt et al. 2006; Tate et al. 2001). MC is a unique polymer that responds to temperature changes as it forms a hydrogel at temperatures above the lower critical solution temperature (LCST). This property of MC facilitates the injection of MC into a defined space in liquid phase, which then forms a hydrogel in response to temperature increases from the surrounding environment. In peripheral nerve and spinal cord transection models, MC and MC

polymer blends have facilitated neurite outgrowth and improved functional recovery (Gupta et al. 2006; Tsai et al. 2006; Wells et al. 1997).

Laminin-1 (LN) is an ECM protein that has been shown to improve NSC survival, proliferation, migration, and differentiation (Aarum et al. 2003; Flanagan et al. 2006; Kearns et al. 2003; Leone et al. 2005; Nakajima et al. 2007; Recknor et al. 2006; Tate et al. 2004). In neural tissue engineering, scaffolds coated with or tethered to LN have been found to promote neurite outgrowth in transected peripheral nerves (Hadlock et al. 2000; Yu and Bellamkonda 2003). Therefore, we hypothesize that a neural tissue engineering scaffold composed of MC and LN has the potential to enhance NSC survival in a neural injury environment.

The aim of this study was to evaluate the potential positive effect MC-x-LN imposes on NSC survival, migration, and differentiation when delivered in concert into a host environment displaying components of neural injury. This goal was achieved by utilizing a multi-level analysis with both *in vitro* and *in vivo* injury models. First, the acute apoptotic activity of NSCs was evaluated with an *in vitro* neural co-culture (neurons and astrocytes). This co-culture system has been shown to exhibit hallmark signs of astrogliosis following mechanical deformation (Cullen et al. 2007b). Subsequently, an *in vivo* TBI model (controlled cortical impact) enabled a more long-term evaluation of NSC co-delivered with MC-x-LN. Collectively, the results from these models indicated that MC-x-LN enhanced NSC survival in the short term, which potentially influenced the differences in engraftment and migration locations in the long term.

Methods

All animal procedures were approved by the Institutional Animal Care and Use Committee (IACUC) of the Georgia Institute of Technology. All reagents were purchased from Invitrogen (Carlsbad, CA) unless otherwise noted.

Neural Stem Cell Harvest and Culture

NSC neurospheres were obtained from primary fetal transgenic B6-TgN(β-act-EGFP)osbY01 mice (C57BL6 background). The use of NSCs constitutively expressing GFP enabled time-course 3-D imaging on a confocal microscope to evaluate migration and neurite outgrowth. Pregnant mice (gestational day 14.5) were anesthetized with isoflurane and sacrificed. The fetuses were then isolated by Caesarian section and decapitated; the scalp and skull were removed. Next, the germinal zone was isolated and mechanically dissociated in HBSS. Cells were maintained in suspension culture in NSC medium comprised of serum-free DMEM/F12 containing insulin (25 μg/mL; Sigma Aldrich, St. Louis, MO), transferrin (100 μg/mL; Sigma), putrescine (60 μM), sodium selenite (30 nM), progesterone (20 nM), and glucose (6 μg/mL; Sigma). Cultures were maintained in a tissue culture incubator of 37ºC, 5% CO_2, and 95% relative humidity. Human recombinant basic fibroblast growth factor (FGF, 20 ng/mL; Peprotech) supplements were added every other day to maintain proliferating neurospheres. The resulting neurospheres were passaged every 7-10 days, which were used at passages 3-5.

Tethering of Laminin-1 to Methylcellulose

MC (methylcellulose, M_w~40kDa; Sigma) hydrogels were prepared in 1X Dulbecco's Phosphate-Buffered Saline (D-PBS) according to a dispersion technique

previously reported (Kobayashi et al. 1999; Tate et al. 2001). Tethering of laminin-l (LN) to MC was accomplished via photocrosslinker N-sulfosuccinimidyl-6-[4´-azido-2´-nitrophenylamino] hexanoate (sulfo-SANPAH; Pierce Biotechnology, Inc, Rockford, IL). Briefly, LN (200 μg/mL) was incubated with a 0.5 mg/mL sulfo-SANPAH solution in absence of light for 2.5 hours. Residual unreacted sulfo-SANPAH was removed with micro-centrifuge filters. LN-SANPAH (200 μg/mL) was reconstituted and thoroughly mixed on ice with MC (7.2% w/v). A thin layer of the MC+LN-SANPAH mixture was then cast onto a glass slide and exposed to UV light for four minutes (100 W, 365 nm; BP-100AP lamp, UVP, Upland, CA) to initiate the photocrosslinking reaction. Upon completion of the tethering scheme, unbound LN was removed by rinsing with D-PBS supplemented with 0.1% Tween-20 followed by three rinses with D-PBS. MC tethered to LN is referred to as MC-x-LN and unmodified MC is referred to as MC. This tethering scheme resulted in 8.2 ± 1.4 μg LN per ml of MC.

In vitro Neural Injury Model Methods

A portion of the data presented in this study was a included in a collaborative publication that utilized a well-characterized neuron astrocyte co-culture to evaluate acute apoptotic NSC activity delivered with and without a tissue engineering scaffold (Appendix A) (Cullen et al. 2007c). In addition to the published active pan-caspase results, a more specific analysis of active caspase 3 and 7 in NSCs delivered into neuron-astrocyte co-cultures was performed. All methods were based on the collaborative publication and are outlined below.

Neuron and Astrocyte Co-cultures

Co-cultures consisting of primary cortical neurons and astrocytes were plated in 3-D within Matrigel® (Becton Dickinson Biosciences; Bedford, MA). Culture methods were based on previous publications (Cullen et al. 2007b). Primary cortical neurons (embryonic day 18) and cortical astrocytes (postnatal day one) were harvested from Sasco Sprague–Dawley rats (Charles River, Wilmington, MA).

The cortical neurons harvest and dissociation was as follows. Timed-pregnant dams (E18) were anesthetized with isoflurane and rapidly decapitated. Fetuses were removed by Caesarian section, placed into Hanks Balanced Salt Solution (HBSS), rapidly decapitated, and the brain was removed. Next, the cerebral cortices were isolated. Tissue was dissociated with trypsin (0.25%) and 1 mM EDTA (10 min at 37 °C). The trypsin–EDTA was exchanged for HBSS supplemented with DNase I (0.15 mg/mL; Sigma). The tissue was gently vortexed for 30s, centrifuged at 1000 rpm for 3 min, then the supernatant was aspirated and the cells were resuspended in Neurobasal medium supplemented with 2% B-27, 1% G-5, and 500 μM L-glutamine (co-culture medium).

Astrocytes were harvested from day one postnatal pups. Pups were anesthetized with isoflurane and rapidly decapitated. The brains were removed and the cerebral cortices isolated. Upon isolation, cortices were minced and treated with trypsin–EDTA (37 °C for 5 min). The DNase – HBSS solution was added and the tissue was triturated with a flame-narrowed Pasteur pipette. Astrocyte medium (DMEM/F12 supplemented with 10% fetal bovine serum) was added and the cells were centrifuged (1000 rpm, 3 min). The supernatant was aspirated and the cells were resuspended and transferred to T-75 tissue culture flasks. Upon reaching 90% confluency, cells were passaged and

replated at a density of 300 cells/mm^2. Astrocytes of passage 4-12 were used for the 3-D co-cultures.

Co-cultures were plated with the neurons and astrocytes isolated from the protocols above. Cultures were plated in custom-made cell culture chambers designed for the cell shearing device; they were constructed with a glass coverslip and silicone-based elastomer mold (Sylgard 184 and 186, Dow Corning; Midland, MI). The chambers were pre-treated with 0.05 mg/mL poly-L-lysine (PLL, Sigma; 4 hrs) followed by Matrigel (0.5 mL/well at 0.6 mg/mL) in Neurobasal medium (4 hrs). Co-cultures were plated within Matrigel matrix (2500 cells/mm^3, 1:1 neuron:astrocyte ratio) at a final Matrigel concentration 7.5 mg/mL and thickness of 500–750 μm. Co-cultures were then incubated at 37 °C to permit matrix gelation and 3-D cell entrapment for 1 hour at which point 0.5 mL of co-culture medium was added to each well. Cultures were maintained at 37 °C and 5% CO2–95% humidified air, and medium was exchanged at 24 h post-plating and every 2 days thereafter.

In vitro Mechanical Injury Model: Cell Shearing Device

After 21 days post-plating, the 3-D co-cultures were subjected mechanical deformation. The injury device imparts a high-strain rate shear deformation to the 3-D cultures; this device and the resulting cellular alterations and death of neural co-cultures has been extensively characterized (Cullen and LaPlaca 2006; Cullen et al. 2007b; LaPlaca et al. 2005). Briefly, co-cultures were subjected to mechanical injury through a rapid horizontal motion of the cell chamber top plate relative to a fixed base resulting in a high-strain-rate simple shear deformation to the co-cultures. This 3-D bulk shear deformation generates heterogeneous local cellular strains in which culture viability is

directly dependent on strain rate (Cullen and LaPlaca 2006; LaPlaca et al. 2005). After mechanical injury or mock loading of control cultures, medium was added and the cultures were returned to the incubator.

Injection of NSC and Delivery Vehicles to Co-Cultures

NSCs were delivered via controlled injection designed to mimic *in vivo* transplant protocols implemented by our group (Shear et al. 2004; Tate et al. 2001). Injection into co-cultures (injured and control) occurred 2 days after mechanical injury. NSCs were delivered with a microsyringe mounted on a micromanipulator 200 μm below the surface of the co-culture. Prior to injections, co-cultures were placed in a laminar flow hood and the majority of the medium was removed. Then, 2.5 μL of NSCs (1.5×10^4 cells total) dispersed within Neurobasal medium, MC, MC+LN, or MC-x-LN to the co-cultures over 2 minutes. The cultures were returned to a tissue culture incubator for 60 min, after which co-culture medium was added.

Acute Survival Analysis: Active Caspase Assay

At 3 days post-injection, the level of activated caspases, a family of proteolytic enzymes central in apoptotic cell death, was measured in order to assess the involvement of pro-apoptotic pathways in NSCs transplanted into injured 3-D cultures using a commercially available kit (CaspaTag™ Pan-Caspase Assay; Chemicon, Temecula, CA; n = 3-4 cocultures per condition). A second round of experiments evaluated exclusively active caspase 3 and 7 by using CaspaTag Caspase 3 and 7 *In Situ* Assay Kit (Chemicon). The kits use fluorochrome inhibitor of caspases (FLICA) , which covalently bind to activated caspase heterodimers. Pan-caspase used the sequence SR-VAD-FMK, while caspase 3 and 7 are targeted with SR-DEVD-FMK. The respective caspase reagent was

mixed in media (1:30) and added to the cocultures. Following incubation at 37°C at 5% CO_2 for 60 min, the cocultures were rinsed. The binding reaction causes the fluorescent indicator to be retained in a cell, therefore permitted fluorometric detection of activated caspases colocalized with GFP^+ cells in 3-D cocultures (4-5 randomly selected regions per coculture were sampled with a LSM confocal microscope).

Statistical Analysis

Data were analyzed by a multi-way analysis of variance (ANOVA) followed by Tukey's pairwise comparisons ($p<0.05$). Means were considered to be statistically significant by using an alpha value of 0.05. Data is reported as mean ± standard deviation.

In Vivo Murine TBI Model

Controlled Cortical Impact Injury

The controlled cortical impact (CCI) device imparts a controlled mechanical compression to the cortical surface of the brain of adult male mice under moderate brain injury parameters. Unilateral contusions were generated using a custom-built controlled cortical impactor (CCI) device as described previously (Dixon et al. 1991; Tate et al. 2002). Adult male C57BL6 mice (8-12 weeks old; 20-25g; Jackson Laboratory, Bar Harbor, MN) were anesthetized with isoflurane (induction 3%; maintenance 1-2%) and placed in a stereotaxic frame. An incision in the scalp was made to expose the skull. A tissue-punch craniotomy (4 mm diameter) was performed over the left frontoparietal cortex (center: 2.0 mm posterior to bregma; 2.0 mm lateral to the midline). The impactor

tip was angled 15º from vertical to ensure the tip was perpendicular to the tangential plane of the brain surface. The metal impactor (3 mm diameter) was controlled with a pneumatically-operated piston. Injury impact was at a velocity of 6.0 m/s to a depth of 1.0 mm below the dura mater for 150 ms duration. Consistencies among injuries were verified by measuring the impact velocity and duration with a linear variable displacement transducer. Following injury, the incision was sutured and animals were allowed to recover on warming pads. Sham surgeries for uninjured controls involved anesthesia, incision, cranectomy, positioning of the impactor, and suturing. Following recovery from surgery, all mice were housed in a temperature and humidity-controlled environment with a 12:12 hour light:dark cycle with food and water available ad libitum.

Transplantation of NSCs

Seven days following the CCI injury, animals were anesthetized with isoflurane (3% induction, 1% maintenance) and placed in a sterotaxic frame. The incision site for injury or sham was re-opened and using a Hamilton microsyringe (27-guage needle; Hamilton, Reno, NV) 7 µl of NSCs in a specified delivery vehicle (passage 3; 6.125×10^4 cells total; 8.75 x 103 cell/µL) were transplanted. Transplants were delivered into the center of the 4 mm crainiectomy circle at a depth 1.1 mm below the dura mater at a rate of 0.7 µL / min using a syringe pump (Sage Instruments). After completion of the injection, the needle was left in place for an additional 5 minutes and then withdrawn slowly over 2 minutes to minimize leakage through the needle track. The incision was sutured and animals were kept on a heating pad for recovery. Vehicle control animals received 7 µL HBSS without cells, sham animals (injured controls, sham, and naïve animals) were anesthetized and the incision was re-opened and sutured, but no injection

was given. Transplant groups were as follows: NSCs + vehicle (n=6), NSCs + scaffold (n=8), vehicle only (n=3), scaffold only (n=8), injured controls (no transplant; n=5), shams (no injury or transplant; n=4), naïve (anesthesia and suturing only; n=3).

Beam Walk Motor Functional Test

The beam walk task was used to assess fine motor coordination and deficits (Fox et al. 1998). Mice were trained one week prior to injury surgery and baseline levels were measured one day prior to injury surgery. The mice were placed at the start point near the end of a narrow beam (12 mm width for the first 50 cm; 6 mm width for the second 50 cm; 25 cm above a padded surface) and were allowed to traverse the beam into a darkened goal box. The CCI injury to the left frontoparietal cortex results in deficits in motor control for the right hindlimb (Fox and Faden 1998; Fox et al. 1998). Therefore, the outcome measure was the percentage of right hindlimb foot slipped 5 mm or more below the beam surface. Mice were tested for three trials per time point to generate a mean value for data analysis. Between trials, mice were allowed to rest for 30 seconds in the goal box. The behavior schedule was as follows: training 1 week prior to injury, testing 1 day prior to CCI-injury, testing 6 days post-injury (1 day prior to transplants), and then testing weekly for 8 weeks post-transplant. All researchers involved in the beam walk data collection and analysis were blinded.

Tissue Harvest and Processing

Animals were sacrificed at 8 weeks post-transplantation and brain tissue was harvested and processed histological analysis. Mice were anesthetized with an intraperitoneal injection of pentobarbital (80 mg/kg) and were perfused with PBS (0.1M; pH 7.4) followed by 4% paraformaldehyde in PBS. Brains were harvested, post-fixed

(4% paraformaldehyde; 4°C for 12 hours), and cryoprotected (phosphate-buffered 30% sucrose; 4°C for 3-5 days). The brains were then embedded in optimal cutting temperature medium (OCT; Sakura, Torrence, CA), frozen, and stored at -80°C. Brains were coronally sectioned in 10 μm thick sections on a Microtome Cyrostat (Richard-Allan Scientific; Kalamazoo, MI). Sections were mounted in sequential series on gelatin-coated glass slides.

Immunohistochemistry

Immunohistochemistry was used to evaluate both the host response to the transplants and the differentiation of the transplanted cells. Methods have been previously established (Shear et al. 2004; Tate et al. 2002). Briefly, cryosectioned tissue was allowed to thaw at 4ºC for 12hrs. Sections were then permeablized with 0.1% Trition X-100 (Sigma) in 8% goat serum (Invitrogen) diluted in PBS for 1 hour at room temperature. Primary antibodies were diluted in 0.1% Triton X-100 and 4% goat serum to achieve the appropriate concentration for Immunohistochemistry. Diluted primary solutions were then added atop of the brain sections and incubated overnight at 4°C. Upon rinsing thrice with PBS, the appropriate secondary antibodies diluted in 4% goat serum added atop of the sections and incubated at room temperature for 2 hrs. Sections were then rinsed 3 times in PBS and treated with a DNA counterstain (Hoechst; Molecular Probes) for 10 min. Sections were rinsed 3 times in PBS and mounted with Fluoromount-G medium. Slides were stored at 4°C until analyzed. Primary antibodies and dilutions used in this study were as follows: anti-nestin (1:200; Promega), anti-β-tubulin III (1:1000; Promega), anti-glial fibrillary acid protein (GFAP; 1:200; Chemicon), anti-oligodendrocyte marker 4 (O4; 1:200; Chemicon), anti-NG2 chondroitin sulfate

proteoglycan (NG2; 1:200; Chemicon), anti-neuronal nuclei (NeuN; 1:100; Chemicon), and *Griffonia simplicifolia* isolectin IB_4 conjugated to Alexa 568 (1:100; Invitrogen). Appropriate secondary antibodies of goat-anti-mouse IgG Alexa 546 (1:1000; Molecular Probes) or goat-anti-rabbit IgG Alexa 633 (1:1000; Molecular Probes) were used to visualize primary staining with a fluorescent microscope.

Host Response: GFAP intensity Quantification and Isolectin B4 Analysis

At 8 weeks post-transplant (9 weeks post-injury), the peak host inflammatory response has subsided. However, host GFAP response was evaluated to ensure the MC-x-LN scaffold and / or NSC transplants did not exacerbate the chronic glial response. The intensity of GFAP immunostaining was quantified with a previously developed MATLAB program (Jain et al. 2006). Fluorescent images were obtained at 20x magnification under constant gain and exposure settings. The MATLAB program then generated radial sections (30 sections per image) starting from the injury cavity and branching out. The fluorescent intensity was then quantified, recorded, and averaged as a function of distance from the injury cavity. For this analysis, n= 2 brains per group with n = 4 serial sections (80 μm apart; ~640μm from the start of the injury cavity) where 6-8 images per section was analyzed.

IB_4 staining was performed to further evaluate the host response. IB_4 is a glycoprotein isolated from *Griffonia simplicifolia* that binds to various cell surface markers. It was used in this study initially to evaluate the presence of microglia. Images of ranging magnification were recorded and examined. IB_4 not only binds to microglia, but also perivascular cells, stimulated macrophages, and some forms of laminin. Therefore, the morphology of the IB_4+ cells was also analyzed. For analysis, n = 2 brains

per group and n = 4 serial sections (80 µm apart; ~640µm from the start of the injury cavity) where IB_4+ regions were examined with 4-5 images per section.

Donor Cell Phenotype and Migration Analysis

Immunostained sections with donor cells were analyzed on a LSM confocal microscope (n=4-6 sections per brain, n = 2-3 brains per condition). Confocal z-stack images were acquired to confirm co-localization of a specific phenotypic marker with GFP expression from the donor cells.

To evaluate donor cell migration, sequential serial sections were analyzed beginning ~1.0mm anterior to the lesion cavity and continued through 0.5mm posterior to the injury cavity. The engraftment location and relative number of cells was recorded (n = 3 brains per NSC group).

Statistical Analysis

Behavioral data were analyzed by a repeated measures parametric multi-way analysis of variance (ANOVA) followed by Tukey's pairwise comparisons ($p < 0.05$). All other data was analyzed with a multi-way ANOVA followed by Tukey's pariwise comparisons ($p < 0.05$). Data is reported as mean ± standard deviation. A posthoc power analysis on the behavior data was calculated to determine the minimal number of subjects needed to have 80% power ($\alpha = 0.05$, $\beta = 0.2$; assuming 100% prevalence) at detecting a 15 - 30% improvement effect.

Results

In vitro Neural Injury Model

Injury Model Validation

A neural 3-D co-culture injury system that exhibited key components of neural injury allowed the evaluation of NSCs in a controlled setting. The co-cultures were subjected to moderate injury conditions that results in both significant cell death 2 days after injury and hypertrophic astrocytes 5 days after injury (Cullen et al. 2007c). The co-culture system was utilized to mimic the *in vivo* injury environment in order to evaluate the acute response of donor NSCs and begin to determine mechanisms of cell death.

Neural Injury Environment Influenced NSC Caspase Activity

Pan-Caspase Activity

When NSCS were delivered in liquid suspension form to injured neural co-cultures, a significant increase in TUNEL+ NSCs was observed with injured co-cultures compared to control co-cultures (Cullen et al. 2007c). Therefore, this model system demonstrated a negative effect of the injury environment on NSC "transplants". This observation lead to the use of this model for evaluating tissue engineered scaffolds designed to enhance acute donor cell survival. Consequently, active caspases, a class of enzymes that are involved in apoptotic signaling (see Review (Ceccatelli et al. 2004)) were measured 72 hours after co-delivery of NSCs in medium, MC, and MC-x-LN into injured or control co-cultures. Endogenous caspase-3 activity has been reported in NSC neurospheres in the initial phase of differentiation; however, the peak level of activity was observed 24 hours after subjecting NSCs to differentiation medium and returns to

baseline after 48 hours (Fernando et al. 2005). Therefore, caspase activity assessed at 72 hours is expected designate apoptotic activity. Statistical analysis revealed that donor cell caspase activation depended significantly on the co-culture environment (injured vs. control; $p < 0.01$), the delivery method (vehicle vs. MC vs. MC-LN; $p < 0.01$), and interactions of these variables ($p < 0.05$) (Figure 5.1). Moreover, in control co-cultures, low levels of donor cell caspase activity were observed in all delivery groups. However, in the injured co-cultures, a significant increase in donor cell caspase activity was observed when NSCs were delivered within medium compared to control co-cultures ($p < 0.05$). The mean percentage of caspase activated GFP^+ donor cells was similar to the mean percentage of TUNEL+ donor cells, indicating these cells were dying via caspase mediated apoptosis (Cullen et al. 2007c). Alternatively, in injured co-cultures, the presence of MC ($n = 3$) or MC-x-LN ($n = 4$) resulted in a significant decrease in the amount donor cell caspase activity ($p < 0.05$ and $p < 0.001$, respectively) compared to in the vehicle. Although, a post-hoc power analysis assuming similar variability determined that a significant difference between MC and MC-x-LN could be detected with n=5 for each group. Therefore, a supplemental experiment was performed to not only decrease the variability, but also to examine more specific effector caspases 3 and 7.

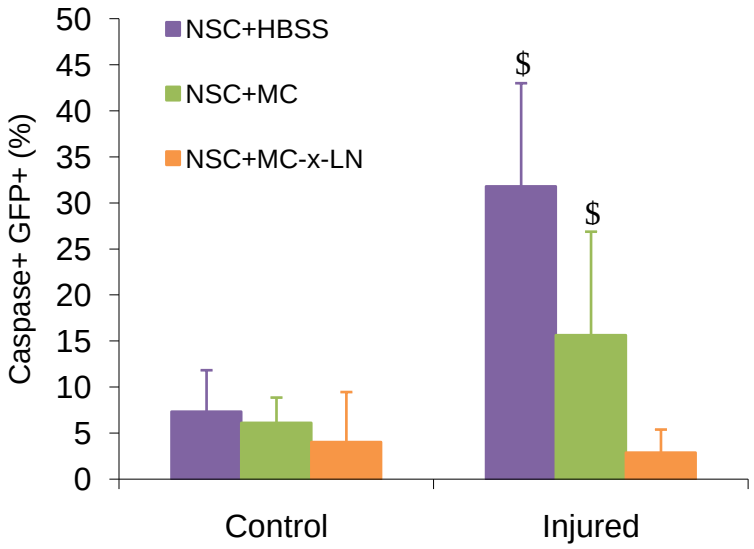

Figure 5.1 – NSC pan-caspase activity. NSCs were delivered with HBSS to the injured co-cultures, the percentage of cells with colocalized GFP and activated caspases significantly increased beyond control levels ($ represents $p < 0.05$). However, delivery in MC-x-LN and MC mitigated this effect. NSCs co-delivered in MC-x-LN to injured co-cultures reduced activated caspases to levels near donor cells in control co-cultures.

Effector Caspase 3 and 7 Activity

The experimental timeline remained the same for this study; the only variation in protocol was the FLICA reagent. Similar to the pan-caspase experiment, effector caspase-3 and -7 activity in donor cells significantly depended on co-culture conditions, delivery vehicle, and the interactions (Figure 5.2). When NSCs were delivered to control co-cultures low levels of donor cell caspase activity were observed in all delivery groups. However, when NSCs were injected to injured co-cultures within HBSS or MC, caspase 3 and 7 activity significantly increased ($p < 0.05$). Delivery in MC-x-LN significantly decreased the number of caspase+ donor cells compared to HBSS and MC delivery vehicles ($p < 0.05$). Caspase levels for all groups were moderately higher compared to the pan-caspase assay, but within one standard deviation of the respective groups. However, a notably increase was observed in the injured co-culture MC delivery group. As mentioned above, that group in the pan-caspase assay had an $n = 3$, while in the caspase 3 and 7 assay $n = 5$ cultures were evaluated. Collectively however, these two caspase assays demonstrated the benefit of co-delivering NSCs with MC-x-LN when transplanting into a hostile injury environment.

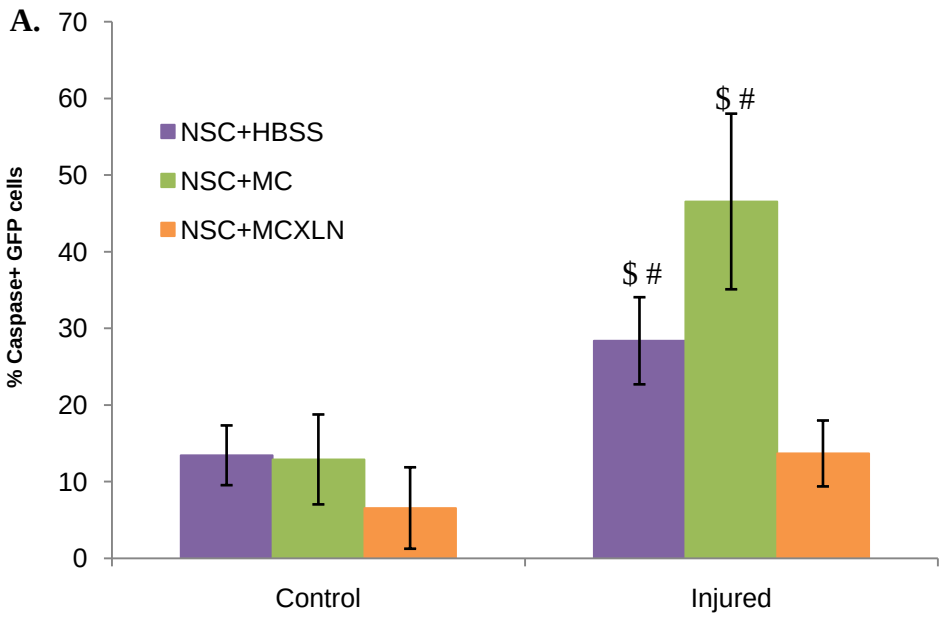

Figure 5.2 – NSC Caspase-3 and -7 Activity. (A)NSCs delivered to control co-cultures expressed low levels caspase activity in all delivery groups. However, when NSCs were injected to injured co-cultures within HBSS or MC, caspase 3 and 7 activity significantly increased. Co-delivery in MC-x-LN into injured co-cultures significantly decreased the number of caspase+ NSCs compared to HBSS and MC. Data presented as mean ± standard deviation. $ represents $p < 0.05$ relative injured MC-x-LN. # represents $p < 0.05$ relative to respective control culture group. Scale bar = 50 µm.

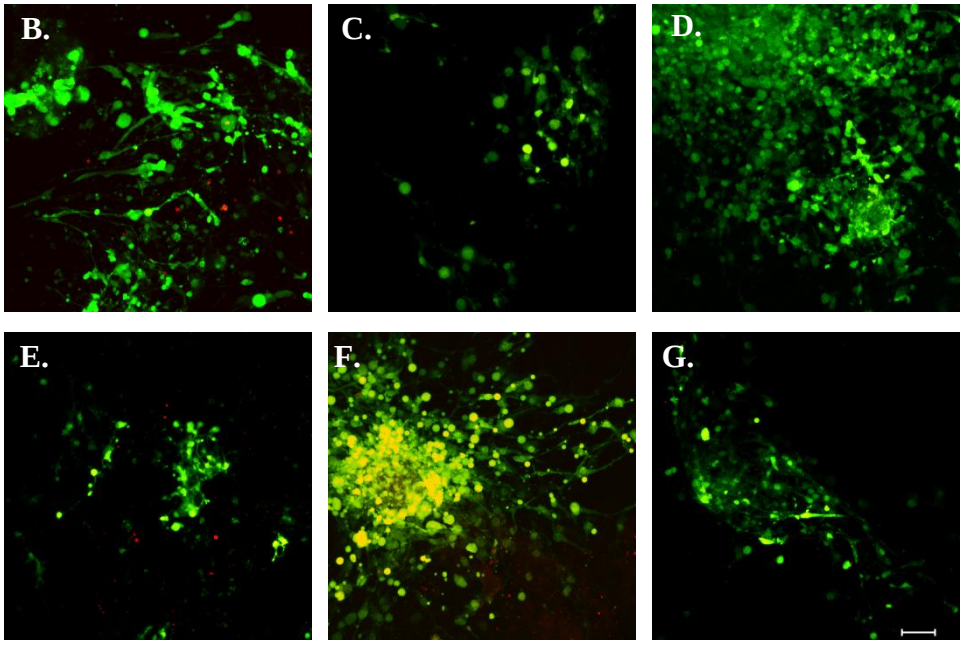

Figure 5.2 Continued – Representative confocal reconstructions of GFP^+ donor cells co-delivered with (B, E) HBSS, (C, F) MC, or (D, G) MC-x-LN in 3-D cocultures following exposure to control conditions (B-D) or mechanical injury (E-G), where the colocalization of the active caspases (red) with GFP (green) is identified by the yellow cell bodies.

In Vivo TBI Model: Neural Tissue Engineering for NSC Support

Behavior Results: Beam Walk

Motor coordination was tested throughout the duration of the transplant study with the beam walk task. Mice must traverse a 100cm beam which is divided in equal lengths into two widths, 12mm for the first 50cm and 6mm for the last 50cm. The data are presented as the percentage of right hindlimb footfalls of more than 5mm below the top of the beam. For both the 12mm (Figure 5.3) and the 6mm beams (Figure 5.4), an injury deficit was sustained; however, the sensitivity of the 12mm beam task to detect an injury deficit diminished towards the end of the testing period. Among the injured groups, no differences were evident for the various treatments tested. A post hoc power analysis for 6mm beam walk task at 8 weeks, assuming a confidence interval of 95% and a power of 0.80, a sample size of 12 animals per group would have been required to observe a difference of 20% improvement in foot falls and a sample size of 22 animals per group would have been required to detect a 30% improvement in foot falls. More extreme, the post hoc power analysis for the 12mm beam walk task at 8 weeks, to observe a only a 15% improvement effect a sample size of 53 per group would be required. Collectively, these results and analyses indicate that the 12mm beam walk task may not be sensitive enough to detect motor deficits necessary to compare treatment groups. However, the 6mm task was able to identify to finer motor deficit, but significant recovery effects may not be detected until later time points or with a large sample size.

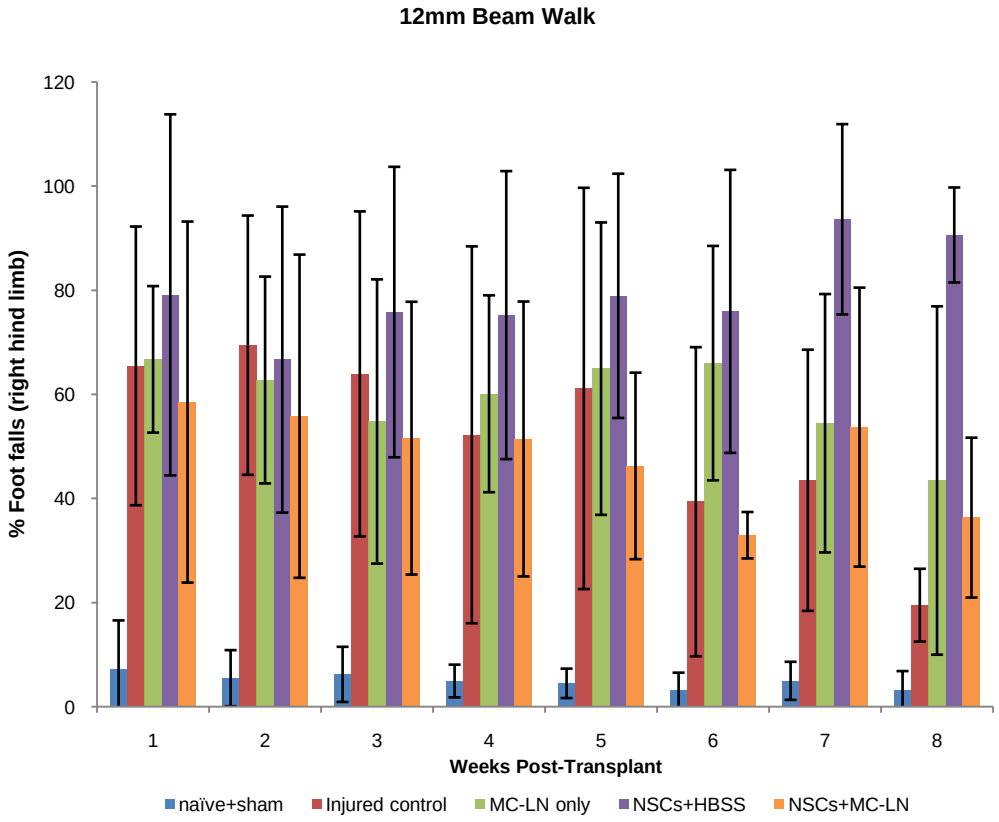

Figure 5.3 – Beam Walk Task (12mm) – Weekly behavioral test for 8 weeks post-transplantation, demonstrated a sustained injury deficit. The sensitivity of this task to detect an injury deficit in the injury controls diminished towards the end of the testing period. No differences were evident for the various treatments tested. Data presented as mean ± SEM.

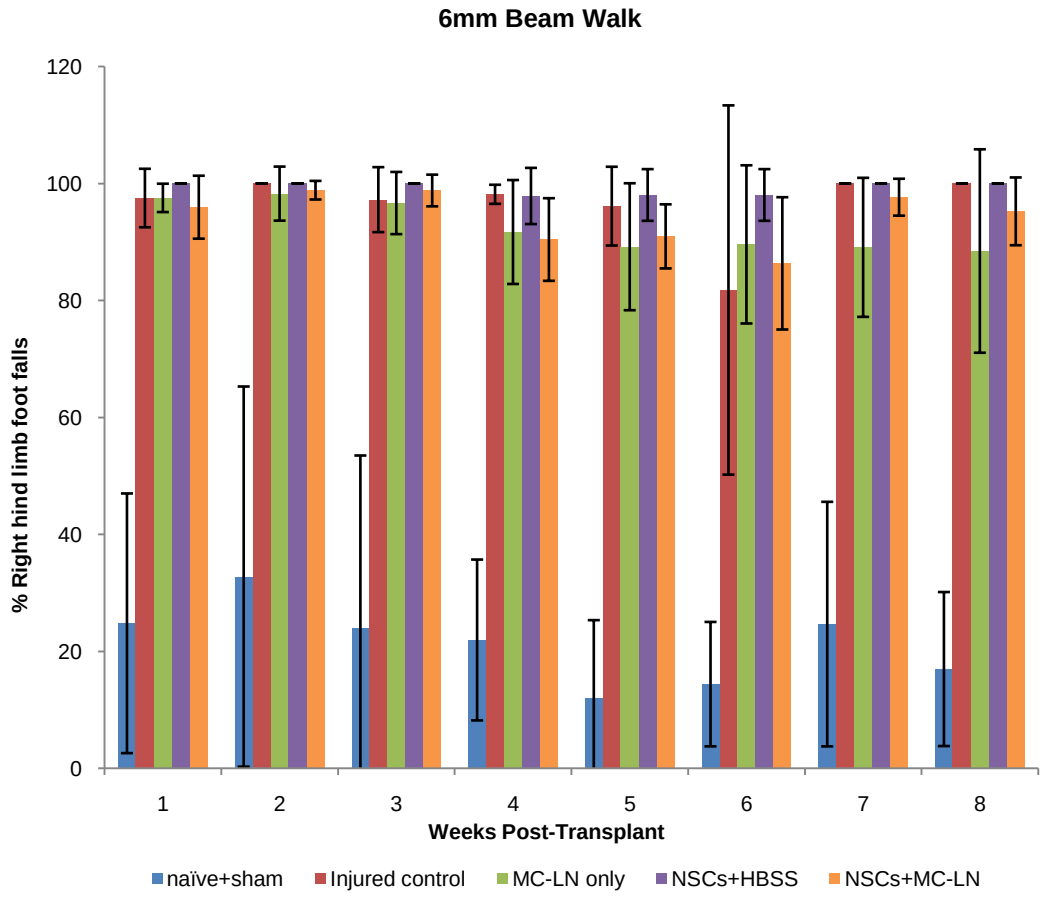

Figure 5.4 –Beam Walk Task (6mm) – Weekly behavioral test for 8 weeks post-transplantation, demonstrated a sustained injury deficit. No differences were evident for the various treatments tested. Data presented as mean ± SEM.

Host Response: GFAP intensity and Isolectin IB4

GFAP Intensity Does Not Increase with Transplantation

At 8 weeks, analysis of GFAP immunostaining intensity was performed to verify that the transplantation of the tissue engineered construct did not exacerbate the chronic glial response. It has been shown previously that MC alone implanted into a TBI injury cavity did not intensify the glial scar beyond injury controls at 1 and 4 weeks post-implant (Tate et al. 2001). The intensity of the GFAP immunostaining did not significantly change across treatment groups (MC-x-LN, NSC+HBSS, and NSC+MC-x-LN) compared to control injury. A thin section of GFAP+ tissue was located at the edge of the lesion cavity and more disperse astrocytic cell bodies observed at distances greater than 100 μm away from the cavity leading the variability in intensity measurements (Figure 5.5). Thus, the findings in this study validated the previous study demonstrating that a MC-containing tissue engineered construct does not exacerbate glial reactivity above that of the injury itself.

Isolectin IB_4^+ Immunostaining Patterns

Isolectin IB_4 staining was performed to evaluate the host tissue microglia. IB_4 not only binds to the surface of microglia, but also perivascular cells, stimulated macrophages, and laminin. Therefore, the morphology of the positive fluorescent signal must be examined prior to determining the cell type. Moderate levels of IB_4 staining were observed in all groups; however, based on morphology, minimal microglial staining was observed.

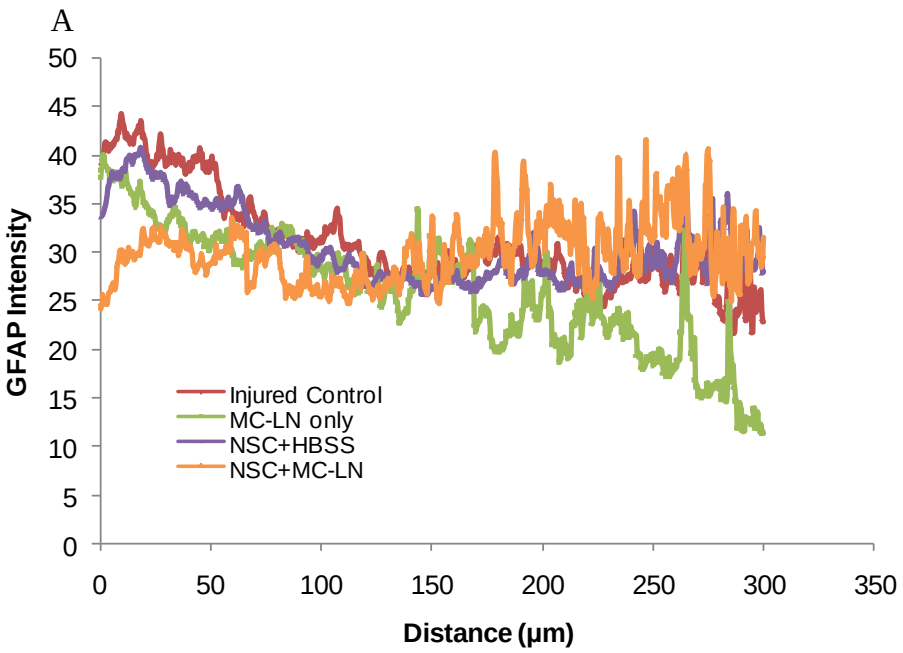

Figure 5.5 – Host Tissue GFAP Intensity. (A) Quantification of GFAP intensity as a function of distance from the injury cavity revealed no statistical difference across the groups. The intensity of 30 radial sections was averaged.

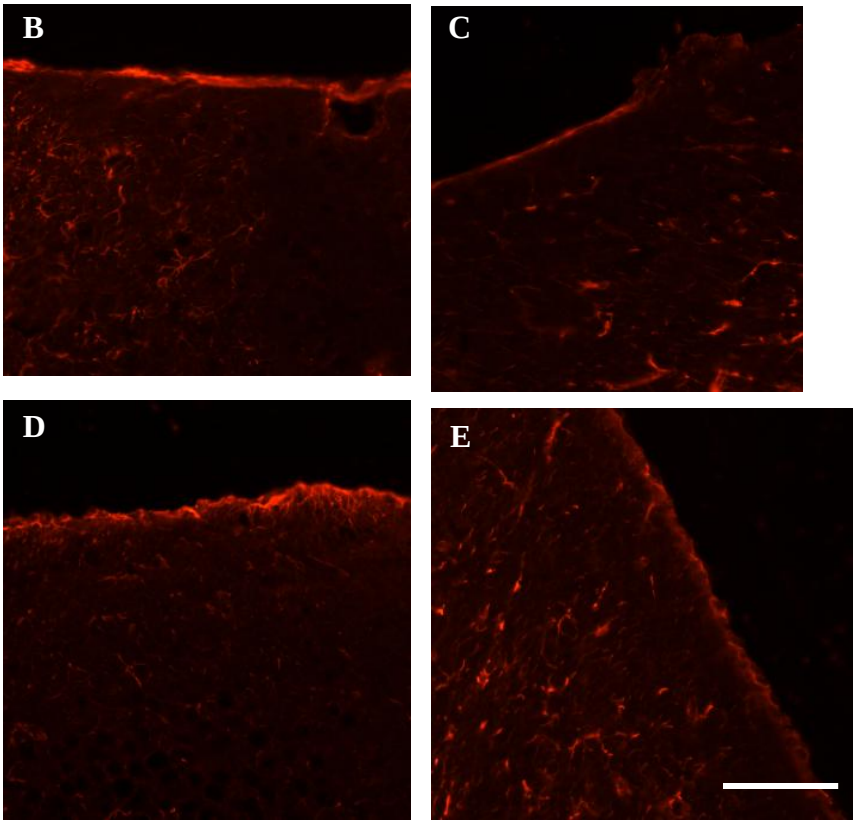

Figure 5.5 Continued – Host Tissue GFAP Intensity. (B-E) Representative images illustrating the thin strip of GFAP+ tissue at the edge of the lesion cavity; more disperse astrocytic cell bodies observed at distances greater than 100 µm away from the cavity leading the variability in intensity measurements. (B) Injury control, (C) MC-x-LN only, (D) NSC+HBSS, (D) NSC+MC-x-LN. (Scale bar = 100 µm)

Donor Cell Migration

Previous studies have demonstrated the migratory capacity of NSCs transplanted into a TBI lesion cavity (Shear et al. 2004; Tate et al. 2002). Qualitative evaluation of the donor cell engraftment location demonstrated subtle differences when NSCs were delivered within a MC-x-LN construct (n = 3 brains per group). In both HBSS and MC-x-LN delivery vehicles, the bulk of surviving donor cells were located at the anterior end of the lesion cavity. NSCs delivered in suspension form had engrafted in clusters randomly along the edges of the injury cavity; whereas, delivery within MC-x-LN resulted in engraftment at the innermost edge of the cavity near the corpus callosum (Figure 5.6). Furthermore, if NSCs engrafted to the innermost edge of the cavity, they migrated into the white matter tracts; this occurred regardless of the delivery medium. To summarize, donor cell engraftment of NSC delivered in suspension form was more random than the MC-x-LN scaffold.

Donor Cell Phenotype

The phenotypic profile of the donor cells was evaluated with immunohistochemistry and confocal laser microscopy to determine co-localization. In both HBSS and MC-x-LN modes of delivery, donor cells residing at the interior edge of the injury cavity stained with the astrocytic marker GFAP (Figure 5.7). However, the remainder of the donor cells in either group residing elsewhere in the tissue did not co-localize with any of the following immunomarkers; nestin, NG2, O4, β-tubulin III, and NeuN. This array of phenotypic markers was chosen to examine a broad range of phenotypes.

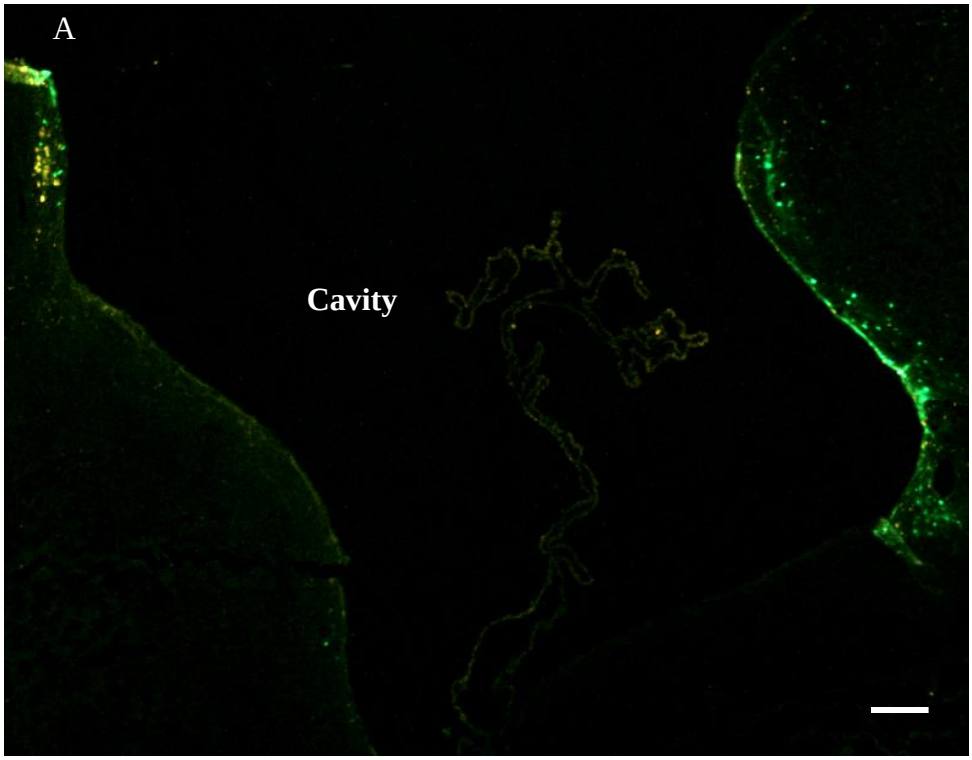

Figure 5.6 – Donor Cell Migration. (A) The distribution of donor cell engraftment when NSCs were delivered in HBSS appeared to be more random compared to the NSC+MC-x-LN groups (B) (scale bar = 200µm).

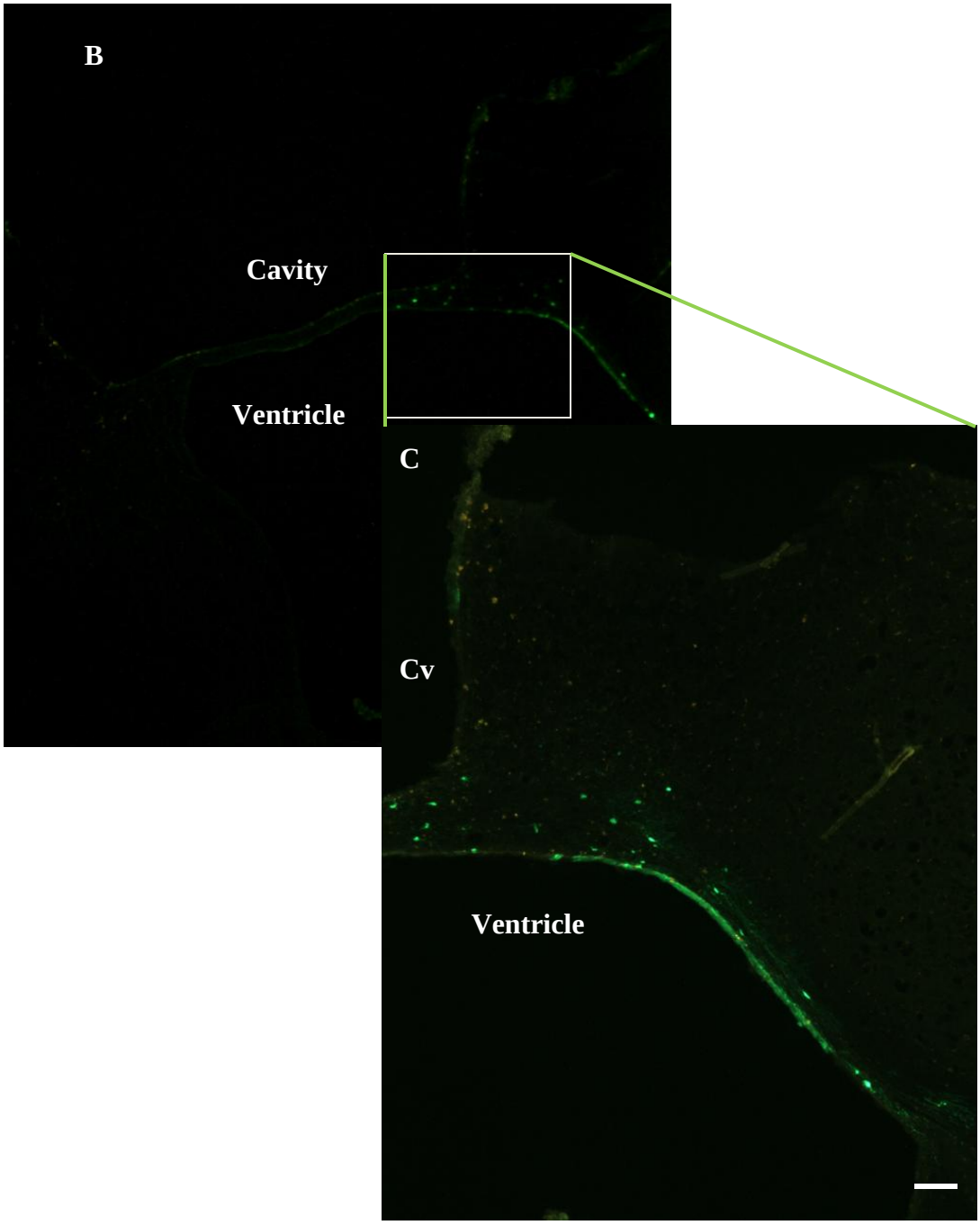

Figure 5.6 Continued – Donor Cell Migration. (A) The distribution of donor cell engraftment when NSCs were delivered in HBSS appeared to be more random compared to the NSC+MC-x-LN groups (B) (scale bar = 200µm). The higher magnification image (C) demonstrates the migration along the white matter track away from the cavity. (scale bar = 100 µm)

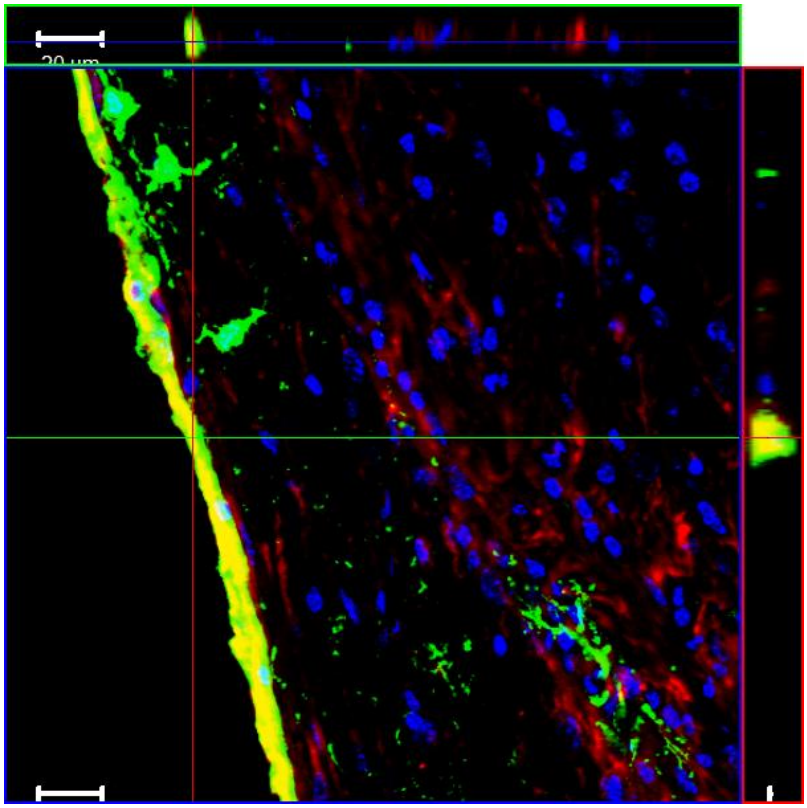

Figure 5.7 – Donor Cell Phenotype. Orthogonal view of a confocal micrograph along the medial edge of the injury cavity of a NSC+MC-x-LN transplant demonstrates the co-localization of GFP (green) and GFAP (red). Similar observations were made with most donor cells lining the injury cavity regardless of the transplant vehicle. Blue = Hoechst counterstain, scale bar = 20µm.

Discussion

This study combined an *in vivo* transplant model with an innovative *in vitro* model in order to evaluate the ability of tissue engineered construct scaffold to support NSCs in a neural injury environment. *In vitro*, the MC-x-LN scaffold protected the NSCs from apoptosis when injected into an injured co-culture. Specifically, effector caspases-3 and -7 activity was reduced when NSCs were delivered in a MC-x-LN scaffold. Although recovery of motor function, as tested with the beam walk task, was not observed *in vivo*, differences in donor cell engraftment and migratory locations were detected. Collectively, this study reinforced the significant role the extracellular environment plays in NSC fate.

Apoptosis of neural transplantation has been recorded in a range of injurious and neurodegenerative pathologies (Bakshi et al. 2005; Chen et al. 2002; Emgard et al. 2003; Marchionini et al. 2004). Activation of apoptotic signaling pathways has been detected as early as 90 minutes after transplantation in Parkinson's model and 24 hrs in a TBI model (Bakshi et al. 2005; Emgard et al. 2003). Furthermore, a significantly higher percentage of donor cells were shown to undergo caspase-mediated apoptosis in the traumatically injured brain compared to transplants delivered to sham brains (Bakshi et al. 2005). Therefore, the milieu within a traumatically injured brain induces detrimental effects on neural transplants. The results from the *in vitro* co-culture study support this theory, as an increase in caspase activity was observed following injection of unsupported NSCs into the injured neuron-astrocyte culture (Cullen et al. 2007c). Moreover, this response has been shown to be specific to the factors within a mechanically injured co-culture, as chemical induction of astrogliosis in the same co-

culture did not affect NSC apoptosis (Cullen et al. 2007c). In order to mitigate this cell death a 3-D matrix decorated with LN protected NSCs caspase-mediated apoptosis.

Previous *in vitro* studies have examined NSC response to reactive astrocyte or 2-D injured neural co-cultures to primarily examine NSC differentiation and migratory patterns (Chang et al. 2003; Faijerson et al. 2006; Song et al. 2002). Specifically, culturing NSCs on reactive astrocytes (scratch injury model) or in the presence of injury conditioned media has shown to increase the NSC propensity to differentiate into astrocytes, while not affecting neuronal or oligodendrocyte differentiation (Faijerson et al. 2006). Reactive astrocytes have been shown to secrete ciliary neurotrophic factor (CNTF) and leukemia inhibitor factor (LIF), both of which induce NSC astrocyte differentiation (Banner et al. 1997; Faijerson et al. 2006; Ilkhanizadeh et al. 2007; Ip et al. 1993; Johe et al. 1996; Nakajima et al. 2007). Transplantation into a TBI lesion cavity consequentially exposes donor cells to a reactive glial environment where levels of CNTF and LIF have been shown to increase after injury (Banner et al. 1997; Ip et al. 1993; Oyesiku et al. 1999). At 8 weeks i*n vivo*, we observed that donor cells residing along the injury cavity were $GFAP^+$, possibly due to secreted factors from host reactive astrocytes. Moreover, donor cells that migrated away from the injury cavity penumbra were not $GFAP^+$; however, the migratory donor cells did not stain for the selection of phenotypic markers we chose to evaluate (NG2, O4, NeuN, β-tubulin III, nestin). Similar TBI transplant studies, in which NSCs have demonstrated that donor NSC are $NG2^+$ at 14 months; however, the transplant site was in the striatum below the injury cavity (Shear et al. 2004). Such comparisons across transplant studies are difficult due to the variations

in the injury model, severity, time of transplantation, donor cell type, and transplant location.

Recently, a side-by-side comparison of transplantation into mild and severe brain injuries demonstrated a significant influence on donor cell survival; the mild injury provided a more hospitable environment for donor cells (Shindo et al. 2006). Moreover, the site of transplantation has been shown to influence donor survival, migration, and differentiation (Watson et al. 2006). Effectively, the interaction between the donor cells and the microenvironment will dictate the success of the transplantation.

Based on qualitative evaluation, the engraftment and migratory location of the donor cells in this study was modified by a tissue engineering scaffold. NSCs transplanted within MC-x-LN were primarily located along the medial wall of the cavity or had migrated into the corpus callosum, while the engraftment pattern for NSCs delivered in HBSS appeared to be more random and clustered. Similarly, a previous study used a collagen I and fibronectin scaffold to transplant NSCs in a TBI model and observed a significant increase in NSC cell number and migration compared to NSCs delivered without the scaffold (Tate et al. 2002). These results strengthen the contention that NSC fate will be affected by incorporating pro-survival and other positive factors into the NSC transplant microenvironment.

In conclusion, the results from this study demonstrated that MC-x-LN had positive influence on acute NSC survival in a hostile neural injury environment. Furthermore, evaluation of the tissue engineering scaffold in a more chronic *in vivo* TBI model indicated alterations in NSC engraftment compared to NSCs delivered in HBSS. Further *in vivo* analysis (i.e. additional time points and behavioral tests) would strengthen

this study, yet the results suggest that modifying the transplant microenvironment through an ECM presenting delivery scaffold system will enhance donor cell survival and migration.

Acknowledgements

The *in vitro* co-culture study was a collaborative effort that involved multiple researchers. The neuron-astrocyte co-culture and subsequent injury characterizations was performed primarily by D.K. Cullen with the assistance of C.M. Simon under the direction of M.C. LaPlaca (Cullen and LaPlaca 2006; Cullen et al. 2007b; Cullen et al. 2007c; LaPlaca et al. 2005). We acknowledge Ciara Tate for help with the injury device and behavior studies. We would also like to acknowledge Hillary Irons, who the caspase-3 and-7 assay and the *in vivo* study were performed with. Moreover, the tissue processing for the *in vivo* could not have been done without the help from Sharon Byers and the following undergraduate students: Scott Medway, Vishnu Ambur, and Gautam Munglani.

CHAPTER 6: CONCLUSIONS AND FUTURE DIRECTIONS

Conclusions

In conclusion, the findings of this thesis identified the potential for a MC-LN scaffold to be used for neural tissue engineering. Moreover and possibly more importantly, the sub-studies performed throughout this thesis contributed to the basic knowledge of neural cell response to biomaterials. Two different LN tethering chemistries were evaluated. The first scheme utilized carbohydrate chemistry to immobilize LN on MC. While the viability was shown to increase with this method, neurite outgrowth was not supported. Therefore, an alternative tethering method that employed a heterobifunctional crosslinker (sulfo-SANPAH) was examined and the amount of bound LN increased immensely. By utilizing the sulfo-SANPAH as an intermediate tethering arm, we established that neuronal viability and neurite outgrowth was not solely dependent on LN tethering density. Instead, a prominent interaction between substrate stiffness and ligand density on neuronal survival and neurite outgrowth was observed. Therefore, the beginning segment of this thesis work highlighted critical material properties that need to be considered and evaluated in a cell-type specific manner.

Providing 3-D LN moieties to NSCs proved to influence the survival, differentiation, and production of ECM proteins. Specifically, presentation of LN within the microenvironment of the NSCs decreased the percentage of apoptosis. Furthermore, the spatial profile of both phenotypic differentiation and production of ECM proteins within the neurosphere was altered when NSCs were exposed to MC-x-LN. Differences in differentiation and ECM/integrin production profiles were observed not just at the

periphery of the neurosphere (i.e., cell-ECM interface with MC-x-LN), but variations were noted across the entire neurosphere. These results are particularly exciting as they demonstrated a transducing effect the extracellular environment has on cells within the neurosphere center.

A unique aspect of this thesis was the implementation of multiple injury models to examine the ability of a bioadhesive matrix to protect NSCs from detrimental factors transplants are exposed to in traumatically injured CNS tissue. First, we utilized was a previously established *in vitro* injury model comprised of a 3-D co-culture of primary neurons and astrocytes. After subjecting the 3-D co-culture to a mechanical shear deformation, NSCs were injected into the center of the co-culture thereby immersing the NSCs in a potentially pathological environment. This study reported NSCs delivered in a traditional transplant suspension form had a higher incidence of effector caspase activity than when delivered within MC-x-LN. NSC caspases activity within MC-x-LN delivered to the injured co-culture was maintained at the same level as control co-culture injections. Therefore, this study demonstrated the pro-survival affects of an integrin engaging matrix on cellular transplants delivered to injured environments.

Lastly, we co-transplanted the MC-x-LN with NSCs into a murine *in vivo* TBI model. The construct was transplanted 7 days post-injury into the injury cavity. For 8 weeks post-transplant, weekly motor functional recovery was evaluated with the beam walk task. We performed histological analysis at 8 weeks post-transplant to evaluate donor cell and host response. Collectively, the results from the beam walk task demonstrated a moderated increase in functional recovery when MC-x-LN or MC-x-LN +NSCs were transplanted. Due to the variability among groups and large number of

sample groups, no statistical differences were observed with this motor task. We cannot rule out potential recovery in behavior that was not evaluated with this task. The host response at 8 weeks measured through GFAP staining and IB_4 staining was not exacerbated by any of the experimental transplant groups beyond the injured control. The engraftment and migratory profile of donor cells was altered when NSCs were transplanted into a contused brain with MC-LN. NSCs transplanted with MC-x-LN engrafted in the anterior medial portion of the injury cavity. However, NSCs delivered in HBSS engrafted in a more random pattern along the injury cavity; NSCs were found along the medial and lateral sides of the injury cavity. If the NSCs engrafted near the medial portion of the cavity regardless of the transplant medium, NSCs migrated into the corpus callosum. NSCs that took residence along the injury cavity stained positive for GFAP, indicative of an astrocyte phenotype. However, migrating cells did not stain positive for any of the probed immunomarkers. While we did not observed significant changes in behavioral or histological outcome measures, the results indicated that both microenvironmental factors present in the transplant medium and the injury environment dictate donor cell fate.

Discussion and Future Directions

This project encompassed a multi-level developmental analysis of a biomaterial for neural tissue engineering, a format that has many advantages for biomaterials testing. Challenging a biomaterial with multiple relevant cell types and with both *in vitro* and *in vivo* injury models demonstrates the robustness this material.

Multiple factors influence cell transplant outcome in TBI models, such as time (Zhang et al. 2005), location (Watson et al. 2006), and injury severity (Shindo et al.

2006). TBI initiates a complex set of signaling cascades consisting of excitotoxicity, release of reactive oxygen species, and inflammatory response (McIntosh et al. 1998). According to the literature, much of this initial wave of secondary injury response subsides after one week after injury (Lenzlinger et al. 2001; McIntosh et al. 1998; Ray et al. 2002), therefore, we transplanted at this time. Due to the injectable scaffold design, we transplanted into the injury cavity as an effort to not to disrupt the intact brain. This transplant design may need to be reconsidered based on recent reports indicating that acute transplantation post-injury results in a high incidence of donor cell death whereas transplantation 1 month post-injury resulted in higher levels of donor cell survival (Zhang et al. 2005). Moreover, our transplant location may need to be reevaluated. The injury cavity is at the heart of astrogliosis and inflammatory response. Therefore, injecting donor cells directly to that hostile environment may have detrimental effects on donor cells. Moreover, researchers have reported a correlation between transplantation site and donor cell differentiation (Watson et al. 2006). Ultimately, to achieve transplantation success, the microenvironment in which the donor cells will be immersed needs to be further characterized to predict donor cell response. Several areas for future work using this approach, in light of the above issues, should be considered. A few of these directions are discussed below.

Acute *In Vivo* Transplant Study

An acute transplant study with the *in vivo* mouse TBI model would complement the results gathered in this project. This study would achieve two goals: 1. Assess the efficacy of a MC-LN scaffold to maintain NSC survival, and 2. Evaluate the predictive capacity of the *in vitro* injury model for transplant paradigms. Outcome measures would

include apoptotic assays (e.g., TUNEL, effector caspase activity) and evaluation of suspected pro-survival signaling pathways that may be upregulated in the presence of LN. This acute study would also enable us to evaluate potential pro-survival signaling mechanisms of the donor cells *in vivo*. Proposed signaling pathways for LN-integrin interactions include phosphorylation of AKT.

Polymeric Scaffold Modification

We have established MC for neural tissue engineering applications; however, this system has limits that could be improved upon. Namely, a future system would be a polymeric blend with MC that maintains the thermoreversible component, but also incorporates polymer backbone with multiple branches for tethering chemistries (e.g., polyethylene glycol). By incorporating additional polymer chains, multiple ligands could be immobilized in the scaffold matrix. Additional ligand support would potentially direct differentiation and increase the proliferate capacity of the NSCs. Moreover, inclusion of an enzymatic cleavable region would allow for migrating cells to degrade the matrix and increase the tortuosity of the scaffold for other migratory cells. Collectively, the aforementioned design aspects should be considered when designing the next generation neural tissue engineering scaffold.

Integration of Soluble Factors

This study focused on adhesive ECM to improve NSC survival and did not examine the influence of soluble growth factors. For example, bFGF or EGF could be integrated into the matrix as the compounding effects of the mitogens and LN has been shown to increase the proliferative capacity of NSCs (Nakajima et al. 2007). Furthermore, pro-survival signaling pathways of certain growth factors converge with the

signaling pathways of LN. Therefore, bioadhesive support and growth factors could be coupled together to block apoptosis of donor cells transplanted in TBI models. Various growth factors also target differentiation of NSCs. Ultimately, to overcome pathological signals observed in transplant paradigms, multiple pro-survival cues may need to be integrated into a delivery matrix.

Peptide Sequences

Tethering of peptide sequences instead of proteins enables the generation of a matrix with a high density of specific active sequences. LN is a large heterotrimeric protein with multiple active sequences. Table 6.1 highlights a couple of sequences that interact with specific neural receptors. High density presentation of the sequence IKVAV has been shown to preferentially support the neuronal differentiation of NSCs. Additionally, the sequence IKLLI has been shown to prevent neuronal apoptosis (Gary and Mattson 2001; Gary et al. 2003). Ideally, numerous sequences could be presented in a concerted manner within a synthetic matrix in order to tailor to specific cell types and cell functions. For example, IKLLI and IKVAV could be presented simultaneously to enhance neuronal differentiation while preventing apoptosis.

Table 6.1: LN peptide sequences that have relevant functional responses on neural cells

Peptide Sequence	Origin	Receptor/Cellular Interactions	Functional Response	Reference
E**IKLLI**S	LN α1-chain G domain	$\alpha_3\beta_1$, $\alpha_6\beta_1$ integrins, surface heparan sulfate proteoglycan	Heparin binding, cell adhesion, PC-12 neurite extension, Activates integrin-linked kinase (ILK), prevents Akt-mediated apoptosis	(Gary and Mattson 2001; Gary et al. 2003; Tashiro et al. 1999; Tashiro et al. 1989)
IKVAV	LN α1 chain G domain	110kDa binding protein	Cell adhesion, neurite outgrowth	(Kleinman et al. 1988; Nomizu et al. 1995)
PA – (both **IKLLI** and **IKVAV)**	LN α1 chain G domain	$\alpha_3\beta_1$, $\alpha_6\beta_1$ integrin, surface heparan sulfate proteoglycan	Heparin binding, cell adhesion, PC-12 neurite extension	(Tashiro et al. 1999)

To conclude, this project aimed to address the current limitations in transplant technology for TBI. Tissue engineering may be a solution to this limitation, yet the current in the scaffold design did not conquer these limitations. The theme throughout this thesis is the critical need to improve transplant survival. This goal will not be accomplished until the impact the pathological transplant environment on donor cell is understood. This is not a trivial task considering the dynamic sequence of signaling events that occurs after TBI. Moreover, the time and location of transplant could be the dominating factors in developing an effective transplant paradigm. To this end, future TBI transplantation studies should focus on acute time points post-transplant in an effort to maximize donor survival as well as elucidate the mediators of donor cell death.

In light of the discussed limitations, this project significantly impacted the neurotransplantation field by contributing to the knowledge NSC survival mechanisms. We engineered a delivery scaffold for NSC transplants and established an anti-apoptotic effect of LN on NSCs. More importantly, this effect was not only observed within optimal *in vitro* culture conditions, but also after exposing the NCS-scaffold constructs to an *in vitro* mechanical injury model. Thus, the results from this project will enhance the neurotransplantation field by challenging researchers to respect and work toward modulating the microenvironment for transplanted cells.

REFERENCES

2004. 2004 Annual Statistical Report. Birmingham, AL: National Spinal Cord Injury Statistical Center, University of Alabama at Birmingham. 24 p.

Aarum J, Sandberg K, Haeberlein SL and Persson MA. 2003. Migration and differentiation of neural precursor cells can be directed by microglia. Proc Natl Acad Sci U S A 100(26):15983-15988.

Adekoya N, Thurman DJ, White DD and Webb KW. 2002. Surveillance for Traumatic Brain Injury Deathes - United States, 1989-1998. Morbidity and Mortality Weekly Report 51(SS-10):1-15.

Adelson PD, Ragheb J, Kanev P, Brockmeyer D, Beers SR, Brown SD, Cassidy LD, Chang Y and Levin H. 2005. Phase II clinical trial of moderate hypothermia after severe traumatic brain injury in children. Neurosurgery 56(4):740-754; discussion 740-754.

Bakshi A, Keck CA, Koshkin VS, LeBold DG, Siman R, Snyder EY and McIntosh TK. 2005. Caspase-mediated cell death predominates following engraftment of neural progenitor cells into traumatically injured rat brain. Brain Research 1065:8-19.

Bakshi A, Shimizu S, Keck CA, Cho S, LeBold DG, Morales D, Arenas E, Snyder EY, Watson DJ and McIntosh TK. 2006. Neural progenitor cells engineered to secrete GDNF show enhanced survival, neuronal differentiation and improve cognitive function following traumatic brain injury. European Journal of Neuroscience 23(8):2119-2134.

Balgude AP, Yu X, Szymanski A and Bellamkonda RV. 2001. Agarose gel stiffness determines rate of DRG neurite extension in 3D cultures. Biomaterials 22(10):1077-1084.

Banner LR, Moayeri NN and Patterson PH. 1997. Leukemia inhibitory factor is expressed in astrocytes following cortical brain injury. Exp Neurol 147(1):1-9.

Bellamkonda R, Ranieri JP and Aebischer P. 1995a. Laminin Oligopeptide Derivatized Agarose Gels Allow 3- Dimensional Neurite Extension in-Vitro. Journal of Neuroscience Research 41(4):501-509.

Bellamkonda R, Ranieri JP, Bouche N and Aebischer P. 1995b. Hydrogel-based three-dimensional matrix for neural cells. J Biomed Mater Res 29(5):663-671.

Bhang SH, Lee YE, Cho SW, Shim JW, Lee SH, Choi CY, Chang JW and Kim BS. 2007. Basic fibroblast growth factor promotes bone marrow stromal cell

transplantation-mediated neural regeneration in traumatic brain injury. Biochem Biophys Res Commun 359(1):40-45.

Boley SE, Wong VA, French JE and Recio L. 2002. p53 heterozygosity alters the mRNA expression of p53 target genes in the bone marrow in response to inhaled benzene. Toxicol Sci 66(2):209-215.

Boockvar JA, Schouten J, Royo N, Millard M, Spangler Z, Castelbuono D, Snyder E, O'Rourke D and McIntosh T. 2005. Experimental traumatic brain injury modulates the survival, migration, and terminal phenotype of transplanted epidermal growth factor receptor-activated neural stem cells. Neurosurgery 56(1):163-171.

Boontheekul T and Mooney DJ. 2003. Protein-based signaling systems in tissue engineering. Curr Opin Biotechnol 14(5):559-565.

Brannvall K, Bergman K, Wallenquist U, Svahn S, Bowden T, Hilborn J and Forsberg-Nilsson K. 2007. Enhanced neuronal differentiation in a three-dimensional collagen-hyaluronan matrix. J Neurosci Res 85(10):2138-2146.

Brewer GJ. 1997. Isolation and culture of adult rat hippocampal neurons. Journal of Neuroscience Methods 71(2):143-155.

Busch SA and Silver J. 2007. The role of extracellular matrix in CNS regeneration. Curr Opin Neurobiol 17(1):120-127.

Bussemer T, Dashevsky A and Bodmeier R. 2003. A pulsatile drug delivery system based on rupturable coated hard gelatin capsules. Journal of Controlled Release 93(3):331-339.

Byers BA, Pavlath GK, Murphy TJ, Karsenty G and Garcia AJ. 2002. Cell-type-dependent up-regulation of in vitro mineralization after overexpression of the osteoblast-specific transcription factor Runx2/Cbfa1. Journal of Bone and Mineral Research 17(11):1931-1944.

Calatayud Maldonado V, Calatayud Perez JB and Aso Escario J. 1991. Effects of CDP-choline on the recovery of patients with head injury. J Neurol Sci 103 Suppl:S15-18.

Campos LS. 2004. Neurospheres: insights into neural stem cell biology. J Neurosci Res 78(6):761-769.

Campos LS. 2005. Beta1 integrins and neural stem cells: making sense of the extracellular environment. Bioessays 27(7):698-707.

Campos LS, Leone DP, Relvas JB, Brakebusch C, Fassler R, Suter U and ffrench-Constant C. 2004. Beta1 integrins activate a MAPK signalling pathway in neural stem cells that contributes to their maintenance. Development 131(14):3433-3444.

Ceccatelli S, Tamm C, Sleeper E and Orrenius S. 2004. Neural stem cells and cell death. Toxicology Letters 149(1-3):59-66.

Chang MY, Son H, Lee YS and Lee SH. 2003. Neurons and astrocytes secrete factors that cause stem cells to differentiate into neurons and astrocytes, respectively. Molecular and Cellular Neuroscience 23(3):414-426.

Chao DT and Korsmeyer SJ. 1998. BCL-2 family: regulators of cell death. Annu Rev Immunol 16:395-419.

Chen J, Li Y, Wang L, Lu M and Chopp M. 2002. Caspase inhibition by Z-VAD increases the survival of grafted bone marrow cells and improves functional outcome after MCAo in rats. J Neurol Sci 199(1-2):17-24.

Chen S, Pickard JD and Harris NG. 2003. Time course of cellular pathology after controlled cortical impact injury. Experimental Neurology 182(1):87-102.

Chothia C and Jones EY. 1997. The molecular structure of cell adhesion molecules. Annual Review of Biochemistry 66:823-862.

Coats B and Margulies SS. 2006. Material properties of porcine parietal cortex. J Biomech 39(13):2521-2525.

Colognato H and Yurchenco PD. 2000. Form and function: The laminin family of heterotrimers. Developmental Dynamics 218(2):213-234.

Cukierman E, Pankov R, Stevens DR and Yamada KM. 2001. Taking cell-matrix adhesions to the third dimension. Science 294(5547):1708-1712.

Cukierman E, Pankov R and Yamada KM. 2002. Cell interactions with three-dimensional matrices. Current Opinion in Cell Biology 14(5):633-639.

Cullen DK and LaPlaca MC. 2006. Neuronal response to high rate shear deformation depends on heterogeneity of the local strain field. J Neurotrauma 23(9):1304-1319.

Cullen DK, Lessing MC and LaPlaca MC. 2007a. Collagen-dependent neurite outgrowth and response to dynamic deformation in three-dimensional neuronal cultures. Ann Biomed Eng 35(5):835-846.

Cullen DK, Simon CM and Laplaca MC. 2007b. Strain rate-dependent induction of reactive astrogliosis and cell death in three-dimensional neuronal-astrocytic co-cultures. Brain Res 1158:103-115.

Cullen DK, Stabenfeldt SE, Simon CM, Tate CC and Laplaca MC. 2007c. In vitro neural injury model for optimization of tissue-engineered constructs. J Neurosci Res.

Dai WG, Belt J and Saltzman WM. 1994. Cell-Binding Peptides Conjugated to Poly(Ethylene Glycol) Promote Neural Cell-Aggregation. Bio-Technology 12(8):797-801.

Davies AR. 2005. Hypothermia improves outcome from traumatic brain injury. Crit Care Resusc 7(3):238-243.

Decker T and Lohmann-Matthes ML. 1988. A quick and simple method for the quantitation of lactate dehydrogenase release in measurements of cellular cytotoxicity and tumor necrosis factor (TNF) activity. J Immunol Methods 115(1):61-69.

Desbrieres J, Hirrien M and Ross-Murphy SB. 2000. Thermogelation of methylcellulose: rheological considerations. Polymer 41(7):2451-2461.

Dihne M, Bernreuther C, Hagel C, Wesche KO and Schachner M. 2006. Embryonic stem cell-derived neuronally committed precursor cells with reduced teratoma formation after transplantation into the lesioned adult mouse brain. Stem Cells 24(6):1458-1466.

Dixon CE, Clifton GL, Lighthall JW, Yaghmai AA and Hayes RL. 1991. A controlled cortical impact model of traumatic brain injury in the rat. J Neurosci Methods 39(3):253-262.

Dixon CE, Kochanek PM, Yan HQ, Schiding JK, Griffith RG, Baum E, Marion DW and DeKosky ST. 1999. One-year study of spatial memory performance, brain morphology, and cholinergic markers after moderate controlled cortical impact in rats. J Neurotrauma 16(2):109-122.

Dodla MC and Bellamkonda RV. 2006. Anisotropic scaffolds facilitate enhanced neurite extension in vitro. J Biomed Mater Res A 78(2):213-221.

Duan WM, Zhao LR, Westerman M, Lovick D, Furcht LT, McCarthy JB and Low WC. 2000. Enhancement of nigral graft survival in rat brain with the systemic administration of synthetic fibronectin peptide V. Neuroscience 100(3):521-530.

El-Khatib RM. 2002. Spectrophotometric detection of methyl cellulose-manganate(VI) intermediate complex in the oxidation of methyl cellulose by alkaline permanganate. Carbohydrate Polymers 49:337-345.

Emgard M, Hallin U, Karlsson J, Bahr BA, Brundin P and Blomgren K. 2003. Both apoptosis and necrosis occur early after intracerebral grafting of ventral mesencephalic tissue: a role for protease activation. J Neurochem 86(5):1223-1232.

Engstrom CM, Demers D, Dooner M, McAuliffe C, Benoit BO, Stencel K, Joly M, Hulspas R, Reilly JL, Savarese T, Recht LD, Ross AH and Quesenberry PJ. 2002. A method for clonal analysis of epidermal growth factor-responsive neural progenitors. J Neurosci Methods 117(2):111-121.

Faijerson J, Tinsley RB, Aprico K, Thorsell A, Nodin C, Nilsson M, Blomstrand F and Eriksson PS. 2006. Reactive astrogliosis induces astrocytic differentiation of adult neural stem/progenitor cells in vitro. J Neurosci Res 84(7):1415-1424.

Fann JR, Uomoto JM and Katon WJ. 2001. Cognitive improvement with treatment of depression following mild traumatic brain injury. Psychosomatics 42(1):48-54.

Fawcett JW and Asher RA. 1999. The glial scar and central nervous system repair. Brain Research Bulletin 49(6):377-391.

Fernando P, Brunette S and Megeney LA. 2005. Neural stem cell differentiation is dependent upon endogenous caspase 3 activity. FASEB J 19(12):1671-1673.

Flanagan LA, Ju YE, Marg B, Osterfield M and Janmey PA. 2002. Neurite branching on deformable substrates. Neuroreport 13(18):2411-2415.

Flanagan LA, Rebaza LM, Derzic S, Schwartz PH and Monuki ES. 2006. Regulation of human neural precursor cells by laminin and integrins. J Neurosci Res 83(5):845-856.

Flynn L, Dalton PD and Shoichet MS. 2003. Fiber templating of poly(2-hydroxyethyl methacrylate) for neural tissue engineering. Biomaterials 24(23):4265-4272.

Fox GB and Faden AI. 1998. Traumatic brain injury causes delayed motor and cognitive impairment in a mutant mouse strain known to exhibit delayed Wallerian degeneration. J Neurosci Res 53(6):718-727.

Fox GB, Fan L, Levasseur RA and Faden AI. 1998. Sustained sensory/motor and cognitive deficits with neuronal apoptosis following controlled cortical impact brain injury in the mouse. J Neurotrauma 15(8):599-614.

Freire E, Gomes FCA, Linden R, Neto VM and Coelho-Sampaio T. 2002. Structure of laminin substrate modulates cellular signaling for neuritogenesis. Journal of Cell Science 115(24):4867-4876.

Friedl P and Brocker EB. 2000. The biology of cell locomotion within three-dimensional extracellular matrix. Cell Mol Life Sci 57(1):41-64.

Fujimoto ST, Longhi L, Saatman KE and McIntosh TK. 2004. Motor and cognitive function evaluation following experimental traumatic brain injury. Neuroscience & Biobehavioral Reviews 28(4):365-378.

Gao J, Prough DS, McAdoo DJ, Grady JJ, Parsley MO, Ma L, Tarensenko YI and Wu P. 2006. Transplantation of primed human fetal neural stem cells improves cognitive function in rats after traumatic brain injury. Exp Neurol 201(2):281-292.

Garcia AJ, Vega MD and Boettiger D. 1999. Modulation of cell proliferation and differentiation through substrate-dependent changes in fibronectin conformation. Molecular Biology of the Cell 10(3):785-798.

Gary DS and Mattson MP. 2001. Integrin signaling via the PI3-kinase-Akt pathway increases neuronal resistance to glutamate-induced apoptosis. Journal of Neurochemistry 76(5):1485-1496.

Gary DS, Milhavet O, Camandola S and Mattson MP. 2003. Essential role for integrin linked kinase in Akt-mediated integrin survival signaling in hippocampal neurons. Journal of Neurochemistry 84(4):878-890.

Gefen A and Margulies SS. 2004. Are in vivo and in situ brain tissues mechanically similar? J Biomech 37(9):1339-1352.

Georges PC, Miller WJ, Meaney DF, Sawyer ES and Janmey PA. 2006. Matrices with compliance comparable to that of brain tissue select neuronal over glial growth in mixed cortical cultures. Biophys J 90(8):3012-3018.

Gersbach CA, Byers BA, Pavlath GK and Garcia AJ. 2004. Runx2/Cbfa1 stimulates transdifferentiation of primary skeletal myoblasts into a mineralizing osteoblastic phenotype. Experimental Cell Research 300(2):406-417.

Grasso G, Sfacteria A, Meli F, Passalacqua M, Fodale V, Buemi M, Giambartino F, Iacopino DG and Tomasello F. 2007. The role of erythropoietin in neuroprotection: therapeutic perspectives. Drug News Perspect 20(5):315-320.

Gray DS, Tien J and Chen CS. 2003. Repositioning of cells by mechanotaxis on surfaces with micropatterned Young's modulus. J Biomed Mater Res A 66(3):605-614.

Gupta D, Tator CH and Shoichet MS. 2006. Fast-gelling injectable blend of hyaluronan and methylcellulose for intrathecal, localized delivery to the injured spinal cord. Biomaterials 27(11):2370-2379.

Hadlock T, Sundback C, Hunter D, Cheney M and Vacanti JP. 2000. A polymer foam conduit seeded with Schwann cells promotes guided peripheral nerve regeneration. Tissue Eng 6(2):119-127.

Hall PE, Lathia JD, Miller NG, Caldwell MA and ffrench-Constant C. 2006. Integrins are markers of human neural stem cells. Stem Cells 24(9):2078-2084.

Hern DL and Hubbell JA. 1998. Incorporation of adhesion peptides into nonadhesive hydrogels useful for tissue resurfacing. Journal of Biomedical Materials Research 39(2):266-276.

Hirrien M, Chevillard C, Desbrieres J, Axelos MAV and Rinaudo M. 1998. Thermogelation of methylcelluloses: new evidence for understanding the gelation mechanism. Polymer 39(25):6251-6259.

Hoane MR, Becerra GD, Shank JE, Tatko L, Pak ES, Smith M and Murashov AK. 2004. Transplantation of neuronal and glial precursors dramatically improves sensorimotor function but not cognitive function in the traumatically injured brain. J Neurotrauma 21(2):163-174.

Hohenester E and Engel J. 2002. Domain structure and organisation in extracellular matrix proteins. Matrix Biology 21(2):115-128.

Hubbell JA. 1999. Bioactive biomaterials. Current Opinion in Biotechnology 10(2):123-129.

Ilkhanizadeh S, Teixeira AI and Hermanson O. 2007. Inkjet printing of macromolecules on hydrogels to steer neural stem cell differentiation. Biomaterials 28(27):3936-3943.

Ip NY, Wiegand SJ, Morse J and Rudge JS. 1993. Injury-induced regulation of ciliary neurotrophic factor mRNA in the adult rat brain. Eur J Neurosci 5(1):25-33.

Jacques TS, Relvas JB, Nishimura S, Pytela R, Edwards GM, Streuli CH and ffrench-Constant C. 1998. Neural precursor cell chain migration and division are regulated through different beta 1 integrins. Development 125(16):3167-3177.

Jain A, Kim YT, McKeon RJ and Bellamkonda RV. 2006. In situ gelling hydrogels for conformal repair of spinal cord defects, and local delivery of BDNF after spinal cord injury. Biomaterials 27(3):497-504.

Jeong B, Bae YH, Lee DS and Kim SW. 1997. Biodegradable block copolymers as injectable drug-delivery systems. Nature 388:860-862.

Jiang G, Huang AH, Cai Y, Tanase M and Sheetz MP. 2006. Rigidity sensing at the leading edge through alphavbeta3 integrins and RPTPalpha. Biophys J 90(5):1804-1809.

Johe KK, Hazel TG, Muller T, Dugich-Djordjevic MM and McKay RD. 1996. Single factors direct the differentiation of stem cells from the fetal and adult central nervous system. Genes Dev 10(24):3129-3140.

Jucker M, Kleinman HK, Hohmann CF, Ordy JM and Ingram DK. 1991. Distinct immunoreactivity to 110 kDa laminin-binding protein in adult and lesioned rat forebrain. Brain Res 555(2):305-312.

Kapur TA and Shoichet MS. 2004. Immobilized concentration gradients of nerve growth factor guide neurite outgrowth. Journal of Biomedical Materials Research Part A 68A(2):235-243.

Kearns SM, Laywell ED, Kukekov VK and Steindler DA. 2003. Extracellular matrix effects on neurosphere cell motility. Experimental Neurology 182(1):240-244.

Keener CR, Wolfe CAC and Hage DS. 1994. Optimization of oxidized antibody labeling with lucifer yellow. BioTechniques 16(5):894-897.

Kelly S, Bliss TM, Shah AK, Sun GH, Ma M, Foo WC, Masel J, Yenari MA, Weissman IL, Uchida N, Palmer T and Steinberg GK. 2004. Transplanted human fetal neural stem cells survive, migrate, and differentiate in ischemic rat cerebral cortex. Proc Natl Acad Sci U S A 101(32):11839-11844.

Kerever A, Schnack J, Vellinga D, Ichikawa N, Moon C, Arikawa-Hirasawa E, Efird JT and Mercier F. 2007. Novel Extracellular Matrix Structures in the Neural Stem Cell Niche Capture the Neurogenic Factor FGF-2 from the Extracellular Milieu. Stem Cells.

Keselowsky BG, Collard DM and Garcia AJ. 2003. Surface chemistry modulates fibronectin conformation and directs integrin binding and specificity to control cell adhesion. Journal of Biomedical Materials Research Part A 66A(2):247-259.

Kim DE, Tsuji K, Kim YR, Mueller FJ, Eom HS, Snyder EY, Lo EH, Weissleder R and Schellingerhout D. 2006. Neural stem cell transplant survival in brains of mice: assessing the effect of immunity and ischemia by using real-time bioluminescent imaging. Radiology 241(3):822-830.

Kleinman HK, Ogle RC, Little CD, Sweeney TM and Luckenbilledds L. 1988. Laminin Receptors for Neurite Formation. Proceedings of the National Academy of Sciences of the United States of America 85(4):1282-1286.

Kobayashi K, Huang CI and Lodge TP. 1999. Thermoreversible gelation of aqueous methylcellulose solutions. Macromolecules 32(21):7070-7077.

Kumar S, Haglund BO and Himmelstein KJ. 1994. In situ-forming gels for ophthalmic drug delivery. Journal of Ocular Pharmacology 10(1):47-56.

Labrador RO, Buti M and Navarro X. 1998. Influence of collagen and laminin gels concentration on nerve regeneration after resection and tube repair. Experimental Neurology 149:243-252.

LaPlaca MC, Cullen DK, McLoughlin JJ and Cargill RS, 2nd. 2005. High rate shear strain of three-dimensional neural cell cultures: a new in vitro traumatic brain injury model. J Biomech 38(5):1093-1105.

LaPlaca MC, Lee VMY and Thibault LE. 1997. An in vitro model of traumatic neuronal injury: Loading rate- dependent changes in acute cytosolic calcium and lactate dehydrogenase release. Journal of Neurotrauma 14(6):355-368.

Leach JB, Brown XQ, Jacot JG, Dimilla PA and Wong JY. 2007. Neurite outgrowth and branching of PC12 cells on very soft substrates sharply decreases below a threshold of substrate rigidity. J Neural Eng 4(2):26-34.

Legrand C, Bour JM, Jacob C, Capiaumont J, Martial A, Marc A, Wudtke M, Kretzmer G, Demangel C, Duval D and et al. 1992. Lactate dehydrogenase (LDH) activity of the cultured eukaryotic cells as marker of the number of dead cells in the medium [corrected]. J Biotechnol 25(3):231-243.

Lenzlinger PM, Morganti-Kossmann MC, Laurer HL and McIntosh TK. 2001. The duality of the inflammatory response to traumatic brain injury. Mol Neurobiol 24(1-3):169-181.

Leone DP, Relvas JB, Campos LS, Hemmi S, Brakebusch C, Fassle R, Ffrench-Constant C and Suter U. 2005. Regulation of neural progenitor proliferation and survival by β1 integrins. Journal of Cell Science 118:2589-2599.

Lesny P, De Croos J, Pradny M, Vacik J, Michalek J, Woerly S and Sykova E. 2002. Polymer hydrogels usable for nervous tissue repair. Journal of Chemical Neuroanatomy 23(4):243-247.

Li J and Kao WJ. 2003. Synthesis of polyethylene glycol (PEG) derivatives and PEGylated-peptide biopolymer conjugates. Biomacromolecules 4(4):1055-1067.

Liesi P, Fried G and Stewart RR. 2001. Neurons and glial cells of the embryonic human brain and spinal cord express multiple and distinct isoforms of laminin. Journal of Neuroscience Research 64(2):144-167.

Liesi P, Kirkwood T and Vaheri A. 1986. Fibronectin is expressed by astrocytes cultured from embryonic and early postnatal rat brain. Exp Cell Res 163(1):175-185.

Longhi L, Zanier ER, Royo N, Stocchetti N and McIntosh TK. 2005. Stem cell transplantation as a therapueutic strategy for traumatic brain injury. Transplantation Immunology 15:143-148.

Lu D, Sanberg PR, Mahmood A, Li Y, Wang L, Sanchez-Ramos J and Chopp M. 2002. Intravenous administration of human umbilical cord blood reduces neurological deficit in the rat after traumatic brain injury. Cell Transplant 11(3):275-281.

LuckenbillEdds L. 1997. Laminin and the mechanism of neuronal outgrowth. Brain Research Reviews 23(1-2):1-27.

Lutolf MP and Hubbell JA. 2005a. Synthetic biomaterials as instructive extracellular microenvironments for morphogenesis in tissue engineering. Nat Biotechnol 23(1):47-55.

Lutolf MP and Hubbell JA. 2005b. Synthetic biomaterials as instructive extracellular microenvironments for morphogenesis in tissue engineering. Nature Biotechnology 23(1):47-55.

Ma W, Chen S, Fitzgerald W, Maric D, Lin HJ, O'Shaughnessy TJ, Kelly J, Liu XH and Barker JL. 2005. Three-dimensional collagen gel networks for neural stem cell-based neural tissue engineering. Macromolecular Symposia 227:327-333.

Mahmood A, Lu D and Chopp M. 2004. Marrow stromal cell transplantation after traumatic brain injury promotes cellular proliferation within the brain. Neurosurgery 55(5):1185-1193.

Mahmood A, Lu D, Qu C, Goussev A and Chopp M. 2006. Long-term recovery after bone marrow stromal cell treatment of traumatic brain injury in rats. J Neurosurg 104(2):272-277.

Mahoney MJ and Anseth KS. 2006. Three-dimensional growth and function of neural tissue in degradable polyethylene glycol hydrogels. Biomaterials 27(10):2265-2274.

Mahoney MJ and Anseth KS. 2007. Contrasting effects of collagen and bFGF-2 on neural cell function in degradable synthetic PEG hydrogels. J Biomed Mater Res A 81(2):269-278.

Mann BK, Schmedlen RH and West JL. 2001. Tethered-TGF-beta increases extracellular matrix production of vascular smooth muscle cells. Biomaterials 22(5):439-444.

Marchionini DM, Collier TJ, Camargo M, McGuire S, Pitzer M and Sortwell CE. 2003. Interference with anoikis-induced cell death of dopamine neurons: implications for augmenting embryonic graft survival in a rat model of Parkinson's disease. J Comp Neurol 464(2):172-179.

Marchionini DM, Collier TJ, Pitzer MR and Sortwell CE. 2004. Reassessment of caspase inhibition to augment grafted dopamine neuron survival. Cell Transplant 13(3):273-282.

Margutti S, Vicini S, Proietti N, Capitani D, Conio G, Pedemonte E and Segre AL. 2002. Physical-chemical characterisation of acrylic polymers grafted on cellulose. Polymer 43(23):6183-6194.

Marklund N, Bakshi A, Castelbuono DJ, Conte V and McIntosh TK. 2006. Evaluation of pharmacological treatment strategies in traumatic brain injury. Curr Pharm Des 12(13):1645-1680.

Massia SP and Stark J. 2001. Immobilized RGD peptides on surface-grafted dextran promote biospecific cell attachment. Journal of Biomedical Materials Research 56(3):390-399.

McIntosh TK. 1994. Neurochemical Sequelae of Traumatic Brain Injury - Therapeutic Implications. Cerebrovascular and Brain Metabolism Reviews 6(2):109-162.

McIntosh TK, Saatman KE, Raghupathi R, Graham DI, Smith DH, Lee VMY and Trojanowski JQ. 1998. The molecular and cellular sequelae of experimental traumatic brain injury: pathogenetic mechanisms. Neuropathology and Applied Neurobiology 24(4):251-267.

McIntosh TK, Smith DH, Meaney DF, Kotapka MJ, Gennarelli TA and Graham DI. 1996. Neuropathological sequelae of traumatic brain injury: Relationship to neurochemical and biomechanical mechanisms. Laboratory Investigation 74(2):315-342.

Mercier F, Kitasako JT and Hatton GI. 2002. Anatomy of the brain neurogenic zones revisited: fractones and the fibroblast/macrophage network. J Comp Neurol 451(2):170-188.

Mercier F, Kitasako JT and Hatton GI. 2003. Fractones and other basal laminae in the hypothalamus. J Comp Neurol 455(3):324-340.

Michael KE, Vernekar VN, Keselowsky BG, Meredith JC, Latour RA and Garcia AJ. 2003. Adsorption-induced conformational changes in fibronectin due to interactions with well-defined surface chemistries. Langmuir 19(19):8033-8040.

Molcanyi M, Riess P, Bentz K, Maegele M, Hescheler J, Schafke B, Trapp T, Neugebauer E, Klug N and Schafer U. 2007. Trauma-associated inflammatory response impairs embryonic stem cell survival and integration after implantation into injured rat brain. Journal of Neurotrauma 24(4):625-237.

Na K and Park KH. 2000. Conjugation of Arg-Gly-Asp sequence into thermo-reversible gel as an extracellular matrix for 3T3-L1 fibroblast cell culture. Biotechnology Letters 22(19):1553-1556.

Nakajima M, Ishimuro T, Kato K, Ko IK, Hirata I, Arima Y and Iwata H. 2007. Combinatorial protein display for the cell-based screening of biomaterials that direct neural stem cell differentiation. Biomaterials 28(6):1048-1060.

Nevell TP. 1963. Methods in carbohydrate chemistry. Whistler RL and Wolfrom ML, editors. New York: Academic Press.

Nolan S. 2005. Traumatic brain injury: a review. Crit Care Nurs Q 28(2):188-194.

Nomizu M, Weeks BS, Weston CA, Kim WH, Kleinman HK and Yamada Y. 1995. Structure-Activity Study of a Laminin Alpha-1 Chain Active Peptide Segment Ile-Lys-Val-Ala-Val (Ikvav). Febs Letters 365(2-3):227-231.

O'Connor SM, Stenger DA, Shaffer KM and Ma W. 2001. Survival and neurite outgrowth of rat cortical neurons in three-dimensional agarose and collagen gel matrices. Neuroscience Letters 304(3):189-193.

Oyesiku NM, Evans CO, Houston S, Darrell RS, Smith JS, Fulop ZL, Dixon CE and Stein DG. 1999. Regional changes in the expression of neurotrophic factors and their receptors following acute traumatic brain injury in the adult rat brain. Brain Research 833(2):161-172.

Philips MF, Muir JK, Saatman KE, Raghupathi R, Lee VM, Trojanowski JQ and McIntosh TK. 1999. Survival and integration of transplanted postmitotic human neurons following experimental brain injury in immunocompetent rats. J Neurosurg 90(1):116-124.

Phillips JB, Bunting SC, Hall SM and Brown RA. 2005. Neural tissue engineering: a self-organizing collagen guidance conduit. Tissue Eng 11(9-10):1611-1617.

Pinkse GG, Bouwman WP, Jiawan-Lalai R, Terpstra OT, Bruijn JA and de Heer E. 2006. Integrin signaling via RGD peptides and anti-beta1 antibodies confers resistance to apoptosis in islets of Langerhans. Diabetes 55(2):312-317.

Pinkse GG, Voorhoeve MP, Noteborn M, Terpstra OT, Bruijn JA and De Heer E. 2004. Hepatocyte survival depends on beta1-integrin-mediated attachment of hepatocytes to hepatic extracellular matrix. Liver Int 24(3):218-226.

Pittier R, Sauthier F, Hubbell JA and Hall H. 2005. Neurite extension and in vitro myelination within three-dimensional modified fibrin matrices. Journal of Neurobiology 63(1):1-14.

Powell SK and Kleinman HK. 1997. Neuronal laminins and their cellular receptors. International Journal of Biochemistry & Cell Biology 29(3):401-414.

Prange MT and Margulies SS. 2002. Regional, directional, and age-dependent properties of the brain undergoing large deformation. J Biomech Eng 124(2):244-252.

Quirk RA, Davies MC, Tendler SJB, Chan WC and Shakesheff KM. 2001. Controlling biological interactions with poly(lactic acid) by surface entrapment modification. Langmuir 17(9):2817-2820.

Ray SK, Dixon CE and Banik NL. 2002. Molecular mechanisms in the pathogenesis of traumatic brain injury. Histol Histopathol 17(4):1137-1152.

Recknor JB, Sakaguchi DS and Mallapragada SK. 2006. Directed growth and selective differentiation of neural progenitor cells on micropatterned polymer substrates. Biomaterials 27(22):4098-4108.

Reynolds BA, Tetzlaff W and Weiss S. 1992. A multipotent EGF-responsive striatal embryonic progenitor cell produces neurons and astrocytes. J Neurosci 12(11):4565-4574.

Riess P, Molcanyi M, Bentz K, Maegele M, Simanski C, Carlitscheck C, Schneider A, Hescheler J, Bouillon B, Schafer U and Neugebauer E. 2007. Embryonic stem cell transplantation after experimental traumatic brain injury dramatically improves neurological outcome, but may cause tumors. J Neurotrauma 24(1):216-225.

Riess P, Zhang C, Saatman KE, Laurer HL, Longhi LG, Raghupathi R, Lenzlinger PM, Lifshitz J, Boockvar J, Neugebauer E, Snyder EY and McIntosh TK. 2002a. Transplanted neural stem cells survive, differentiate, and improve neurological motor function after experimental traumatic brain injury. Neurosurgery 51(4):1043-1052; discussion 1052-1044.

Riess P, Zhang C, Saatman KE, Laurer HL, Longhi LG, Raghupathi R, Lenzlinger PM, Lifshitz J, Boockvar J, Neurgebauer E, Snyder EY and McIntosh TK. 2002b. Transplanted neural stem cells survive, differentiate, and improve neurological motor function after experimental traumatic brain injury. Neurosurgery 51:1043-1054.

Rutland-Brown W, Langlois JA, Thomas KE and Xi YL. 2006. Incidence of traumatic brain injury in the United States, 2003. J Head Trauma Rehabil 21(6):544-548.

Saatman KE, Feeko KJ, Pape RL and Raghupathi R. 2006. Differential behavioral and histopathological responses to graded cortical impact injury in mice. J Neurotrauma 23(8):1241-1253.

Saha K, Irwin EF, Kozhukh J, Schaffer DV and Healy KE. 2007. Biomimetic interfacial interpenetrating polymer networks control neural stem cell behavior. J Biomed Mater Res A 81(1):240-249.

Sakiyama-Elbert SE and Hubbell JA. 2000. Controlled release of nerve growth factor from a heparin-containing fibrin-based cell ingrowth matrix. Journal of Controlled Release 69(1):149-158.

Schense JC, Bloch J, Aebischer P and Hubbell JA. 2000. Enzymatic incorporation of bioactive peptides into fibrin matrices enhances neurite extension. Nature Biotechnology 18(4):415-419.

Schmidt C and Leach J. 2003. Neural tissue engineering: Strategies for repair and regeneration. Annual Review of Biomedical Engineering 5:293-347.

Shear DA, Tate MC, Archer DR, Hoffman SW, Hulce VD, LaPlaca MC and Stein DG. 2004. Neural progenitor cell transplants promote long-term functional recovery after traumatic brain injury. Brain Research 1026(1):11-22.

Shin H, Jo S and Mikos AG. 2002. Modulation of marrow stromal osteoblast adhesion on biomimetic oligo poly(ethylene glycol) fumarate hydrogels modified with Arg-Gly-Asp peptides and a poly(ethylene glycol) spacer. Journal of Biomedical Materials Research 61(2):169-179.

Shindo T, Matsumoto Y, Wang Q, Kawai N, Tamiya T and Nagao S. 2006. Differences in the neuronal stem cells survival, neuronal differentiation and neurological improvement after transplantation of neural stem cells between mild and severe experimental traumatic brain injury. J Med Invest 53(1-2):42-51.

Siesjo BK and Wieloch T. 1988. Brain Injury: Neurochemical Aspects. Central Nervous System Trauma Status Report. Washington, D.C.: U.S. Government Printing Office. p 513-532.

Silva GA, Czeisler C, Niece KL, Beniash E, Harrington DA, Kessler JA and Stupp SI. 2004. Selective differentiation of neural progenitor cells by high-epitope density nanofibers. Science 303(5662):1352-1355.

Sinson G, Voddi M and McIntosh TK. 1996. Combined fetal neural transplantation and nerve growth factor infusion: effects on neurological outcome following fluid-percussion brain injury in the rat. Journal of Neurosurgery 84:655-662.

Smets FN, Chen Y, Wang LJ and Soriano HE. 2002. Loss of cell anchorage triggers apoptosis (anoikis) in primary mouse hepatocytes. Mol Genet Metab 75(4):344-352.

Smith E, Bai J, Oxenford C, Yang J, Somayaji R and Uludag H. 2003. Conjugation of arginine-glycine-aspartic acid peptides to thermoreversible N-isopropylacrylamide polymers. Journal of Polymer Science Part a-Polymer Chemistry 41(24):3989-4000.

Song H, Stevens CF and Gage FH. 2002. Astroglia induce neurogenesis from adult neural stem cells. Nature 417(6884):39-44.

Soria JM, Martinez Ramos C, Salmeron Sanchez M, Benavent V, Campillo Fernandez A, Gomez Ribelles JL, Garcia Verdugo JM, Pradas MM and Barcia JA. 2006. Survival and differentiation of embryonic neural explants on different biomaterials. J Biomed Mater Res A 79(3):495-502.

Stabenfeldt SE, Garcia AJ and LaPlaca MC. 2006. Thermoreversible laminin-functionalized hydrogel for neural tissue engineering. Journal of Biomedical Materials Research Part A 77A(4):718-725.

Stile RA, Burghardt WR and Healy KE. 1999. Synthesis and characterization of injectable poly(N- isopropylacrylamide)-based hydrogels that support tissue formation in vitro. Macromolecules 32(22):7370-7379.

Studer L, Tabar V and McKay RDG. 1998. Transplantation of expanded mesencephalic precursors leads to recovery in parkinsonian rats. Nature Neuroscience 1(4):290-295.

Subramanian T. 2001. Cell transplantation for the treatment of Parkinson's disease. Seminars of Neurology 21(1):103-115.

Suslov ON, Kukekov VG, Ignatova TN and Steindler DA. 2002. Neural stem cell heterogeneity demonstrated by molecular phenotyping of clonal neurospheres. Proc Natl Acad Sci U S A 99(22):14506-14511.

Sutton RL, Lescaudron L and Stein DG. 1993. Unilateral cortical contusion injury in the rat: Vascular disruption and temporal development of cortical necrosis. Journal of Neurotrauma 10(2):135-149.

Tashiro K, Monji A, Yoshida I, Hayashi Y, Matsuda K, Tashiro N and Mitsuyama Y. 1999. An IKLLI-containing peptide derived from the laminin alpha 1 chain mediating heparin-binding, cell adhesion, neurite outgrowth and proliferation, represents a binding site for integrin alpha 3 beta 1 and heparan sulphate proteoglycan. Biochemical Journal 340:119-126.

Tashiro K, Sephel GC, Weeks B, Sasaki M, Martin GR, Kleinman HK and Yamada Y. 1989. A Synthetic Peptide Containing the Ikvav Sequence from the a-Chain of Laminin Mediates Cell Attachment, Migration, and Neurite Outgrowth. Journal of Biological Chemistry 264(27):16174-16182.

Tate MC, Garcia AJ, Keselowsky BG, Schumm MA, Archer DR and LaPlaca MC. 2004. Specific Beta-1 integrins mediate adhesion, migration, and differentiation of neural progenitors derived from the embryonic striatum. Molecular and Cellular Neuroscience 27(1):22-31.

Tate MC, Shear DA, Hoffman SW, Stein DG, Archer DR and LaPlaca MC. 2002. Fibronectin promotes survival and migration of primary neural stem cells transplanted into the traumatically injured mouse brain. Cell Transplantation 11(3):283-295.

Tate MC, Shear DA, Hoffman SW, Stein DG and LaPlaca MC. 2001. Biocompatibility of methylcellulose-based constructs designed for intracerebral gelation following experimental traumatic brain injury. Biomaterials 22(10):1113-1123.

Taylor SJ, McDonald JW and Sakiyama-Elbert SE. 2004. Controlled release of neurotrophin-3 from fibrin gels for spinal cord injury. Journal of Controlled Release 98:281-294.

Temenoff JS, Shin H, Conway DE, Engel PS and Mikos AG. 2003. In vitro cytotoxicity of redox radical initiators for cross-linking of oligo(poly(ethylene glycol) fumarate) macromers. Biomacromolecules 4(6):1605-1613.

Thibault KL and Margulies SS. 1998. Age-dependent material properties of the porcine cerebrum: effect on pediatric inertial head injury criteria. J Biomech 31(12):1119-1126.

Thomas FT, Contreras JL, Bilbao G, Ricordi C, Curiel D and Thomas JM. 1999. Anoikis, extracellular matrix, and apoptosis factors in isolated cell transplantation. Surgery 126(2):299-304.

Thurman DJ, Alverson C, Dunn KA, Guerrero J and Sniezek JE. 1999. Traumatic brain injury in the United States: A public health perspective. J Head Trauma Rehabil 14(6):602-615.

Tsai EC, Dalton PD, Shoichet MS and Tator CH. 2006. Matrix inclusion within synthetic hydrogel guidance channels improves specific supraspinal and local axonal regeneration after complete spinal cord transection. Biomaterials 27(3):519-533.

Unterberg AW, Stover J, Kress B and Kiening KL. 2004. Edema and brain trauma. Neuroscience 129(4):1021-1029.

Varma AJ and Chavan VB. 1995. A Study of Crystallinity Changes in Oxidized Celluloses. Polymer Degradation and Stability 49(2):245-250.

Varma AJ and Kulkarni MP. 2002. Oxidation of cellulose under controlled conditions. Polymer Degradation and Stability 77(1):25-27.

Wach RA, Mitomo H and Yoshii F. 2004. ESR investigation on gamma-irradiated methylcellulose and hydroxyethylcellulose in dry state and in aqueous solution. Journal of Radioanalytical and Nuclear Chemistry 261(1):113-118.

Warden D. 2006. Military TBI during the Iraq and Afghanistan wars. J Head Trauma Rehabil 21(5):398-402.

Watson DJ, Walton RM, Magnitsky SG, Bulte JW, Poptani H and Wolfe JH. 2006. Structure-specific patterns of neural stem cell engraftment after transplantation in the adult mouse brain. Hum Gene Ther 17(7):693-704.

Webb K, Budko E, Neuberger TJ, Chen SZ, Schachner M and Tresco PA. 2001. Substrate-bound human recombinant L1 selectively promotes neuronal attachment and outgrowth in the presence of astrocytes and fibroblasts. Biomaterials 22(10):1017-1028.

Wells MR, Kraus K, Batter DK, Blunt DG, Weremowitz J, Lynch SE, Antoniades HN and Hansson HA. 1997. Gel matrix vehicles for growth factor application in nerve gap injuries repaired with tubes: A comparison of biomatrix, collagen, and methylcellulose. Experimental Neurology 146(2):395-402.

Willerth SM and Sakiyama-Elbert SE. 2007. Approaches to neural tissue engineering using scaffolds for drug delivery. Adv Drug Deliv Rev 59(4-5):325-338.

Willits RK and Skornia SL. 2004. Effect of collagen gel stiffness on neurite extension. J Biomater Sci Polym Ed 15(12):1521-1531.

Woerly S, Petrov P, Sykova E, Roitbak T, Simonova Z and Harvey AR. 1999. Neural tissue formation within porous hydrogels implanted in brain and spinal cord lesions: Ultrastructural, immunohistochemical, and diffusion studies. Tissue Engineering 5(5):467-488.

Woerly S, Plant GW and Harvey AR. 1996. Cultured rat neuronal and glial cells entrapped within hydrogel polymer matrices: A potential tool for neural tissue replacement. Neuroscience Letters 205(3):197-201.

Wolfe CAC and Hage DS. 1995. Studies on the rate and control of antibody oxidation by periodate. Analytical Biochemistry 231:123-130.

Wright DW, Ritchie JC, Mullins RE, Kellermann AL and Denson DD. 2005. Steady-state serum concentrations of progesterone following continuous intravenous infusion in patients with acute moderate to severe traumatic brain injury. J Clin Pharmacol 45(6):640-648.

Yang F, Xu CY, Kotaki M, Wang S and Ramakrishna S. 2004. Characterization of neural stem cells on electrospun poly(L-lactic acid) nanofibrous scaffold. Journal of Biomaterials Science-Polymer Edition 15(12):1483-1497.

Yeung T, Georges PC, Flanagan LA, Marg B, Ortiz M, Funaki M, Zahir N, Ming W, Weaver V and Janmey PA. 2005. Effects of substrate stiffness on cell morphology, cytoskeletal structure, and adhesion. Cell Motil Cytoskeleton 60(1):24-34.

Young RJ and Lovell PA. 1991. Introduction to Polymers. New York: Chapman & Hall. 443 p.

Yu XJ and Bellamkonda RV. 2003. Tissue-engineered scaffolds are effective alternatives to autografts for bridging peripheral nerve gaps. Tissue Engineering 9(3):421-430.

Yu XJ, Dillon GP and Bellamkonda RV. 1999. A laminin and nerve growth factor-laden three-dimensional scaffold for enhanced neurite extension. Tissue Engineering 5(4):291-304.

Zafonte RD, Cullen N and Lexell J. 2002. Serotonin agents in the treatment of acquired brain injury. J Head Trauma Rehabil 17(4):322-334.

Zhang C, Saatman KE, Royo NC, Soltesz KM, Millard M, Schouten JW, Motta M, Hoover RC, McMillan A, Watson DJ, Lee VM, Trojanowski JQ and McIntosh TK. 2005. Delayed transplantation of human neurons following brain injury in rats: a long-term graft survival and behavior study. J Neurotrauma 22(12):1456-1474.

Zhbankov RG. 1966. Infrared Spectra of Cellulose. Densham AB, translator. Stepanov BI, editor. New York: Consultants Bureau. 333 p.

Zhou FC. 1990. Four patterns of laminin-immunoreactive structure in developing rat brain. Brain Res Dev Brain Res 55(2):191-201.